Chapter 5

Reactivity of Small Gold Clusters: Results and Discussion

In this chapter, the experimental results for the reactivity of small gold clusters towards molecular oxygen (O_2) and carbon monoxide (CO) in the gas-phase will be presented. As mentioned in section 2.3.2, the charge, the electronic and geometrical structure as well as the chemical composition of the clusters have a significant influence on their chemical reactivity. First, the influence of the charge on the reactivity of gold clusters with oxygen and carbon monoxide will be discussed. The study of the reactivity of gold anions towards O_2 and CO as a function of temperature will follow this discussion. For the first time, temperature-dependent kinetic measurements for the reactivity of gold clusters with oxygen and carbon monoxide were performed. Furthermore, a full catalytic cycle for the CO oxidation reaction on anionic gold dimers will be described. Finally, a comparison between the reactivities of gold, silver and mixed silver-gold clusters will be presented, demonstrating the influence of the chemical composition on the cluster reactivity.

5.1 Reactions of Gold Cations with O_2 and CO

The reactivity of positively charged gold clusters (Au_n^+, $n \leq 11$) with molecular oxygen was investigated as a function of cluster size and temperature. In Fig. 5.1, typical mass spectra of cationic gold clusters, obtained after the alignment of the

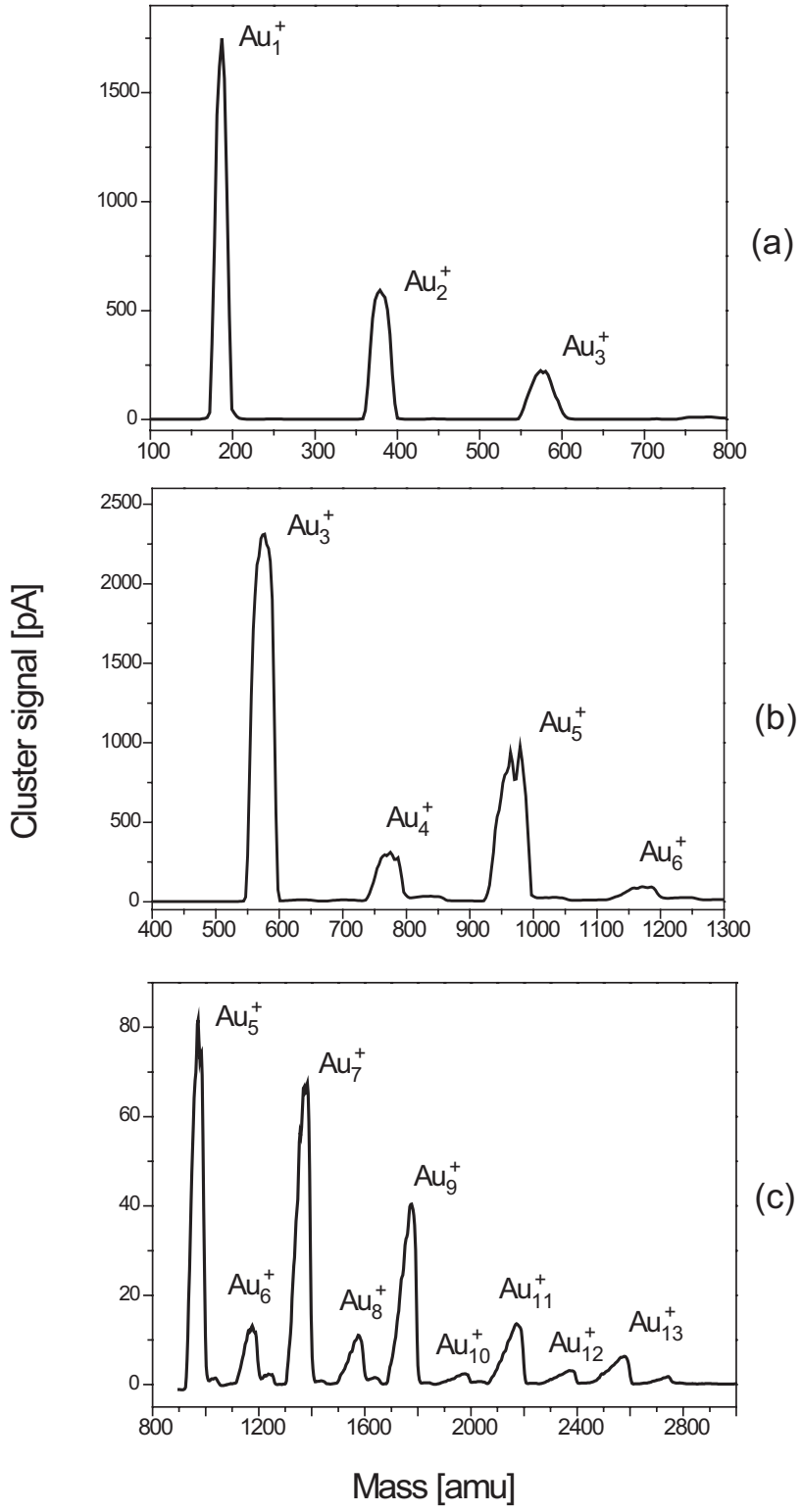

Figure 5.1: Typical mass spectra of gold cations. The cluster signal is depicted as a function of the cluster mass. (a), (b) Mass spectra measured after mass selection in Q_1 (see chapter 4, Fig. 4.1) with alignment for maximum intensity of Au_2^+ and Au_3^+ clusters, respectively. (c) Mass spectrum measured after mass selection in Q_3 (see chapter 4, Fig. 4.1) with alignment for maximum intensity of Au_6^+ clusters.

CORDIS source as well as the series of quadrupoles and electrostatic lenses, are presented (see section 4.1.1). Since gold has only one isotope (^{197}Au), the peaks in Fig. 5.1 (a), (b), (c) can be unambiguously assigned. From the mass spectra, it can be clearly seen that the signal intensity for the odd numbered clusters (Au_3^+, Au_5^+, Au_7^+, Au_9^+, Au_{11}^+, Au_{13}^+) is higher than for the even numbered clusters (Au_4^+, Au_6^+, Au_8^+, Au_{10}^+, Au_{12}^+). This odd-even alternation appears due to the well known electron pairing effect.[110] For all metals which have a s^1 valence electron, like coinage metals (copper, silver, gold) and alkaline metals, the positively or negatively charged clusters with an odd number of atoms, *i.e* an even number of valence electrons are more stable and hence more abundant than the clusters with an even number of atoms, *i.e* an odd number of valence electrons.[110]

After the optimization of all experimental parameters for obtaining a maximum signal intensity of the desired cluster size, the measurement procedure was carried out as previously described in section 4.1.3. The reactivity of all available cationic gold clusters (Au_n^+, $n = 2 - 11$) with oxygen was systematically investigated as a function of ion trap temperature $T_{octopole}$, which was varied between 70 K and 300 K. No reaction product with oxygen is detected for any cluster size at any investigated temperature. For exemplification, the mass spectra for Au_2^+, Au_3^+ and Au_7^+ in the presence of molecular oxygen are shown in Fig. 5.2 (a), (b), (c) for an ion trap temperature of $T_{octopole} = 300$ K. It can be seen that no reaction products appear in the mass spectra presented in Fig. 5.2.

The non-reactivity of cationic gold clusters towards oxygen was previously observed by Cox *et al.*[111] The authors investigated the reactivity of gold clusters (Au_n^+, $n \leq 20$) with O_2, CH_4 and H_2, as a function of cluster size and cluster charge state by using the flow reactor technique. It was shown that the reactivity of gold clusters is strongly size- and charge-state dependent and from the cationic gold clusters, only Au_{10}^+ was found to be reactive towards molecular oxygen. Under the experimental conditions used for the measurements presented in this work, no reaction product with oxygen is detected for gold cations, including Au_{10}^+. The absence of a reaction product for the case of Au_{10}^+ clusters is a result of the experimental restrictions that allow only the presence of small amounts of reactive gases inside the octopole ion trap in comparison to the experiments performed by Cox *et al.*[111]

Due to the lack of theoretical calculations and experimental data for the reactivity

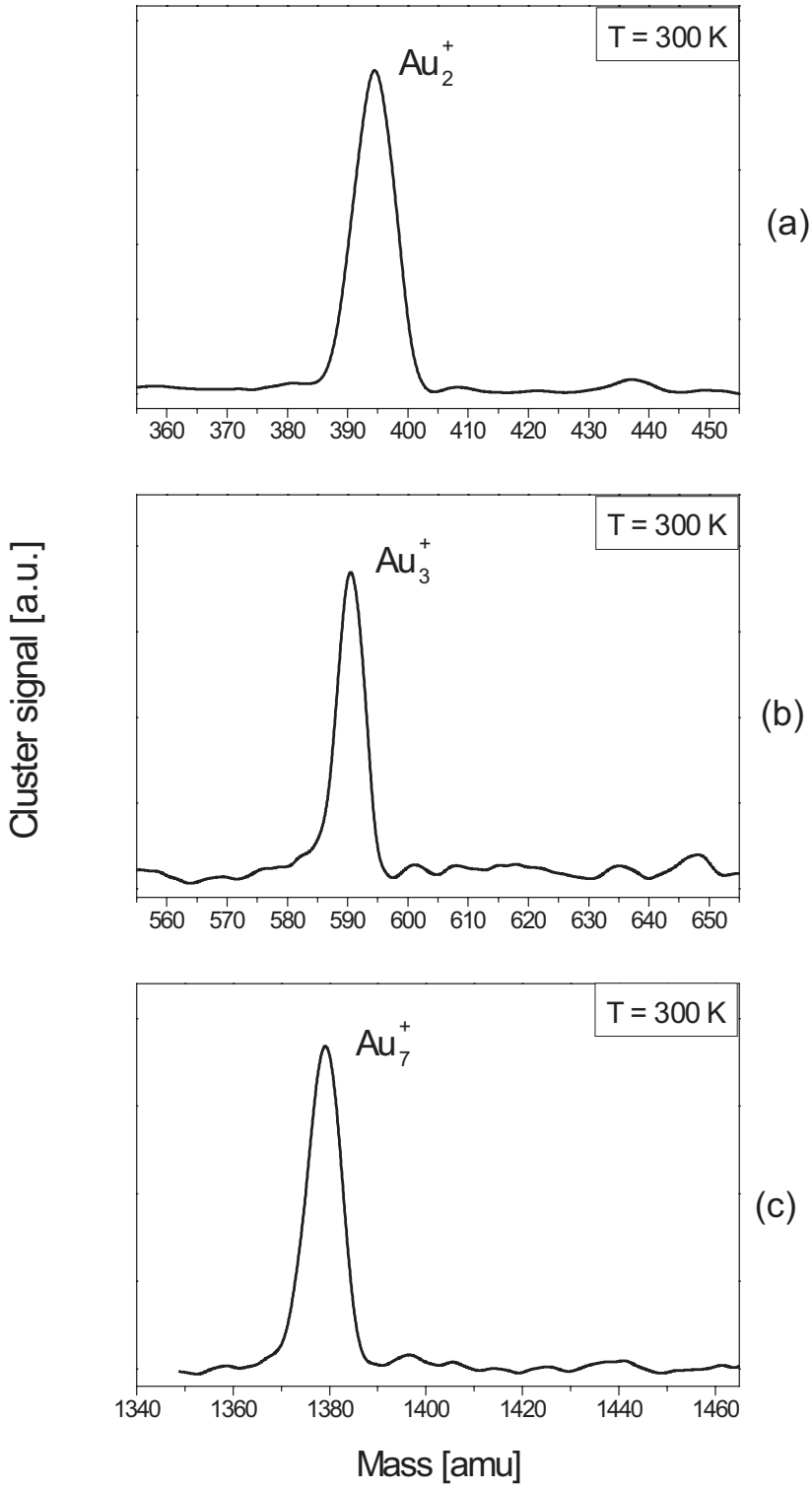

Figure 5.2: Reactivity of Au_2^+, Au_3^+ and Au_7^+ with O_2 at room temperature. The reaction parameters are: (a) $p_{He} = 0.57\ Pa$, $p_{O_2} = 0.63\ Pa$, $t_{reaction} = 1000\ ms$, $T_{octopole} = 300\ K$; (b) $p_{He} = 1.16\ Pa$, $p_{O_2} = 0.15\ Pa$, $t_{reaction} = 500\ ms$, $T_{octopole} = 300\ K$; (c) $p_{He} = 1.12\ Pa$, $p_{O_2} = 0.36\ Pa$, $t_{reaction} = 500\ ms$, $T_{octopole} = 300\ K$.

of gold cations towards oxygen, only trends in the reactive behavior of gold will be outlined in the following. The influence of relativistic effects on the physical and chemical properties of gold will be emphasized by making a comparison with the reactivity of other coinage metals like silver (Ag) and copper (Cu).

In the following, the non-reactivity of small, positively charged gold clusters with oxygen will be discussed with respect to the reactive behavior towards O_2 of neutral and negatively charged clusters as well as bulk surfaces of coinage metals. Theoretical calculations for small neutral and negatively charged gold clusters ($Au_n,\ n \leq 11$) based on density functional theory (DFT) show that the binding energy between neutral gold clusters and oxygen is weaker than the binding energy of O_2 on anionic gold clusters and has values between $E_{BE}(Au_7O_2) = 0.17\ eV$ and $E_{BE}(Au_3O_2) = 0.66\ eV$ for molecularly adsorbed oxygen. Furthermore, the $O-O$ bond is elongated when oxygen binds on gold anions, whereas only small changes in the oxygen bond length (an elongation of 0.018 $\mathring{A}$ for Au_6O_2 complex) are predicted for the reaction with neutral clusters.[112] Although predicted by theory, no reaction products of neutral gold dimer with oxygen molecules have been experimentally observed.[113] This can be attributed to the small values of the binding energy of O_2 calculated for neutral gold clusters,[112,114,115] which makes an experimental detection extremely difficult. In the case of surfaces, oxygen does not adsorb on clean $Au(110)$ and $Au(111)$ and gold oxides can only be formed when gold is exposed to excited molecular oxygen or to ozone.[6] On silver surfaces, oxygen can be physisorbed[a], molecularly and dissociatively chemisorbed[b] and even subsurface states have been identified, while on copper surfaces oxygen usually adsorbs dissociatively.[116,117]

In order to understand the non-reactivity of positively charged gold clusters towards oxygen, a closer look into the bonding mechanism of molecular oxygen is necessary. The gas-phase O_2 molecule has the following electronic configuration: $1s\sigma^2 1s\sigma^{*2} 2s\sigma^2 2s\sigma^{*2} 2p_x\pi^2 2p_y\pi^2 2p_z\sigma^2 2p_x\pi^{*1} 2p_y\pi^{*1}$, where z defines the axis between the two oxygen atoms. One can notice that the degenerate $2p\pi^*$ orbitals are half-filled, each having only one electron. The $2p\pi^*$ orbitals have an antibonding character and, for simplification, the π^* notation will be used. Oxygen acts usually as an electron

[a] Physisorption occurs when the interaction forces between the adsorbed molecules and surfaces are van der Waals type forces.

[b] Chemisorption occurs when the interaction forces between the adsorbed molecules and surfaces possess a covalent nature.

acceptor and the O_2 bonding to clusters occurs when an electron from the highest occupied molecular orbital (HOMO) of the cluster is transferred into one of the antibonding π^* orbitals of O_2 molecule.[85] In the case of cations, which already have an electron less than neutral clusters, this charge transfer is energetically unfavorable.

In contrast to gold cations, the absorption of up to two oxygen molecules on positively charged silver dimers (Ag_2^+) was observed in the experiments carried out in the group of Prof. L. Wöste.[79,90] A combined experimental and theoretical study of the oxygen adsorption on cationic silver monomers and dimers was reported by Manard *et al.*[118] The authors explained the weak O_2 bonding on silver cations through a charge-induced dipole moment in the oxygen molecule which causes a polarization of the oxygen electron density towards the positively charged silver ions.

In the case of copper cations, no adsorption of oxygen molecules could be measured by using Fourier Transform Ion Cyclotron Resonance technique (FT-ICR) but, it is important to note, that a strong fragmentation pattern of the positive copper clusters was observed in these experiments.[119] This could be an indication of a highly exothermic binding of oxygen on cationic copper clusters. The absence of thermal oxygen association reaction is interpreted to be the result of the extremely low-pressure reaction conditions which implies that the low concentration of the buffer gas does not provide a sufficient thermalization of the possible reaction products.[85]

The particular reactive behavior of gold, compared to its neighboring metals from the periodic table of elements and especially to those from the same group (silver, copper) can be understood as a consequence of the relativistic effects, which are much stronger in gold than in silver or copper. The relativistic contraction of the *s*-orbitals, the delocalization of the *d*-orbitals as well as a stronger spin-orbit interaction are important consequences of the relativistic effects present in heavy atoms.[120] Compared to its neighboring atoms in the periodic table, the relativistic contraction of the $6s$-orbitals of gold is unusually high.[121]

The uniqueness of gold can also be seen, when a closer look at the structure of coinage metal clusters is taken. For positively charged clusters, the transition from two-dimensional to three-dimensional structures ($2D \rightarrow 3D$ transition) occurs at different sizes for silver and copper than for gold:

- Theoretical studies predict that Cu_n^+ clusters are two-dimensional up to $n = 4$. Starting with Cu_5^+ a three-dimensional structure is energetically preferred.[122]

- For Ag_n^+ clusters, experimental and theoretical works established that the $2D \rightarrow 3D$ transition occurs, as in the case of copper clusters, at $n = 5$.[123,124]

- Experimental and theoretical studies showed that, in contrast to Cu_n^+ and Ag_n^+, Au_n^+ clusters have planar structures up to $n = 7$. For the case of the Au_8^+ cluster, a planar isomer is predicted from DFT calculations as the most stable structure. The theory also calculates a three-dimensional isomer for Au_8^+, which is only 0.06 eV higher in energy than the planar structure. From ion mobility measurements, only the $3D$-structure was observed for Au_8^+.[125] The tendency of gold clusters to favor planar structures is a result of a strong s-d hybridization in the cluster bonding, due to the presence of the relativistic effects.[126]

This unique behavior of gold compared with silver and copper which has its origins in the strong relativistic effects, is likely to influence the reactivity of gold clusters and could explain the non-reactivity of positively charged gold clusters towards oxygen.

Cooling the trap down to 70 K and measuring the reactivity of Au_2^+ clusters with oxygen reveals another interesting feature: the dimer cation does not react with O_2, but reaction products with residual amounts of carbon monoxide present in the ion trap are observed. Fig. 5.3 shows the mass spectrum for Au_2^+ clusters after 1000 ms reaction time. It can be seen that the reaction products Au_2CO^+ and $Au_2(CO)_3^+$ appear in the mass spectrum. The proposed reaction mechanism involves the sequential adsorption of individual CO molecules. Since no $Au_2(CO)_2^+$ product is observed at any reaction time, the adsorption of the third CO molecule should occur on a very fast time scale, compared to the experimental time resolution.

As in the case of the cationic gold clusters reactivity towards oxygen described previously, the interpretation of the measured data should take into account the electronic structure and properties of the ligand and cluster. The electronic structure of a CO molecule is: $1s\sigma^2 1s\sigma^{*2} 2s\sigma^2 2p_z\sigma^2 2p_x\pi^2 2p_y\pi^2 2s\sigma^{*2}$, where the z axis defines the axis between the C and O atoms. The binding mechanism of carbon monoxide on transition metals can be described within the *Blyholder model*,[127] which implies a double charge transfer between carbon monoxide molecule and the metal cluster: CO donates its lone-pair of σ electrons ($2s\sigma^{*2}$) into an empty orbital of the metal cluster, while occupied π and δ orbitals from the metal cluster back-donate into the lowest unoccupied molecular orbital (LUMO) of the CO molecule, which is an antibonding

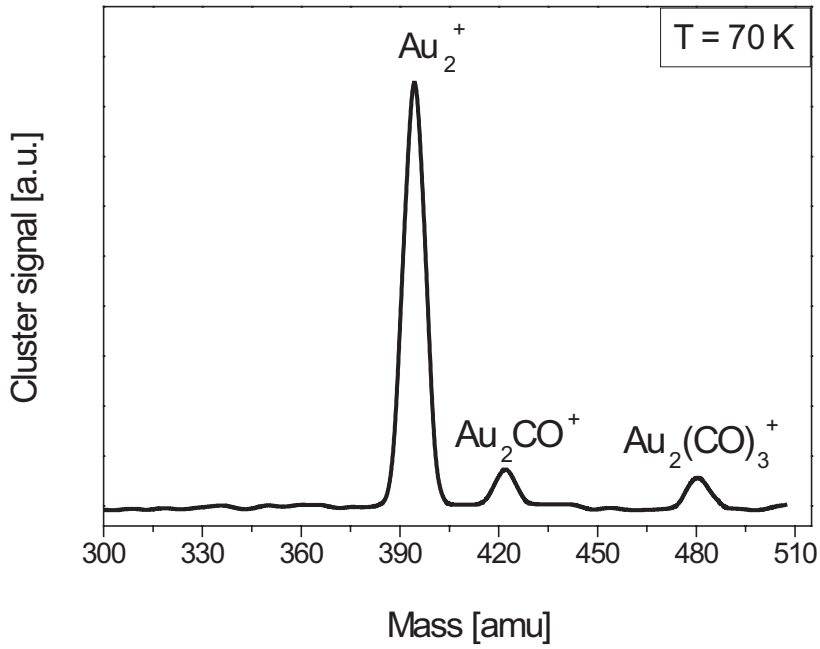

Figure 5.3: Reactivity of Au_2^+ clusters at low temperatures with residual amounts of carbon monoxide present in the vacuum chamber: $p_{He} = 1.13\ Pa$, $p_{O_2} = 0.07\ Pa$, $t_{reaction} = 1000\ ms$, $T_{octopole} = 70\ K$.

π^* orbital ($2p_x\pi^*$ or $2p_y\pi^*$). The strength of these interactions (σ donation and π back-donation) depends on the details of the orbital overlaps.

Theoretical calculations based on DFT theory, have been employed to analyze the binding of the first CO molecule on negative, neutral and positive gold clusters. For Au_2CO^+ and Au_2CO a linear geometry was predicted, where the carbon monoxide bond length is longer in the neutral complex than in the cationic carbonyl complex. These calculations suggest that the CO molecule binds stronger on gold cluster cations than on neutral and anionic gold clusters and the forward donation ($CO \rightarrow$ metal) is the dominant mechanism in this case.[128]

For closed d-shell metals, which are less reactive than metals with an open d-shell, the adsorption of up to three carbon monoxide molecules on cationic gold dimer is surprising at first, but this phenomenon was experimentally measured and theoretically described for all group 11 metals (Cu, Ag, Au).

For bulk copper, silver and gold surfaces the heat of adsorption of CO molecules

at low coverage is smaller in the case of silver surfaces than for gold and copper surfaces.[85] Therefore, it could be assumed that CO is only physisorbed on bulk silver surfaces and chemisorbed on gold and copper surfaces. In his PhD. thesis, Jan Hagen investigated the reactivity of small silver and silver-gold clusters with oxygen and carbon monoxide. In the case of Ag_2^+ clusters, the adsorption of up to two CO molecules at room temperature was observed.[79] For small, positively charged copper clusters, it was experimentally determined that a minimum of three CO molecules adsorb on monomer, dimer and trimer, whereas for Cu_4^+ up to Cu_7^+, at least one or two CO ligands more than the number of atoms contained in the cluster were identified.[32] In the case of neutral dimers of copper, silver and gold, it was observed that Ag_2 cluster does not react with CO, while Cu_2 and Au_2 neutral clusters show a strong reactivity towards carbon monoxide, with gold dimer being about three times more reactive than Cu_2.[113]

The differences discussed above in the reactivity of group 11 metals towards carbon monoxide, with special emphasis on the unique behavior of gold clusters can be understood as a manifestation of the strong relativistic effects. The contraction of the *s*-orbitals leads to a screening of the nuclei and therefore to a destabilization of the *d*-orbitals. Compared to silver, where the position of the *d*-orbitals is energetically unfavorable for the π back-donation with CO molecule, the relativistic destabilization of the *d*-orbitals in gold increases their availability for the π back-donation in the bonding of CO molecules, thus strengthening the CO-metal bond.

In conclusion, the bonding of CO molecules to metal clusters is governed by the interplay between the σ forward charge donation and the π back-donation. As shown above for the case of the bonding between gold clusters and carbon monoxide, the σ forward donation is strongly influenced by the charge state of the cluster, while the π back-donation is dependent on the energetic position of the *d*-orbitals in the clusters. Since the presence of the relativistic effects leads to a strong shift of the *d*-orbitals in gold clusters, they should be considered in the treatment of the reactivity of gold clusters towards CO.

5.2 Reactions of Gold Anions with O_2

After the study of small, positively charged gold clusters, negatively charged clusters were investigated in order to determine the influence of the electric charge on the chemical reactivity. It was shown in section 2.3.2, that the presence of a negative charge plays a significant role in the catalytic oxidation of carbon monoxide to carbon dioxide, when gold nanoparticles and clusters supported on oxide thin films are acting as catalysts. In the case of small Au_8 clusters deposited on thin magnesium oxide films, the charge transfer between the substrate and the deposited clusters weakens the $O-O$ bond and initiates the reaction between carbon monoxide and oxygen. In the following, a detailed study of the reactivity of anionic gold clusters towards oxygen will be presented.

Typical mass spectra of negatively charged gold clusters are presented in Fig 5.4, where the cluster signal intensity is depicted as a function of cluster mass. The peaks corresponding to the masses of Au_1^-, Au_2^- and Au_3^- can be unambiguously assigned. In Fig 5.4 (a), the mass spectrum is measured after the optimization of the experimental setup parameters in order to maximize the Au_2^- signal intensity, while in Fig 5.4 (b) the optimization for maximizing the Au_3^- cluster signal is performed. Due to the experimental limitations of the cluster source, no negatively charged gold clusters composed of more than three atoms could be produced.

The reactivity of gold cluster anions (monomer, dimer and trimer) was systematically investigated as a function of different reaction parameters such as ion trap temperature ($T_{octopole}$), reaction time ($t_{reaction}$) and reactive gas pressure (p_{O_2}). In Fig. 5.5 (a) - (f), the mass spectra in the presence of oxygen for anionic gold monomer, dimer and trimer are shown as a function of reaction time and reaction temperature. The mass spectra were measured under comparable experimental conditions with an oxygen pressure of about $p_{O_2} = 0.3\ Pa$ inside the trap and a reaction time of $t_{reaction} = 1000\ ms$, for an ion trap temperature of $T_{octopole} = 100\ K$ and $T_{octopole} = 300\ K$. Due to the high speed of reaction, in the case of Au_2^- clusters, the mass spectra were recorded for $t_{reaction} = 100\ ms$ at $100\ K$ (Fig. 5.5 (c)) and $t_{reaction} = 500\ ms$ at $300\ K$ (Fig. 5.5 (d)), respectively.

From Fig. 5.5 (a) - (f), it can be seen that no reaction product with oxygen appears for the gold monomer and trimer, while in the case of Au_2^- clusters, only one oxygen

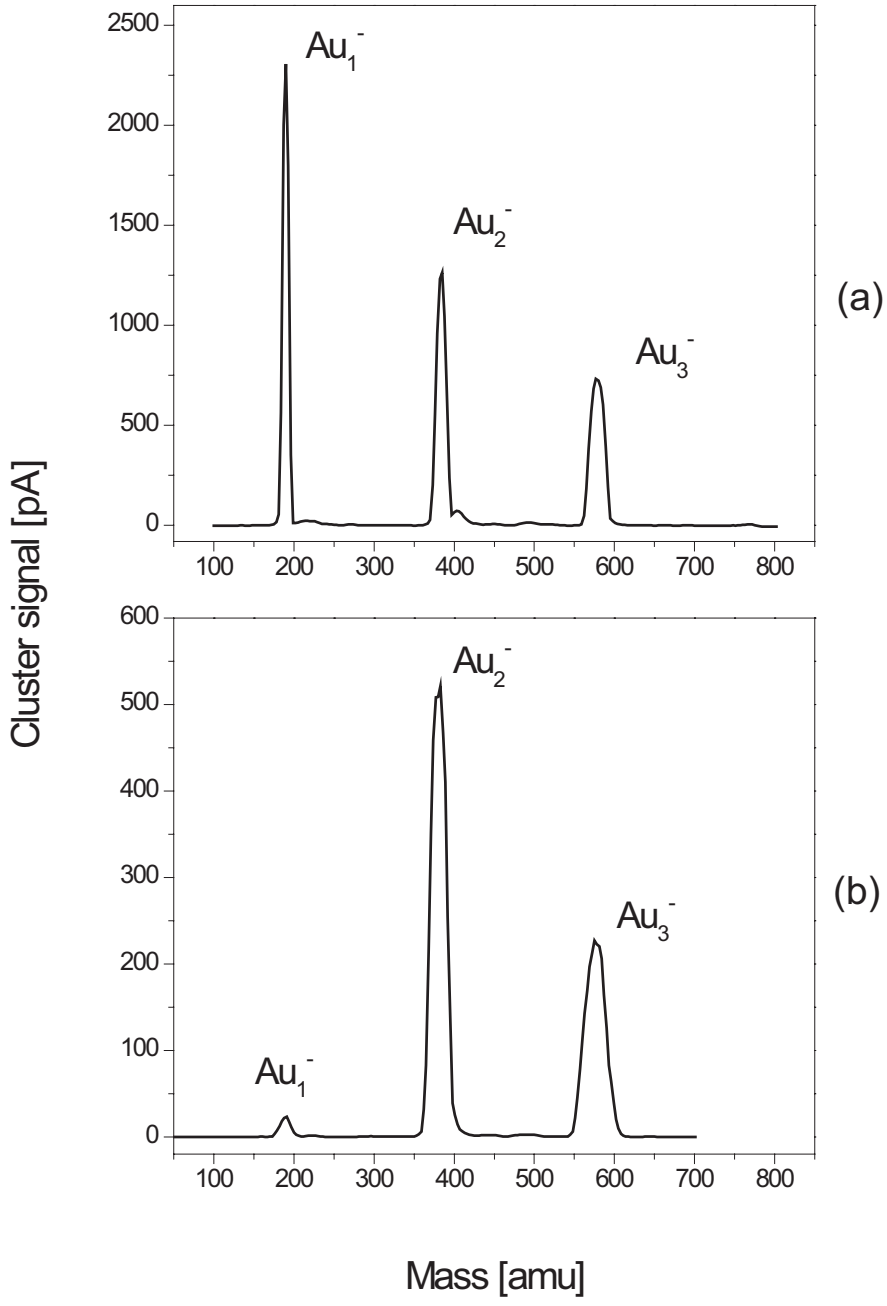

Figure 5.4: Typical mass spectra for negatively charged gold clusters measured after mass selection in Q_1 (see chapter 4, Fig. 4.1). The cluster signal intensity is depicted as a function of cluster mass. (a) Mass spectrum taken after the alignment for maximum intensity of Au_2^- cluster signal. (b) Mass spectrum taken after the alignment for maximum intensity of Au_3^- cluster signal.

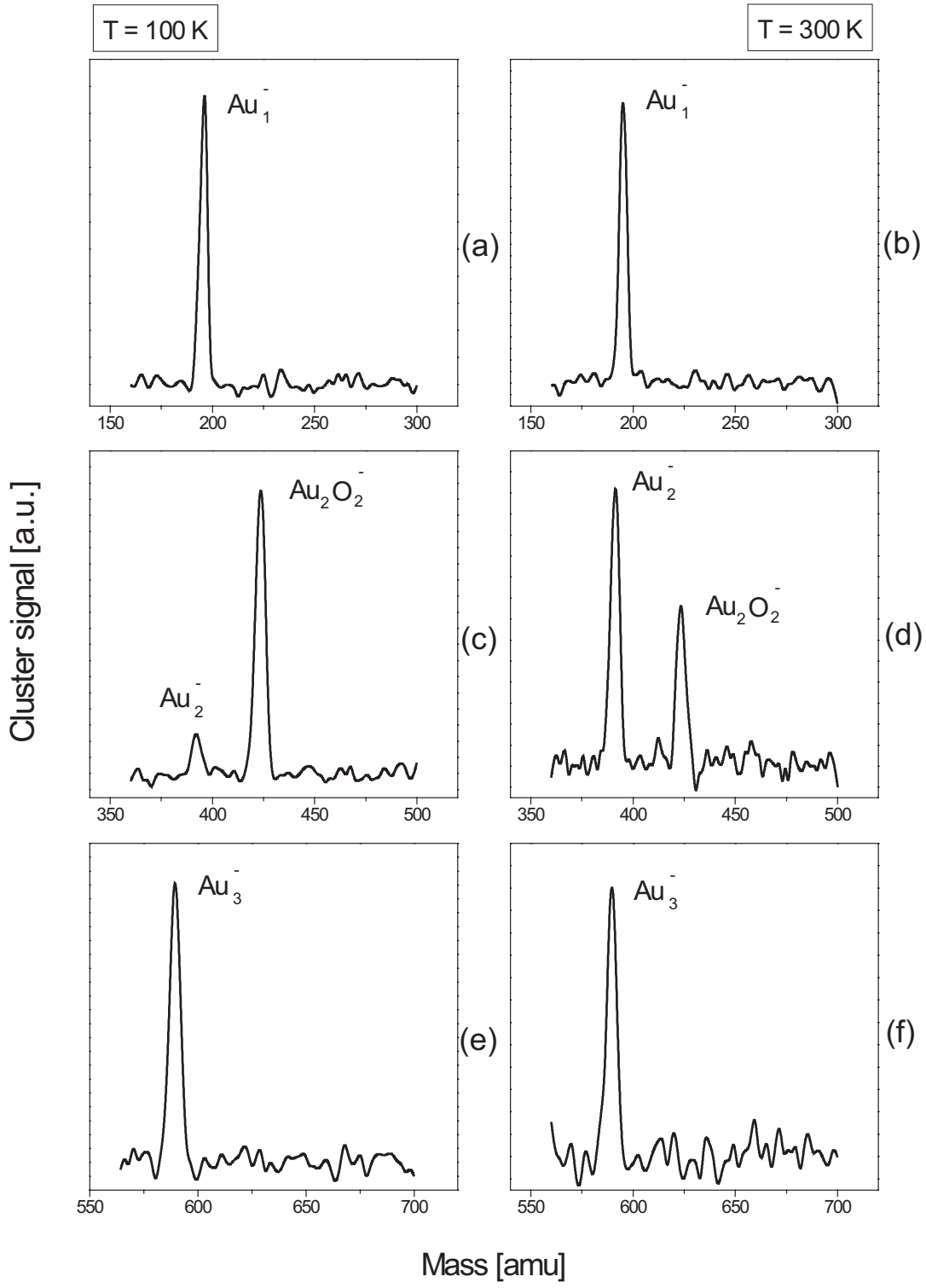

Figure 5.5: Reactivity of Au_1^-, Au_2^- and Au_3^- clusters with oxygen. The reaction parameters are: (a) $p_{He} = 0.94\ Pa$, $p_{O_2} = 0.26\ Pa$, $t_{reaction} = 1000\ ms$, $T_{octopole} = 100\ K$; (b) $p_{He} = 1.01\ Pa$, $p_{O_2} = 0.31\ Pa$, $t_{reaction} = 1000\ ms$, $T_{octopole} = 300\ K$; (c) $p_{He} = 1.00\ Pa$, $p_{O_2} = 0.30\ Pa$, $t_{reaction} = 100\ ms$, $T_{octopole} = 100\ K$; (d) $p_{He} = 1.00\ Pa$, $p_{O_2} = 0.30\ Pa$, $t_{reaction} = 500\ ms$, $T_{octopole} = 300\ K$; (e) $p_{He} = 1.03\ Pa$, $p_{O_2} = 0.32\ Pa$, $t_{reaction} = 1000\ ms$, $T_{octopole} = 100\ K$; (f) $p_{He} = 1.00\ Pa$, $p_{O_2} = 0.30\ Pa$, $t_{reaction} = 1000\ ms$, $T_{octopole} = 300\ K$.

molecule can be adsorbed. Even when the negatively charged gold clusters are stored inside the ion trap for a reaction time of up to 10 seconds, no other reaction product is detected for any investigated ion trap temperature and reactive gas pressure.

The observed odd-even effect in the reactivity of negatively charged gold clusters towards oxygen confirms previous experiments that were carried out at room temperature, where only even-numbered gold anions have been found to react with O_2, adsorbing only one molecule of oxygen and no reaction product was observed for odd-numbered gold anions.[85,111,129] A strong alternating behavior was observed as well in the case of the reactivity of small anionic silver clusters towards oxygen and carbon monoxide. In the experiments performed in the group of Prof. L. Wöste, it was observed that negatively charged silver clusters (Ag_n^-, $n \leq 11$) show an odd-even alternation in the reactivity with oxygen: even numbered clusters adsorb one molecule of oxygen, while odd numbered clusters adsorb two oxygen molecules.[130,131]

The alternating behavior of anionic gold clusters towards the adsorption of oxygen molecules was correlated with the odd-even oscillations in the electron affinity (EA) of anionic gold clusters.[129,132] As described in section 5.1, the binding mechanism of oxygen molecules is based on an electron transfer from the highest occupied molecular orbital (HOMO) of the cluster into one of the antibonding π^* orbitals of the O_2 molecule. The even-numbered negatively charged gold clusters present a low EA and therefore, they can donate more easily an electron to the oxygen ligand than odd-numbered negatively charged gold clusters, which present a higher value for the EA and thus, show no evidence of reactions towards oxygen. In Fig. 5.6, the alternating pattern of the electron affinity for gas-phase gold clusters (Au_n^-, $n = 1-70$) is depicted as a function of cluster size.

Another interesting feature, which can be observed in Fig. 5.5 (c) and (d) is that in the presence of a similar concentration of oxygen in the ion trap, the reaction of Au_2^- clusters with oxygen proceeds faster at low temperature than at room temperature. At an ion trap temperature of 100 K, the Au_2^- cluster signal almost vanishes after 100 ms reaction time and the $Au_2O_2^-$ signal increases significantly, with a ratio of $Au_2^-/Au_2O_2^-$ of 1 : 7. In contrast to this, the ratio of the signal intensities $Au_2^-/Au_2O_2^-$ has a value of 1.7 : 1 at an ion trap temperature of 300 K, after 500 ms reaction time.

In order to deduce the mechanism of the observed reaction of Au_2^- clusters with

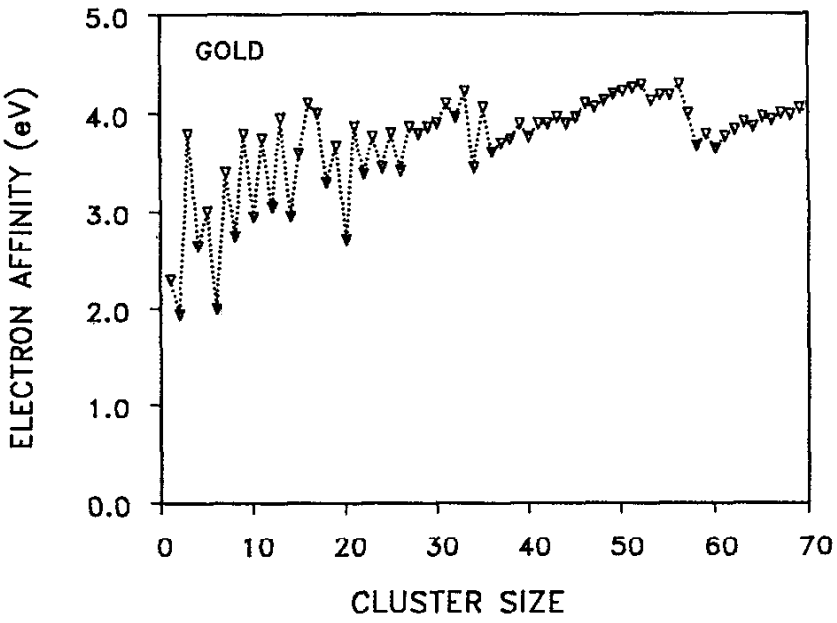

Figure 5.6: The experimental values of the electron affinity (EA) for gold clusters (Au_n^-, $n = 1 - 70$), taken from Taylor *et al.*[132]

O_2, kinetic measurements were performed. As described in section 4.1.3, the analyzed mass was kept constant and the reaction time was varied during this type of experiment. With this method, the time evolution of a reaction educt or product can be monitored. In Fig. 5.7, the kinetic traces for Au_2^- (open triangles) and $Au_2O_2^-$ (open circles) and the sum of the ion signals (filled squares) are shown for a reaction temperature of 300 K. It can be noticed that the sum of the ion signals remains constant during the measurement within the experimental fluctuations. This means that the ions can be stored inside the octopole trap for a reaction time of up to 10 seconds, without significant losses of the total ion signal.

The ion signals for the reaction educts and products are normalized to the total ion signal by using the relation:

$$[X_i]_{normalized} = \frac{[X_i]}{\sum_{j=1}^{j=n}[X_j]} \tag{5.1}$$

where $[X_i]$ represents the ion signal to be normalized and n is the total number of reaction educts and products. The normalization of the cluster signal to the total ion signal was performed for every kinetic measurement.

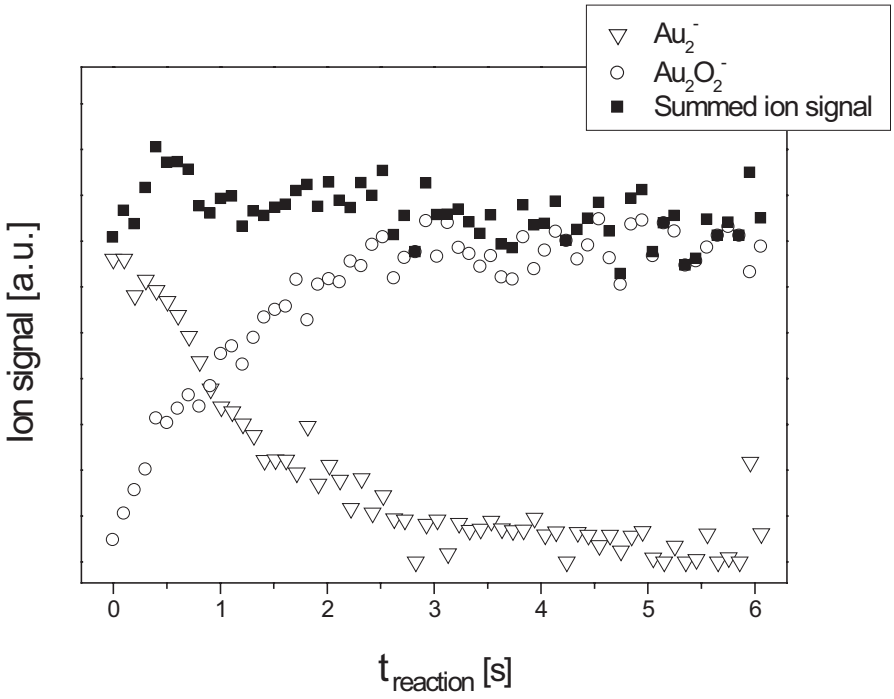

Figure 5.7: Kinetic traces for the reaction of Au_2^- with O_2 at an ion trap temperature of 300 K. The ion signals (open symbols) and the summed signal (filled squares) are depicted as a function of the reaction time. The reaction parameters are: $p_{He} = 1.00\ Pa$, $p_{O_2} = 0.30\ Pa$, $T_{octopole} = 300\ K$.

After the normalization of the signals, the fitting procedure of the kinetic data was performed in order to deduce the reaction mechanism and to calculate the reaction rate constants. The kinetic data were fitted by using the *Detmech* program. This software is a kinetic simulator, which employs an iterative non-linear least-square method for fitting the experimental data. The differential equations of the proposed reaction mechanism are numerically integrated by using the fourth-order Runge-Kutta algorithm.[133] With this fitting procedure the simplest reaction mechanism is searched, *i.e.* a mechanism that describes the experimental data well and contains the lowest possible number of elementary steps. When the simulated product and educt concentrations do not match with the measured data, the proposed reaction mechanism is modified and the procedure is repeated until the simulated data are in good agreement with the experiment. This procedure is very sensitive to the proposed reaction mechanism, *i.e.* a slight modification of the reaction mechanism can lead to

a significant mismatch between simulated and experimental data. For an additional check of the validity of the reaction mechanism obtained from the *Detmech* program, another type of software was used, namely the *Chemical Kinetics Simulator* (IBM, Model *CKS 1.0*), which uses a stochastic algorithm to simulate a chemical reaction.[134] This procedure (normalization and fitting of the measured data) was applied to every kinetic measurement presented in this work.

In Fig. 5.8 (a) - (c), the kinetic traces for the reaction of Au_2^- with O_2 at different reaction temperatures are shown. The normalized ion signals (open symbols) and the simulated signals (solid lines) are represented as a function of the reaction time. From these graphs, it can be observed that the theoretical fit is in very good agreement with the experimental data. As it was already observed from the mass spectra presented in Fig. 5.5, the reaction between Au_2^- and O_2 proceeds faster with decreasing temperature. From Fig. 5.8, it can be seen that at a reaction temperature of 300 K the Au_2^- signal is depleted completely after a reaction time of 5 s, while at a temperature of 100 K, the Au_2^- cluster signal already vanishes after 0.5 s. This observation can be rationalized with the help of the theory of ion-molecule reactions described in section 2.2, where it was shown that ion-molecule reactions that have no activation barrier exhibit a negative temperature dependence.

In the case of the oxidation reaction of Au_2^- clusters, the reaction mechanism is easy to elucidate, since only one oxygen molecule is adsorbed on anionic gold dimers and no other reaction product aside from $Au_2O_2^-$ is detected for the whole investigated temperature and reactive gas pressure range. The reaction mechanism derived from the mass spectra and the kinetic measurements can be written as:

$$Au_2^- + O_2 \quad \rightarrow \quad Au_2O_2^- \qquad\qquad k \tag{5.2}$$

with k as the reaction rate constant. Since the oxygen concentration can be assumed to be constant during the measurements ($[O_2] = \text{const.}$), the reaction of Au_2^- with O_2 can be treated as a pseudo-first-order reaction.[c] Taking into account equation 2.9, the differential rate equations can be written as follows:

$$-\frac{d[Au_2^-]}{dt} = \frac{d[Au_2O_2^-]}{dt} = k^{(2)}[O_2][Au_2^-] = k^{(1)}[Au_2^-] \tag{5.3}$$

[c]The ion concentration is orders of magnitude smaller than the oxygen concentration ($[Au_2^-] \ll [O_2]$)

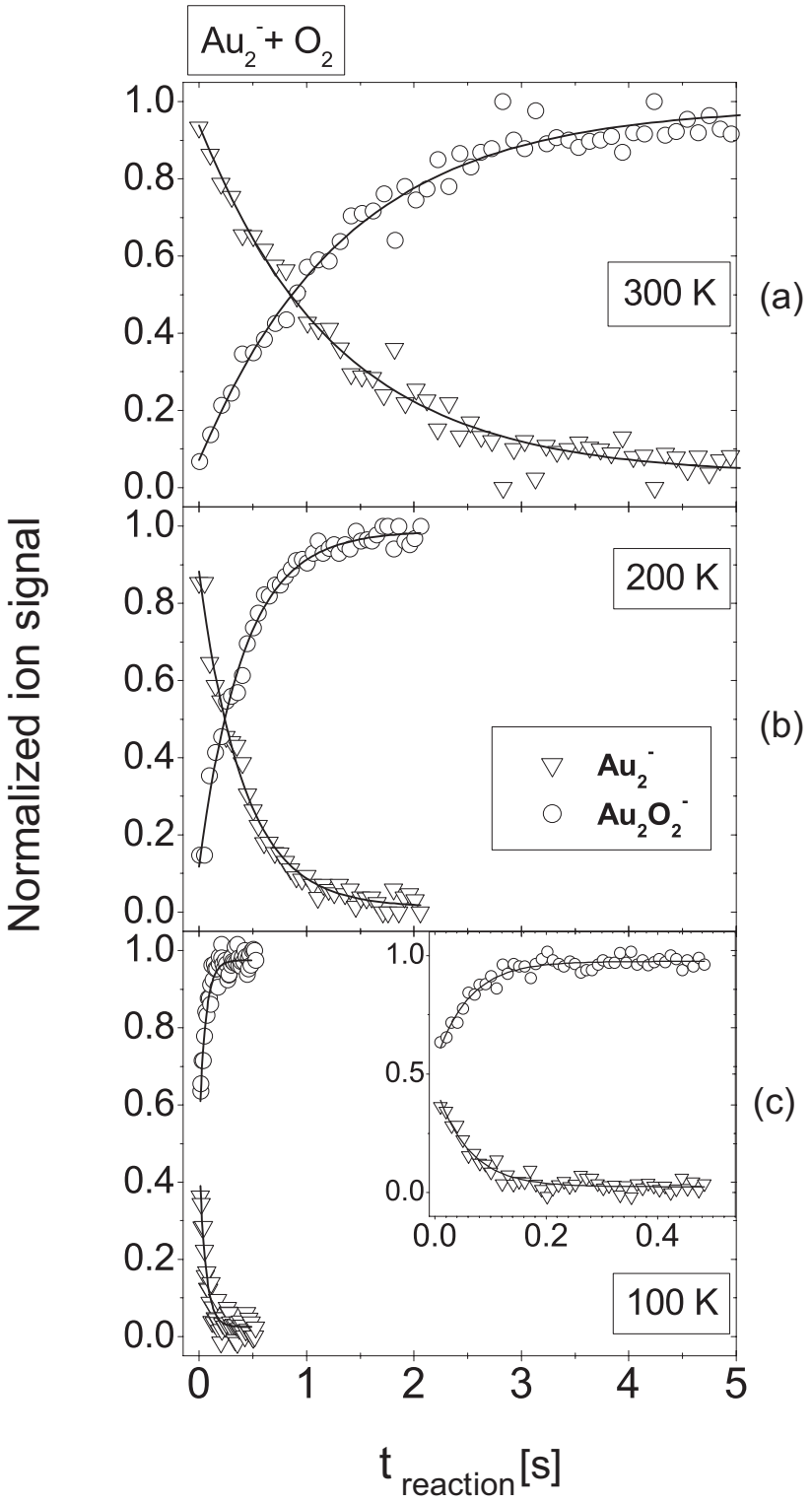

Figure 5.8: Kinetic traces for the reaction of Au_2^- with O_2 at different temperatures. The normalized cluster ion signals (open symbols) and the simulated signals (solid lines) are depicted as a function of the reaction time. The reaction parameters are: (a) $p_{He} = 1.00\ Pa$, $p_{O_2} = 0.30\ Pa$, $T_{octopole} = 300\ K$; (b) $p_{He} = 1.00\ Pa$, $p_{O_2} = 0.30\ Pa$, $T_{octopole} = 200\ K$; (c) $p_{He} = 1.00\ Pa$, $p_{O_2} = 0.30\ Pa$, $T_{octopole} = 100\ K$. The inlet in graph (c) shows the magnified kinetic measurement for the reaction of Au_2^- with O_2 at 100 K.

where $k^{(2)}$ is the second-order rate constant and $k^{(1)}$ is the pseudo-first-order reaction rate constant.

For the reaction of Au_2^- with O_2, the differential rate laws can be solved analytically and the time dependence of the concentration of the reaction product and educt can be obtained:

$$[Au_2^-]_{(t)} = [Au_2^-]_{(0)} \cdot exp\,(-k^{(1)}\,t) \tag{5.4}$$

$$[Au_2O_2^-]_{(t)} = [Au_2^-]_{(0)} \cdot (1 - exp\,(-k^{(1)}\,t)) \tag{5.5}$$

where $[Au_2^-]_{(t)}$ and $[Au_2O_2^-]_{(t)}$ represent the concentration after a given reaction time t, while $[Au_2^-]_{(0)}$ represents the initial concentration of the anionic gold clusters. By employing equations 5.4 and 5.5, the kinetic measurements presented in Fig. 5.8 can be fitted by using an exponential decay for the Au_2^- normalized signal and an exponential growth for the $Au_2O_2^-$ normalized signal, respectively. In order to verify the obtained values for the reaction rate constants, fitting procedures with the *Detmech* program have also been performed and both fitting procedures deliver the same value for the reaction rate constants.

As shown in section 2.2.2, the reaction between cluster anions and molecules, carried out under the experimental conditions for the measurements presented here, can be described by using the Lindemann mechanism, which implies the formation of an intermediate, energetically excited ion-molecule complex (in this case $(Au_2O_2^-)^*$). This excited complex can decompose *via* unimolecular decay back to the reactants if no stabilizing collision with a buffer gas molecule takes place. Thus, in analogy to equation 2.40 and 2.41, the reaction between Au_2^- clusters and O_2 can be reformulated as:

$$Au_2^- + O_2 \rightleftarrows (Au_2O_2^-)^* \qquad k_a,\ k_d \tag{5.6}$$

$$(Au_2O_2^-)^* + He \rightarrow Au_2O_2^- + He^* \qquad k_s \tag{5.7}$$

where k_a, k_d and k_s represent the rate coefficients for the association, decomposition and stabilization processes, respectively. As mentioned in section 2.2.2, the experiments presented in this work are performed in the low-pressure regime of the Lindeman mechanism, where the condition $k_d \gg k_s[He]$ is fulfilled and in this case,

the oxidation reaction is described by the overall third-order reaction rate constant (termolecular reaction rate constant), which has the following form:

$$k^{(3)} = \frac{k_a k_s}{k_d} \tag{5.8}$$

k_a and k_s can be described by using the ion-molecule collision rate coefficients according to the Langevin theory. As shown in section 2.2.1, k_a and k_s are almost independent of cluster size. Furthermore, k_a and k_s do not depend on the reaction temperature. By using the expression 2.32 for the Langevin rate coefficient, k_a and k_s can be calculated for the case of reaction between Au_2^- clusters and O_2 and have the values: $k_a \cong 5.43 \cdot 10^{-10}\ cm^3 s^{-1}$, $k_s \cong 5.23 \cdot 10^{-10}\ cm^3 s^{-1}$. Thus, the temperature and cluster size dependence is contained in the unimolecular decomposition rate coefficient k_d. As shown in section 2.2.3, k_d is obtained from the statistical theories RRK and RRKM.

The measured unimolecular, bimolecular and termolecular reaction rate constants for different reaction temperatures, as well as different oxygen pressures in the case of the reaction between Au_2^- clusters and O_2, are presented in table 5.1. The errors in the unimolecular $k^{(1)}$ constant are mainly due to the uncertainties in the fitting procedure, while the errors for the bimolecular and termolecular rate coefficients $k^{(2)}$ and $k^{(3)}$ are mainly due to the error in the measured gas pressure, which is considered to be $\pm$ 0.01 Pa (the last digit of the measured pressure value that can be read on the manometer display) for all the experiments presented in this work.

The unimolecular rate coefficients ($k^{(1)}$) are extracted directly from the fitted experimental data, while the bimolecular ($k^{(2)}$) and termolecular ($k^{(3)}$) rate coefficients are calculated as:

$$k^{(2)} = \frac{k^{(1)}}{[O_2]} \tag{5.9}$$

$$k^{(3)} = \frac{k^{(1)}}{[He] \cdot [O_2]} = \frac{k^{(2)}}{[He]} \tag{5.10}$$

$[O_2]$ and $[He]$ represent the concentration of the oxygen and helium gas molecules, present in the octopole ion trap for a given reaction temperature T. The gas concentration can be derived from the ideal gas law: $[X] = n/V = p/k_B T$, where n

$\mathbf{T[K]}$	$\mathbf{p_{He}[Pa]}$	$\mathbf{p_{O_2}[Pa]}$	$\mathbf{k^{(1)}[s^{-1}]}$	$\mathbf{k^{(2)}[cm^3s^{-1}]}$	$\mathbf{k^{(3)}[cm^6s^{-1}]}$
100	1.03	0.04	5.52±0.60	$(3.38\pm0.85)\cdot10^{-13}$	$(8.11\pm2.03)\cdot10^{-28}$
150	1.05	0.06	2.49±0.35	$(1.25\pm0.21)\cdot10^{-13}$	$(3.29\pm0.55)\cdot10^{-28}$
190	1.05	0.08	1.13±0.11	$(4.77\pm0.60)\cdot10^{-14}$	$(1.54\pm0.19)\cdot10^{-28}$
200	1.00	0.16	1.38±0.12	$(3.00\pm0.26)\cdot10^{-14}$	$(1.04\pm0.10)\cdot10^{-28}$
300	1.05	0.13	0.62±0.03	$(2.03\pm0.16)\cdot10^{-14}$	$(8.24\pm0.71)\cdot10^{-29}$

Table 5.1: Unimolecular $k^{(1)}$, bimolecular $k^{(2)}$ and termolecular $k^{(3)}$ reaction rate constants for the reaction of Au_2^- clusters with O_2 measured for different ion trap temperatures and different gas pressures.

represent the number of gas molecules, V represents the volume of the gas, p denotes the gas pressure and k_B denotes the Boltzmann constant.

From table 5.1, it can clearly be seen that the values for $k^{(1)}$, $k^{(2)}$ and $k^{(3)}$ rate coefficients decrease with increasing temperature, as it was expected for the case of ion-molecule reactions described in section 2.2.2. For the first time, the negative temperature dependence for the reaction between Au_2^- clusters and O_2 could be experimentally determined and quantitatively described.

By using the expression 5.8 and the values for the termolecular rate coefficients presented in table 5.1, the unimolecular decomposition rate coefficient k_d can be calculated as well as the mean lifetime of the activated complex τ, which is defined as:

$$\tau = \frac{1}{k_d} \tag{5.11}$$

The temperature dependence of k_d and τ is presented in table 5.2. One can notice that k_d increases with increasing temperature, while τ decreases with increasing temperature. For a reaction temperature of 300 K, the activated complex lives about 0.3 ns. Lee *et al.* found a lifetime of about $\tau = (1.4 \pm 0.9)\ ns$ for the $(Au_2O_2^-)^*$ activated complex at 300 K.[85] Taking into account the large error bars in the value given by Lee *et al.*,[85] a good agreement with the values obtained from the experiments presented here is found.

T [K]	$\mathbf{k_d}$ **[s^{-1}]**	τ **[s]**
100	$(3.50 \pm 0.88)\cdot 10^{8}$	$(2.86 \pm 0.72)\cdot 10^{-9}$
150	$(8.63 \pm 1.44)\cdot 10^{8}$	$(1.16 \pm 0.19)\cdot 10^{-9}$
190	$(1.84 \pm 0.23)\cdot 10^{9}$	$(5.43 \pm 0.68)\cdot 10^{-10}$
200	$(2.73 \pm 0.26)\cdot 10^{9}$	$(3.67 \pm 0.35)\cdot 10^{-10}$
300	$(3.45 \pm 0.30)\cdot 10^{9}$	$(2.90 \pm 0.25)\cdot 10^{-10}$

Table 5.2: The unimolecular decomposition rate coefficient k_d and the lifetime τ of the activated complex $(Au_2O_2^-)^*$ calculated as a function of reaction temperature.

By plotting the rate coefficient k_d *versus* the reaction temperature and employing a fitting procedure, which uses the program *Mass Kinetics 1.4*,[135,136] the binding energy of the oxygen molecule on anionic gold dimer can be inferred. The *Mass Kinetics 1.4* program calculates the decomposition rate coefficients k_d by applying the RRKM theory. This program requires the input of the vibrational frequencies of the reaction product, as well as the energy of the activated complex $(Au_2O_2^-)^*$. As described in section 2.2.3, the energy of the activated complex can be calculated by using the model proposed by Cox *et al.*[52] In the case of the activated complex $(Au_2O_2^-)^*$, the energy has the following expression:

$$E(T) = E_0 + 3k_BT \tag{5.12}$$

where $E(T)$ represents the energy of the activated complex $(Au_2O_2^-)^*$ for a given reaction temperature T, E_0 represents the binding energy of the O_2 molecule on Au_2^- clusters and k_B denotes the Boltzmann constant. For the calculation of the activated complex energy, a non-linear geometry of the $(Au_2O_2^-)$ molecule was considered (see Fig. 5.10). The vibrational frequencies of the reaction product $Au_2O_2^-$ are taken from literature.[112,115,137–139] The temperature dependence of the decomposition rate constant k_d is shown in Fig. 5.9. From this graph, it can be seen that the experimental data matches well with the simulated values for a binding energy of $E_{BE}(Au_2O_2^-) = 0.64 \pm 0.10\ eV$ (open circles), while a binding energy of $E_{BE}(Au_2O_2^-) = 0.57\ eV$ (open squares) or $E_{BE}(Au_2O_2^-) = 0.71\ eV$ (open triangles) overestimates and underestimates the measured values, respectively. The

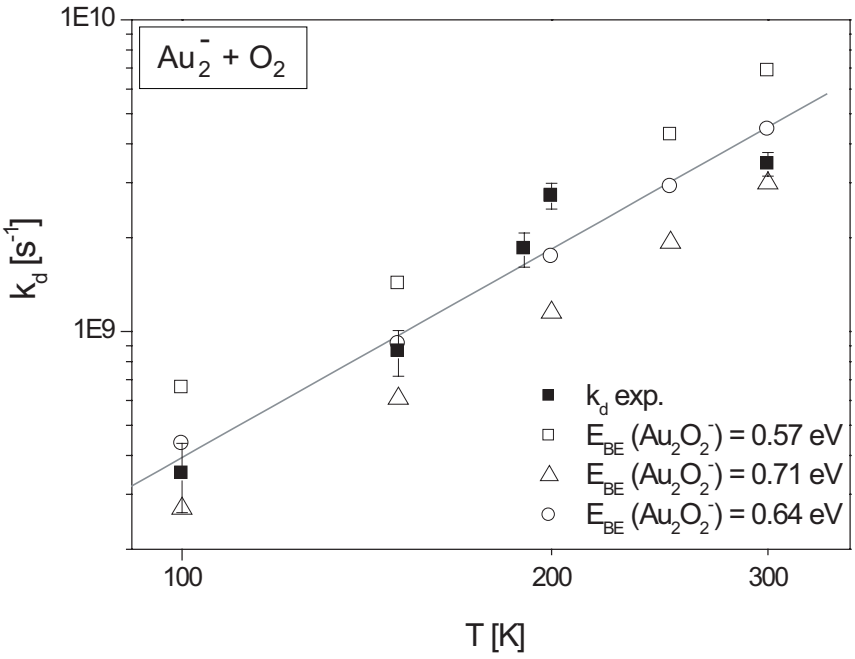

Figure 5.9: Double logarithmic representation of the temperature dependence for the decomposition rate coefficient k_d of the $Au_2O_2^-$ reaction product. The experimental values (filled squares) and the simulated rate coefficients for a binding energy of $E_{BE}(Au_2O_2^-) = 0.57\ eV$ (open squares), $E_{BE}(Au_2O_2^-) = 0.64\ eV$ (open circles) and $E_{BE}(Au_2O_2^-) = 0.71\ eV$ (open triangles) are plotted as a function of temperature. The solid line represents a linear fit of the measured data.

solid line represents a linear fit to the double logarithmic plot of the experimental data and indicates a temperature dependence of the decomposition rate constant $k_d \sim T^{\alpha}$, with $\alpha = 2.22$.

Theoretical calculations based on the density functional theory (DFT) have been performed in order to determine the structure of the $Au_2O_2^-$ reaction complex and the binding energy of the oxygen molecule to the anionic gold dimer.[112,114] It is known that the oxygen molecule presents a variety of activated species and it can be found in a superoxide state (O_2^-) as well as in a peroxide state (O_2^{2-}). As shown in Fig. 5.10, Yoon *et al.* obtained a non-linear structure for $Au_2O_2^-$ cluster in the ground state, with an angle of 115.6° between the Au_2^- cluster and O_2 molecule.[112] The $O-O$ bond length is stretched ($r_{O-O} = 1.34\ \AA$), compared to the bond length of a free oxygen molecule ($r_{O-O} = 1.25\ \AA$). The bonding of the oxygen molecule

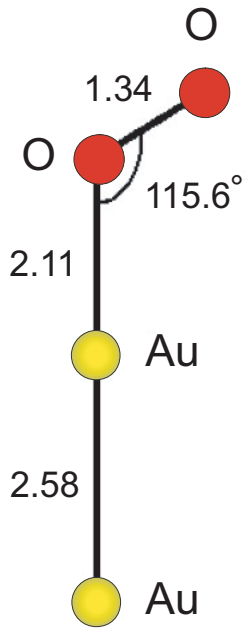

Figure 5.10: Structure of the $Au_2O_2^-$ complex, predicted by DFT theoretical calculations. The bond lengths are given in $\AA$, adapted from Yoon *et al.*[112]

occurs through a charge transfer from the Au_2^- clusters into one of the antibonding π^* orbitals of the oxygen molecule, thus transforming O_2 in a superoxo-like species. According to their calculations, the binding energy of the $Au_2O_2^-$ complex has a value of $E_{BE}(Au_2O_2^-) = 1.39\ eV$. Mills *et al.* performed DFT calculations for the cluster-adsorbate complex $Au_2O_2^-$ as well and obtained a non-linear structure with a binding energy of about $E_{BE}(Au_2O_2^-) = 1.40\ eV$.[114]

From experiments of collision-induced dissociation (CID) performed on $Au_2O_2^-$, a value of about $E_{BE}(Au_2O_2^-) = 1.01\ eV$ is obtained for the binding energy of the oxygen molecule on the gold anionic dimer and according to the authors, this value represents an upper limit for the binding energy of the $Au_2O_2^-$ complex.[140] Recently, Mills *et al.* recalculated the binding energy of the O_2 molecule on Au_2^- clusters and obtained a value of $E_{BE}(Au_2O_2^-) = 1.07\ eV$.[141]

The theoretical calculations performed in the group of Prof. V. Bonačić-Koutecký, based on DFT methods predicted a binding energy of $E_{BE}(Au_2O_2^-) = 1.06\ eV$ for the complex $Au_2O_2^-$.[142] It is important to note that the variation of the employed basis set in these calculations leads to a variation of the oxygen-anionic gold dimer

binding energy in the range of $E_{BE}(Au_2O_2^-) = 0.85\ eV - 1.36\ eV$.[143]

The binding energy of $E_{BE}(Au_2O_2^-) = 0.64\ \pm\ 0.10\ eV$ obtained from the experimental data presented in this work underestimates the bond strength of the $Au_2O_2^-$ complex, compared to other experimental and theoretical data. This could be due to the fact that the statistical RRK and RRKM theories underestimate the complexity of gold-oxygen anionic system. However, this approach still leads to a good qualitative and quantitative description of the experimental data, especially for the temperature dependence of the reaction rate constants.

5.3 Reactions of Gold Anions with *CO*

In order to investigate the catalytic properties of small, negatively charged gold clusters with respect to the oxidation reaction of carbon monoxide, the investigation of the reactive behavior of gas-phase anionic gold clusters towards CO is the next step of the experiment and will be presented in detail in this section.

As in the case of the anionic gold cluster reactivity studies towards oxygen, the reactivity of negatively charged gold clusters (Au_1^-, Au_2^-, Au_3^-) with carbon monoxide was systematically investigated for different ion trap temperatures, as well as different pressures of the reactive gas.[144] In Fig. 5.11, the product ion mass spectra for the reactivity of Au_1^-, Au_2^- and Au_3^- with CO are shown. It is important to note that no reaction products of the anionic gold monomer, dimer and trimer with carbon monoxide are detected at room temperature, even for storage times of the ions inside the trap of up to 10 or even 15 seconds.

From Fig. 5.11 (a), it can be clearly seen that no reaction product with CO is detected over the entire investigated temperature range ($100\ K - 300\ K$) in the case of Au_1^-. For Au_2^- clusters, the formation of mono-carbonyl (Au_2CO^-) and di-carbonyl ($Au_2(CO)_2^-$) complexes can be observed for a reaction temperature of $100\ K$ (Fig. 5.11 (b)). The increase of the ion trap temperature leads to a decrease in the intensity of the observed carbonyl complexes, so that no adsorption of CO molecules onto Au_2^- clusters can be detected at a temperature of $250\ K$ (Fig. 5.11 (c)). Similar to the case of gold dimers, the adsorption of two carbon monoxide molecules can be observed at low temperatures for Au_3^- clusters and the reaction products Au_3CO^-, $Au_3(CO)_2^-$ are detected (Fig. 5.11 (d)). An interesting feature in the case

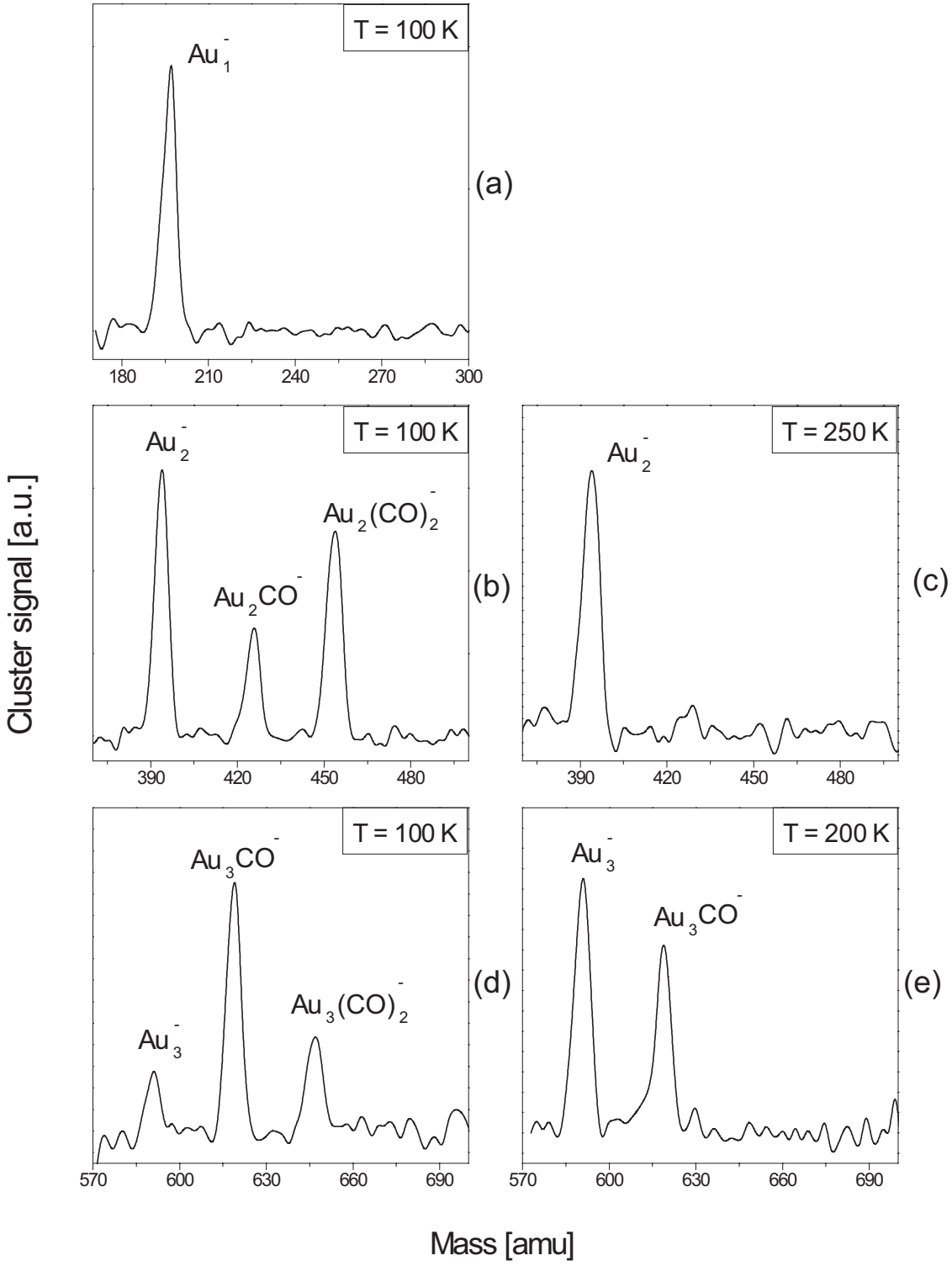

Figure 5.11: Reactivity of negatively charged gold clusters Au_1^-, Au_2^- and Au_3^- with CO. The reaction parameters are: (a) $p_{He} = 1.02\ Pa$, $p_{CO} = 0.28\ Pa$, $t_{reaction} = 1000\ ms$, $T_{octopole} = 100\ K$; (b) $p_{He} = 0.96\ Pa$, $p_{CO} = 0.24\ Pa$, $t_{reaction} = 1000\ ms$, $T_{octopole} = 100\ K$; (c) $p_{He} = 1.04\ Pa$, $p_{CO} = 0.25\ Pa$, $t_{reaction} = 2000\ ms$, $T_{octopole} = 250\ K$; (d) $p_{He} = 1.03\ Pa$, $p_{CO} = 0.02\ Pa$, $t_{reaction} = 500\ ms$, $T_{octopole} = 100\ K$; (e) $p_{He} = 1.05\ Pa$, $p_{CO} = 0.12\ Pa$, $t_{reaction} = 1000\ ms$, $T_{octopole} = 200\ K$.

of negatively charged gold trimers is that at 200 K only one CO molecule is adsorbed and no $Au_3(CO)_2^-$ product can be detected (Fig. 5.11 (e)). These findings are in good agreement with other experimental works, where a very poor reactivity or no reactivity of the gold monomer, dimer and trimer towards carbon monoxide were detected.[85,86,145]

The reaction mechanism of small, negatively charged gold clusters towards CO can be established by performing kinetic measurements in which the reactant and the product ion concentrations are recorded as a function of reaction time. The resulting kinetic traces for the reaction of Au_2^- and Au_3^- clusters towards CO at different reaction temperatures are presented in Fig. 5.12 and Fig. 5.13, respectively. The normalized ion signal (open symbols) and the fitted signal (solid lines) are shown as a function of the reaction time. The fit of the experimental signals is obtained by using the *Detmech* program.[133]

One can observe that the kinetic traces of the gold dimer and trimer have a strikingly different appearance. In both cases, the gold cluster signal shows an exponential decay but the carbonyl complexes present a totally different evolution as a function of the reaction time. In the case of Au_2^- clusters, the carbonyl complexes Au_2CO^- and $Au_2(CO)_2^-$ appear simultaneously and reach an equilibrium after a reaction time of about 5 seconds, at a reaction temperature of 100 K. From Fig. 5.12, it can be seen that the reaction of Au_2^- clusters with CO proceeds faster with decreasing temperature. Furthermore, the equilibrium between Au_2CO^- and $Au_2(CO)_2^-$ products is reached after a longer reaction time at higher temperatures (more than 10 seconds for an ion trap temperature of 200 K). In the case of Au_3^- clusters, the Au_3CO^- product appears first and can be undoubtedly identified as an intermediate complex of the reaction, since its concentration at longer reaction times decreases, while the concentration of the $Au_3(CO)_2^-$ product increases slowly. As in the case of Au_2^- clusters, the reaction proceeds faster with decreasing temperature. The concentration of the di-carbonyl complex $Au_3(CO)_2^-$ decreases as the reaction temperature is increased, so that only the monocarbonyl complex Au_3CO^- can be detected at an ion trap temperature of 200 K. This behavior can be seen in Fig. 5.13.

The kinetic measurements are fitted by using the *Detmech* software,[133] as described previously in section 5.2. The simulated concentrations are plotted in Fig. 5.12 and Fig. 5.13 as solid lines. It is important to note that the same reaction mechanism

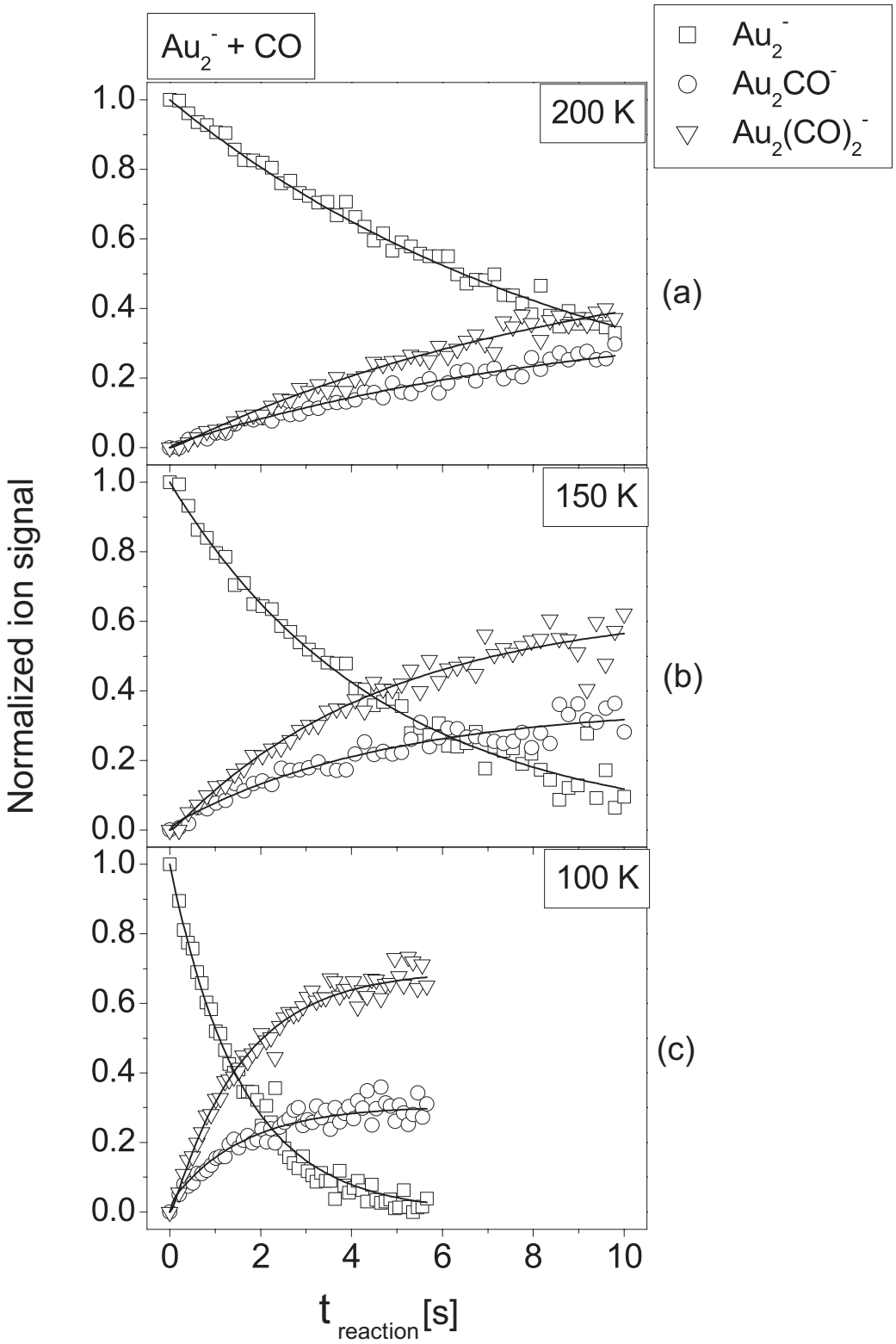

Figure 5.12: Kinetic traces of the reaction of Au_2^- clusters with CO at different temperatures. The normalized ion signals (open symbols) and the simulated signals (solid lines) are shown as a function of the reaction time. The reaction parameters are: (a) $p_{He} = 1.04\ Pa$, $p_{CO} = 0.25\ Pa$, $T_{octopole} = 200\ K$; (b) $p_{He} = 1.04\ Pa$, $p_{CO} = 0.25\ Pa$, $T_{octopole} = 150\ K$; (c) $p_{He} = 0.96\ Pa$, $p_{CO} = 0.24\ Pa$, $T_{octopole} = 100\ K$.

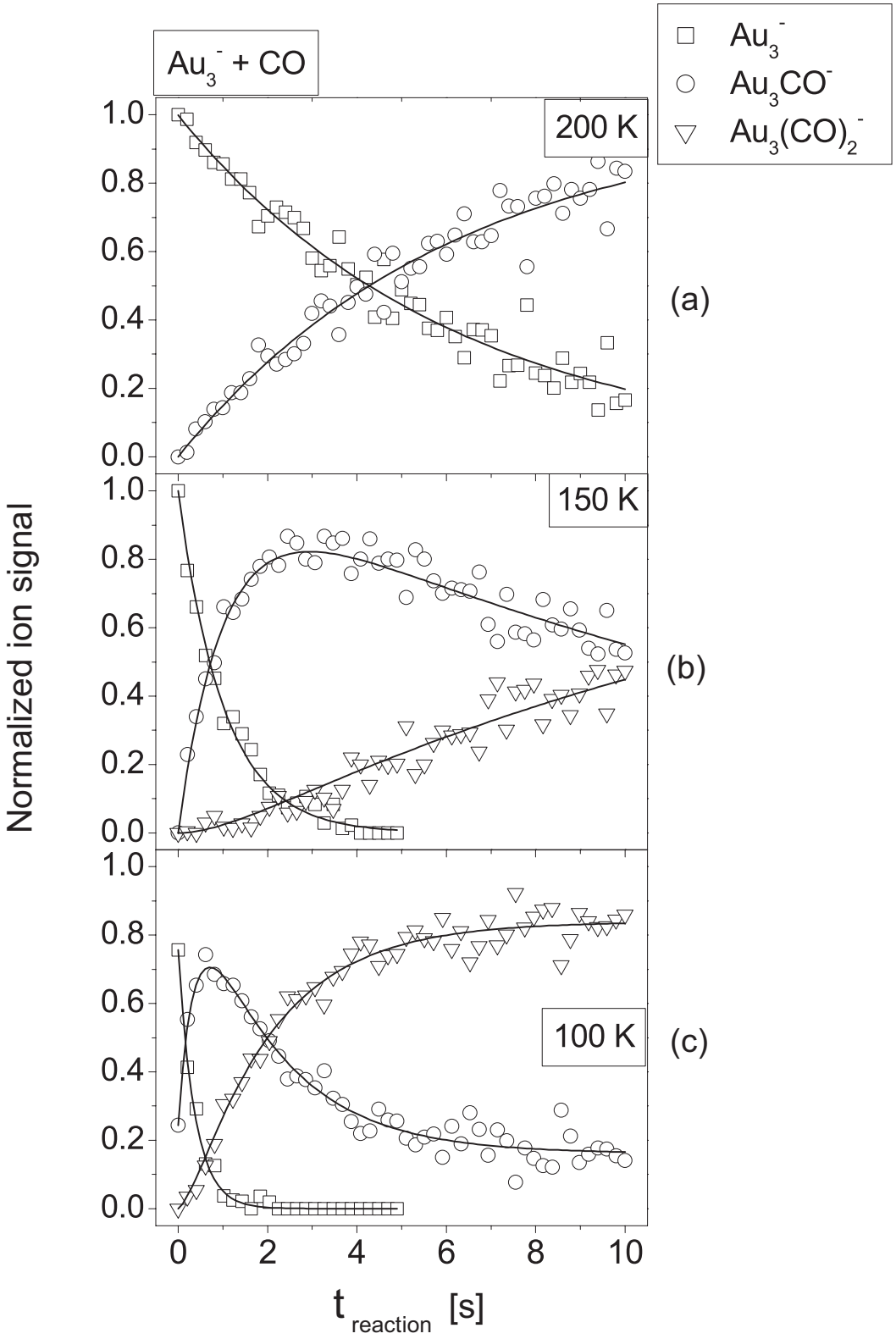

Figure 5.13: Kinetic traces of the reaction of Au_3^- clusters with CO at different temperatures. The normalized ion signals (open symbols) and the simulated signals (solid lines) are shown as a function of the reaction time. The reaction parameters are: (a) $p_{He} = 1.03\ Pa$, $p_{CO} = 0.04\ Pa$, $T_{octopole} = 200\ K$; (b) $p_{He} = 0.99\ Pa$, $p_{CO} = 0.03\ Pa$, $T_{octopole} = 150\ K$; (c) $p_{He} = 1.03\ Pa$, $p_{CO} = 0.02\ Pa$, $T_{octopole} = 100\ K$.

yields the best fit for the measured kinetics in the case of Au_2^- as well as Au_3^- clusters. This mechanism involves a sequential adsorption of carbon monoxide molecules on gold clusters, with Au_nCO^- complex as an intermediate product. The reaction mechanism is described by the following equations:

$$Au_n^- + CO \rightarrow Au_nCO^- \qquad k_1 \tag{5.13}$$

$$Au_nCO^- + CO \leftrightarrows Au_n(CO)_2^- \qquad k_2,\ k_{-2} \tag{5.14}$$

where k_1, k_2 and k_{-2} represent the reaction rates for the different reaction steps and $n = 2,\ 3$.

The fitting procedure is very sensitive to the proposed reaction mechanism. Interestingly, purely consecutive reaction steps, do not fit the experimental data. A good example for the fit quality is given in Fig. 5.14, where the reaction between Au_3^- clusters and CO is fitted without the backward reaction step in expression 5.14.

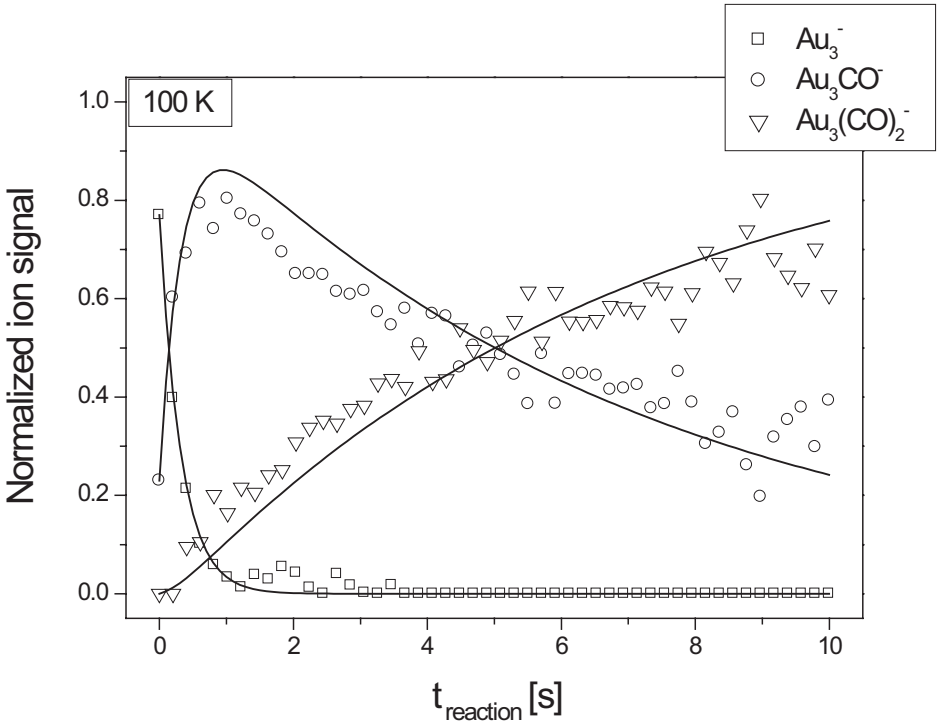

Figure 5.14: Kinetic traces (open symbols) for the reaction of Au_3^- clusters with CO at 100 K. The fitting procedure consists of purely consecutive CO adsorption processes, without the final equilibrium step. The fitted ion signals are depicted as solid lines.

From this figure, it can be observed that the simulated signals do not match the experimental data and thus, the validity of the reaction mechanism described by the expressions 5.13 and 5.14 can be confirmed. The test of the reaction mechanism validity (Fig. 5.14) shows that the reversible adsorption of the second CO molecule (the equilibrium step in expression 5.14) must be taken into account for a good description of the experimental data.

For the reaction of Au_2^- clusters with carbon monoxide, the unimolecular reaction rate coefficients for different reaction temperatures and different concentrations of the reactive gas obtained by fitting the experimental data are presented in table 5.3.

T [K]	$\mathbf{p_{He}}$ **[Pa]**	$\mathbf{p_{CO}}$ **[Pa]**	$\mathbf{k_1^{(1)}}$ **[s^{-1}]**	$\mathbf{k_2^{(1)}}$ **[s^{-1}]**	$\mathbf{k_{-2}^{(1)}}$ **[s^{-1}]**
100	0.96	0.24	0.64 ± 0.14	13.45 ± 2.96	5.89 ± 1.30
150	1.04	0.25	0.21 ± 0.04	8.22 ± 1.56	4.59 ± 0.87
200	1.04	0.25	0.11 ± 0.02	6.88 ± 1.24	4.61 ± 0.83

Table 5.3: $Au_2^- + CO$: the unimolecular rate coefficients $k_1^{(1)}$, $k_2^{(1)}$ and $k_{-2}^{(1)}$ for different reaction temperatures.

Since the experiments are performed in the kinetic low-pressure regime, stabilizing or activating collisions have to be considered in the elementary reaction steps, according to the Lindemann mechanism. Thus, every CO adsorption in the expressions 5.13 and 5.14 involves the formation of an activated complex $(Au_n(CO)_m^-)^*$ with $n = 2,\ 3$ and $m = 1,\ 2$, which can be stabilized through collisions with helium molecules or can decompose back to the reactants, as described in section 5.2. This leads to an overall third-order reaction rate constant for the description of each CO adsorption process ($k_1^{(3)}$ and $k_2^{(3)}$).

Similar to the case of the reaction of negatively charged gold clusters towards oxygen, the bimolecular and termolecular reaction rate constants $k_1^{(2)}$, $k_2^{(2)}$, $k_1^{(3)}$ and $k_2^{(3)}$ are calculated by using the expressions:

$$k_x^{(2)} = \frac{k_x^{(1)}}{[CO]} \tag{5.15}$$

$$k_x^{(3)} = \frac{k_x^{(1)}}{[He]\cdot[CO]} = \frac{k_x^{(2)}}{[He]} \tag{5.16}$$

where $x = 1,\ 2$. The exception is the backward reaction step in expression 5.14, where a Lindemann mechanism for unimolecular decomposition reactions has to be considered. This results in an overall bimolecular rate constant ($k_{-2}^{(2)}$), which can be calculated as:

$$k_{-2}^{(2)} = \frac{k_{-2}^{(1)}}{[He]} \tag{5.17}$$

The equilibrium rate constant K_{eq} for the adsorption and desorption process of the second CO molecule on negatively charged gold dimers and trimers (described by expression 5.14), is given by the following expression:

$$K_{eq} = \frac{k_2^{(2)}}{k_{-2}^{(2)}} \tag{5.18}$$

The bimolecular and termolecular reaction rate coefficients $k_1^{(2)}$, $k_2^{(2)}$, $k_{-2}^{(2)}$, $k_1^{(3)}$ and $k_2^{(3)}$ as well as the equilibrium rate constant K_{eq} for the reaction of Au_2^- clusters with carbon monoxide are shown in table 5.4 and 5.5. The errors in the rate constants presented in tables 5.3 - 5.5 are primarily due to the uncertainties in the fitting procedure. These errors are estimated by fitting the experimental data with *CKS 1.0* software[134] and the obtained error values are at least one order of magnitude higher than the errors due to the uncertainties in the measured gas pressure.

The unimolecular rate coefficients for the reaction of Au_3^- clusters with CO are presented in table 5.6. As in the case of Au_2^- clusters, the bimolecular and the

T[K]	$\mathbf{k_1^{(2)}[cm^3s^{-1}]}$	$\mathbf{k_2^{(2)}[cm^3s^{-1}]}$	$\mathbf{k_{-2}^{(2)}[cm^3s^{-1}]}$	K_{eq}
100	$(0.66 \pm 0.15)\cdot10^{-14}$	$(13.76 \pm 3.03)\cdot10^{-14}$	$(1.51 \pm 0.33)\cdot10^{-14}$	9.11
150	$(0.25 \pm 0.05)\cdot10^{-14}$	$(9.94 \pm 1.89)\cdot10^{-14}$	$(1.33 \pm 0.25)\cdot10^{-14}$	7.47
200	$(0.15 \pm 0.03)\cdot10^{-14}$	$(4.79 \pm 0.86)\cdot10^{-14}$	$(1.54 \pm 0.28)\cdot10^{-14}$	3.11

Table 5.4: $Au_2^- + CO$: the bimolecular rate coefficients $k_1^{(2)}$, $k_2^{(2)}$ and $k_{-2}^{(2)}$, as well as the equilibrium rate constant K_{eq} for different reaction temperatures.

T [K]	p_{He} [Pa]	p_{CO} [Pa]	$k_1^{(3)}$ [$cm^6 s^{-1}$]	$k_2^{(3)}$ [$cm^6 s^{-1}$]
100	0.96	0.24	$(1.69 \pm 0.37) \cdot 10^{-29}$	$(35.33 \pm 7.77) \cdot 10^{-29}$
150	1.04	0.25	$(0.72 \pm 0.14) \cdot 10^{-29}$	$(28.75 \pm 5.46) \cdot 10^{-29}$
200	1.04	0.25	$(0.51 \pm 0.09) \cdot 10^{-29}$	$(16.03 \pm 2.89) \cdot 10^{-29}$

Table 5.5: $Au_2^- + CO$: the termolecular rate coefficients $k_1^{(3)}$ and $k_2^{(3)}$ for different reaction temperatures.

termolecular reaction rate constants are calculated by using the expressions 5.15 - 5.16. Tables 5.7 and 5.8 show the values for the bimolecular and termolecular rate constants for the reaction of Au_3^- clusters with CO. In the case of the reaction of Au_3^- clusters towards carbon monoxide, the errors of the rate constants k_1 and k_2 shown in tables 5.7 - 5.8 are mainly due to the uncertainties in the gas pressure measurement, which has a value of $\pm$ 0.01 Pa, while the errors for k_{-2} rate coefficient are primarily the result of the uncertainties in the fitting procedure.

From tables 5.3 - 5.8, it can be observed that all rate constants show a negative temperature dependence, which is an indication of a barrierless reaction. The exception is the k_{-2} rate coefficient for the reaction of Au_2^- clusters with CO, which does not exhibit a clear dependence on the reaction temperature. In the case of the reaction between Au_2^- clusters and CO (table 5.5), the reaction rate constant $k_2^{(3)}$ is one order of magnitude larger than $k_1^{(3)}$. This shows that the adsorption of the

T [K]	p_{He} [Pa]	p_{CO} [Pa]	$k_1^{(1)}$ [s^{-1}]	$k_2^{(1)}$ [s^{-1}]	$k_{-2}^{(1)}$ [s^{-1}]
100	1.03	0.02	2.69 ± 1.35	0.45 ± 0.23	0.09 ± 0.02
150	0.99	0.03	0.98 ± 0.33	0.06 ± 0.02	0.01 ± 0.002
200	1.03	0.04	0.15 ± 0.04	-	-

Table 5.6: $Au_3^- + CO$: the unimolecular rate coefficients k_1, k_2 and k_{-2} for different reaction temperatures.

T[K]	$\mathbf{k_1^{(2)}[cm^3s^{-1}]}$	$\mathbf{k_2^{(2)}[cm^3s^{-1}]}$	$\mathbf{k_{-2}^{(2)}[cm^3s^{-1}]}$	K_{eq}
100	$(33.04 \pm 16.52)\cdot10^{-14}$	$(5.54 \pm 2.77)\cdot10^{-14}$	$(0.21 \pm 0.05)\cdot10^{-15}$	26.38
150	$(9.87 \pm 3.26)\cdot10^{-14}$	$(0.60 \pm 0.20)\cdot10^{-14}$	$(0.03 \pm 0.01)\cdot10^{-15}$	20.00
200	$(1.31\pm 0.33)\cdot10^{-14}$	-	-	

Table 5.7: $Au_3^- + CO$: the bimolecular rate coefficients $k_1^{(2)}$, $k_2^{(2)}$ and $k_{-2}^{(2)}$, as well as the equilibrium rate constant K_{eq} for different reaction temperatures.

T [K]	$\mathbf{p_{He}}$ **[Pa]**	$\mathbf{p_{CO}}$ **[Pa]**	$\mathbf{k_1^{(3)}}$ $\mathbf{[cm^6s^{-1}]}$	$\mathbf{k_2^{(3)}}$ $\mathbf{[cm^6s^{-1}]}$
100	1.03	0.02	$(79.09 \pm 39.55)\cdot10^{-29}$	$(13.26 \pm 6.63)\cdot10^{-29}$
150	0.99	0.03	$(29.96 \pm 9.89)\cdot10^{-29}$	$(1.82 \pm 0.60)\cdot10^{-29}$
200	1.03	0.04	$(4.44 \pm 1.11)\cdot10^{-29}$	-

Table 5.8: $Au_3^- + CO$: the termolecular rate coefficients $k_1^{(3)}$ and $k_2^{(3)}$ for different reaction temperatures.

second CO molecule on Au_2^- clusters proceeds faster than the adsorption of the first CO molecule. Thus, for the reaction of anionic gold dimer with carbon monoxide, the rate determining step is the adsorption of the first CO molecule.

By comparing the termolecular reaction rates for the anionic gold dimer and trimer (table 5.5 and 5.8), it can be observed that $k_1^{(3)}$ is about one order of magnitude larger in the case of Au_3^- clusters than for Au_2^- clusters. This result shows that the reaction of Au_3^- clusters with carbon monoxide occurs on a much faster time scale than the reaction of Au_2^- clusters with CO. Leuchtner *et al.* measured the gas-phase reactivity of positively charged copper clusters (Cu_n^+, $n = 1 - 14$) towards carbon monoxide and observed an increase of almost four orders of magnitude in the reaction rate coefficient going from the monomer to the heptamer.[32] This significant increase in the reaction rate coefficient was related to the number of internal degrees of freedom, which increases with the cluster size. Since the excess energy released during the adsorption of a CO molecule has to be accommodated by the reaction complex,

an increase in the number of the degrees of freedom facilitates the internal energy redistribution and lowers the dissociation probability. Similar to the case of positive copper clusters, the experiments presented here reflect the important relation between the product formation rate and the possibility of intracluster energy redistribution, which is reflected in the number of internal vibrational degrees of freedom. The dimer has only one vibrational mode, whereas the trimer possesses three internal degrees of freedom. This means that the adsorption energy of the first CO molecule can be more efficiently redistributed in Au_3^- than in Au_2^- clusters.

As mentioned previously, although the kinetic traces for the reaction of the negative gold dimer and trimer with carbon monoxide (Fig. 5.12 and Fig. 5.13) appear clearly dissimilar, they can be described by the same reaction mechanism (expressions 5.13 and 5.14). By comparing the values of $k_{-2}^{(2)}$ for the gold dimer and trimer (table 5.4 and 5.7) it can be seen that the desorption of the second CO molecule (the backward reaction step in expression 5.14) is one order of magnitude faster for Au_2^- clusters than in the case of Au_3^- clusters. This is further illustrated in the values of the equilibrium rate constant K_{eq} for the adsorption and desorption of the second CO molecule on anionic gold clusters, presented in tables 5.4 and 5.7. From these tables, it can be observed that at a reaction temperature of 100 K, the equilibrium is located by a factor of almost 3 more on the side of the final product $Au_3(CO)_2^-$ in comparison to the case of $Au_2(CO)_2^-$ reaction product. This points towards a significantly higher stability of $Au_3(CO)_2^-$ product in comparison to all other investigated carbonyl compounds. Thus, the dissimilarities in the kinetic traces result from the differences in the equilibrium between the Au_nCO^- and $Au_n(CO)_2^-$ ($n = 2,\ 3$) carbonyl complexes.

An enhanced stability of certain gold carbonyl complexes was already observed experimentally. Nygren *et al.* found a particular stability for the complexes Au_7CO^+ and $Au_{19}CO^+$.[146] If the CO molecule is considered as two electron donor (according to the Blyholder model[127]) and taking into account one s valence electron per gold atom, the stable carbonyl complexes correspond to a total valence electron number of 8 and 20, respectively. Similarly stable structures for anionic gold-carbonyl compounds were determined experimentally by Wallace *et al.*[145] They observed peaks with an unusually high intensity which correspond to the products Au_5CO^- as well as $Au_{15}(CO)_2^-$. By employing the same simple electron counting scheme, the total

number of valence electrons for these gold carbonyl compounds is 8 and 20, respectively. These findings were correlated with electronic shell closing known from the *jellium model* proposed for bare clusters which predicts electronic shell closing for 2, 8, 20, etc. valence electrons and implicitly large stabilities of the corresponding clusters.[110,147] In this picture, the $Au_3(CO)_2^-$ product would correspond to a stable 8 valence electron complex which could explain the low value of the $k_{-2}^{(2)}$ reaction rate for the decomposition of this complex. However, recent theoretical calculations performed by Häkkinen *et al.* emphasize the importance of $s-d$ hybridization due to relativistic effects in gold clusters.[126] According to these authors, the role of the d-electrons on the bonding in gold carbonyl complexes should not be neglected and an explanation based on s-electron counting model is not justified. The elucidation of the origin of the observed stability of $Au_3(CO)_2^-$ product will therefore rely on future detailed *ab initio* calculations.

In the following, the discussion will focus on the adsorption of the first CO molecule on negative gold dimer and trimer. It was mentioned previously, that the adsorption of a CO molecule involves the formation of an activated complex, which can decompose back to reactants or can be stabilized through collision with a helium molecule. Schematically, this process can be written as:

$$Au_n^- + CO \leftrightarrows (Au_nCO^-)^* \qquad k_a,\ k_d \tag{5.19}$$

$$(Au_nCO^-)^* + He \rightarrow Au_nCO^- \qquad k_s \tag{5.20}$$

where $n = 2,\ 3$. k_a, k_d and k_s represents the reaction rate coefficients for the association, decomposition and stabilization processes, respectively. As shown by equation 5.8 in section 5.2, by using the termolecular rate constants, the decomposition rate coefficient k_d of the activated complex ($(Au_n(CO)^-)^*$, $n = 2,\ 3$) can be calculated as:

$$k_d = \frac{k_a k_s}{k_1^{(3)}} \tag{5.21}$$

Since CO is a polar molecule, k_a and k_s can be described by ion-dipole and ion-induced dipole collision rate coefficients according to Langevin theory, presented in section 2.2.1. k_s can be derived from equation 2.32 and in the case of gold dimer has the value $k_s(Au_2^-) = 5.26 \cdot 10^{-10}\ cm^3 s^{-1}$, while a value of $k_s(Au_3^-) = 5.25 \cdot 10^{-10}\ cm^3 s^{-1}$ is obtained for the gold trimer. k_a can be calculated by using

the parametrization of Su and Chesnavich[38] for the reaction between an ion and a dipolar molecule, illustrated in the equations 2.37, 2.38 and 2.39, where k_a represents the capture rate constant $k_{cap}(T)$. As shown in section 2.2.1, $k_{cap}(T)$ depends on the reaction temperature T as well as on the Langevin reaction rate k_L, which has the value $k_L(Au_2^-) = 6.39 \cdot 10^{-10}\ cm^3s^{-1}$ for the reaction of negative gold dimer with CO and $k_L(Au_3^-) = 6.32 \cdot 10^{-10}\ cm^3s^{-1}$ in the case of the gold trimer. Since $x = 1/\sqrt{T_R} = \mu_D/(2\alpha k_B T)^{1/2} < 2$ (from equation 2.37), according to the model proposed by Su and Chesnavich,[38] only the expression 2.39 will be utilized for the calculation of the association rate coefficient k_a. The values for the association rate constant in the case of gold dimer ($k_a(Au_2^-)$) and gold trimer ($k_a(Au_3^-)$) as a function of reaction temperature are presented in table 5.9.

T [K]	$\mathbf{k_a(Au_2^-)[cm^3s^{-1}]}$	$\mathbf{k_a(Au_3^-)[cm^3s^{-1}]}$
100	$6.83 \cdot 10^{-10}$	$6.75 \cdot 10^{-10}$
150	$6.72 \cdot 10^{-10}$	$6.65 \cdot 10^{-10}$
200	$6.67 \cdot 10^{-10}$	$6.60 \cdot 10^{-10}$

Table 5.9: The association rate coefficients for the formation of the activated complexes $(Au_2CO^-)^*$ ($k_a(Au_2^-)$) and $(Au_3CO^-)^*$ ($k_a(Au_3^-)$).

T [K]	$\mathbf{k_d(Au_2^-)[s^{-1}]}$	$\tau(\mathbf{Au_2^-})$**[s]**	$\mathbf{k_d(Au_3^-)[s^{-1}]}$	$\tau(\mathbf{Au_3^-})$**[s]**
100	$(2.13\pm0.47)\cdot10^{10}$	$(4.69\pm1.03)\cdot10^{-11}$	$(0.45\pm0.23)\cdot10^{9}$	$(22.22\pm11.11)\cdot10^{-10}$
150	$(4.91\pm0.93)\cdot10^{10}$	$(2.04\pm0.39)\cdot10^{-11}$	$(1.17\pm0.39)\cdot10^{9}$	$(8.55\pm2.82)\cdot10^{-10}$
200	$(6.88\pm1.24)\cdot10^{10}$	$(1.45\pm0.26)\cdot10^{-11}$	$(7.80\pm1.96)\cdot10^{9}$	$(1.28\pm0.32)\cdot10^{-10}$

Table 5.10: The decomposition rate coefficients and the lifetime of the activated complexes $(Au_2CO^-)^*$ ($k_d(Au_2^-)$, $\tau(Au_2^-)$) and $(Au_3CO^-)^*$ ($k_d(Au_3^-)$, $\tau(Au_3^-)$).

The values for the decomposition rate coefficient $k_d(Au_2^-)$ and $k_d(Au_3^-)$ are presented in table 5.10, where $k_d(Au_2^-)$ and $k_d(Au_3^-)$ are calculated by using the expression 5.21. The lifetimes of the activated complexes $(Au_2CO^-)^*$ and $(Au_3CO^-)^*$

denoted as $\tau(Au_2^-)$ and $\tau(Au_3^-)$, are also shown in table 5.10, where $\tau(Au_2^-)$ and $\tau(Au_3^-)$ are calculated as $\tau = 1/k_d$. From this table, it can be seen that the lifetime of the activated complex $(Au_3CO^-)^*$ is one order of magnitude higher than the lifetime of $(Au_2CO^-)^*$, while the decomposition rate coefficient $k_d(Au_3^-)$ is one order of magnitude lower than $k_d(Au_2^-)$.

As in the case of gold anions-oxygen complexes presented in section 5.2, the binding energy of the first CO molecule on Au_2^- and Au_3^- clusters can be estimated by plotting the decomposition rate coefficients $k_d(Au_2^-)$ and $k_d(Au_3^-)$ as a function of the reaction temperature and employing the fitting program *Mass Kinetics 1.4*.[135,136] This program requires the input of the vibrational frequencies of the reaction products (Au_2CO^-, Au_3CO^-) and the energy of the activated complexes ($(Au_2CO^-)^*$, $(Au_3CO^-)^*$). The values of the vibrational frequencies were calculated in the group of Prof. V. Bonačić-Koutecký.[139,148] As shown in section 5.2, the energy of the activated complex can be calculated by using the model proposed by Cox *et al.*.[52] Taking into account that Au_2^- and Au_3^- clusters have a linear geometry[149] and gold-carbonyl complexes have a non-linear structure (see Fig. 5.16),[128,148,150] the energy of the activated complexes $(Au_2CO^-)^*$ and $(Au_3CO^-)^*$ is given by the following expressions:

$$E((Au_2CO^-)^*) = E_0(Au_2CO^-) + 3k_BT \tag{5.22}$$

$$E((Au_3CO^-)^*) = E_0(Au_3CO^-) + 6k_BT \tag{5.23}$$

with k_B being the Boltzmann constant and T the reaction temperature. $E_0(Au_2CO^-)$ and $E_0(Au_3CO^-)$ represent the binding energies of the CO molecule on Au_2^- and Au_3^- clusters, respectively.

Fig. 5.15 shows the temperature dependence of the decomposition rate coefficients in the case of Au_2CO^- (Fig. 5.15 (a)) and Au_3CO^- (Fig. 5.15 (b)) reaction complexes. From Fig. 5.15 (a) it can be seen that the simulated values corresponding to a binding energy $E_{BE}(Au_2CO^-) = 0.15\ eV$ (open squares) overestimate the experimental data, while the values corresponding to a binding energy of $E_{BE}(Au_2CO^-) = 0.20\ eV$ (open triangles) underestimate the measured decomposition rate coefficients. Hence, a value of $E_{BE}(Au_2CO^-) = 0.18 \pm 0.05\ eV$ for the binding energy of the carbon monoxide molecule on the anionic gold dimer is obtained from these simulations. The grey line in Fig. 5.15 (a) represents a linear fit of the double logarithmic plot and indicates a temperature dependence of the decomposition rate coefficient: $k_d(Au_2^-) \sim T^m$, with $m = 1.72$. By employing the same procedure

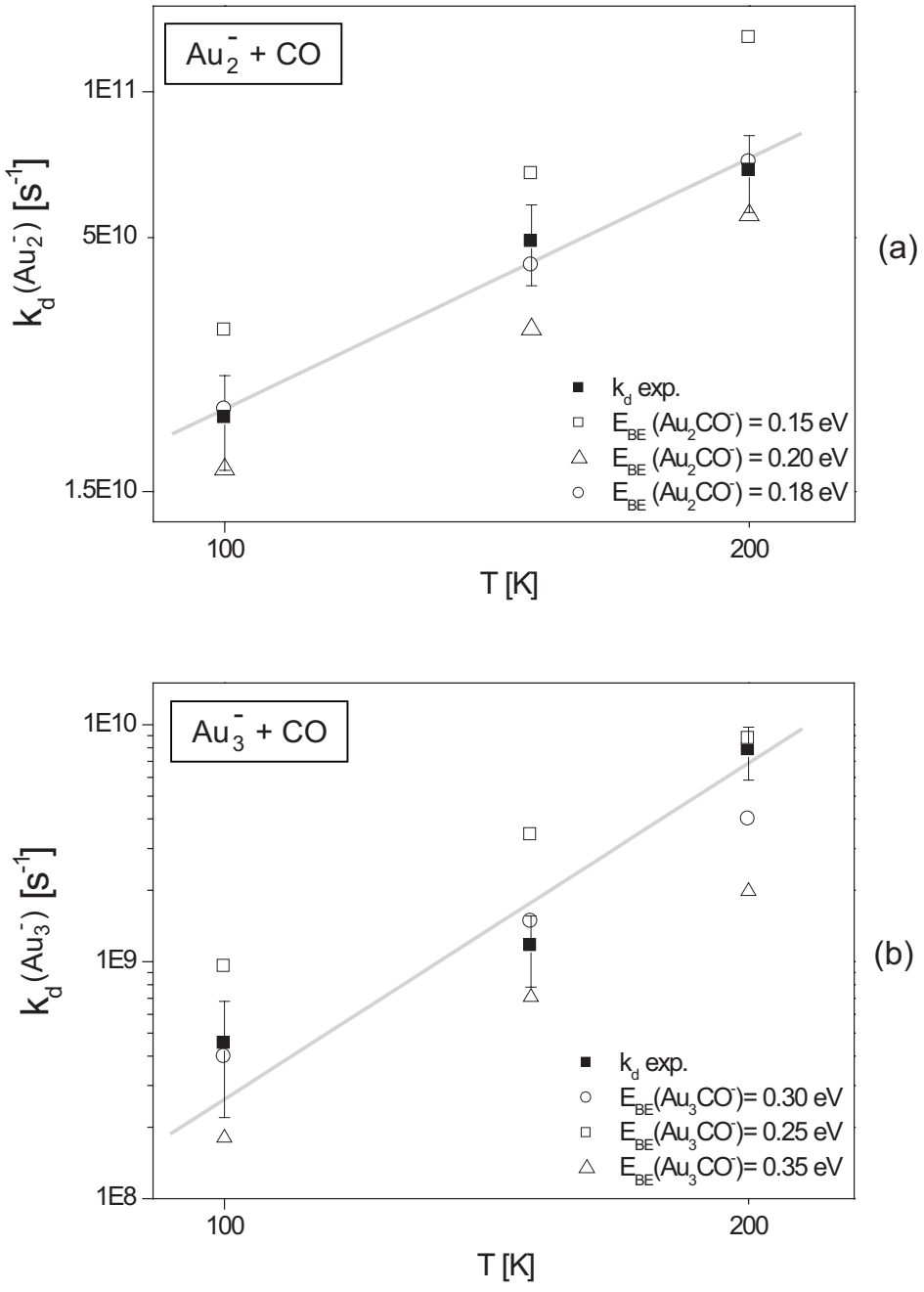

Figure 5.15: Double logarithmic representation of the temperature dependence of the decomposition rate coefficients in the case of (a) Au_2CO^- and (b) Au_3CO^- reaction products. The experimental values are depicted as filled squares, while the simulated rate coefficients are depicted as open symbols. The grey solid lines represent a linear fit of the measured data.

as in the case of Au_2CO^- complex, a value of $E_{BE}(Au_3CO^-) = 0.30 \pm 0.10\ eV$ for the binding energy of the carbon monoxide molecule on the anionic gold trimer is obtained (see Fig. 5.15 (b)). Moreover, a temperature dependence of the decomposition rate constant $k_d(Au_3^-) \sim T^m$, with $m = 4.71$ results from the linear fit of the double logarithmic plot (grey line in Fig. 5.15 (b)). The small values obtained for the binding energies of the first CO molecule on Au_2^- ($E_{BE}(Au_2CO^-) = 0.18 \pm 0.05\ eV$) and Au_3^- ($E_{BE}(Au_3CO^-) = 0.30 \pm 0.10\ eV$) clusters indicate an extremely weak binding of the carbon monoxide molecule on anionic gold dimer and trimer compared to the binding energy obtained for the $Au_2O_2^-$ complex ($E_{BE}(Au_2O_2^-) = 0.64 \pm 0.10\ eV$). These findings are supported by the experimental observation that no reaction product of anionic gold dimer and trimer towards CO appears at reaction temperatures above 200 K. In conclusion, the experimental measurements presented in this work show for the first time that a CO molecule is weaker bound on Au_2^- clusters that an O_2 molecule.

The binding energy of the first CO molecule on anionic gold dimer and trimer can be estimated as well by applying a pure RRK analysis. As described in section 2.2.3, the RRK decomposition rate coefficient is:

$$k_d = \nu \left(\frac{E - E_0}{E}\right)^{s-1} \tag{5.24}$$

where ν represents the frequency of the critical oscillator that leads to dissociation, E denotes the total energy of the activated complex contained in s independent oscillators and E_0 represents the CO binding energy to the cluster.

The energy E of the activated complex can be calculated by using the equations 5.22 - 5.23. The exponent s in expression 5.24 can be written as $s = 3N - 6$ for a molecule with non-linear structure, where N represents the number of atoms in the monocarbonyl complex. Introducing the expressions 5.22 and 5.23 in equation 5.24, the unimolecular RRK decomposition rates for the two cluster sizes are:

$$k_d(Au_2^-) = \nu(Au_2CO^-) \cdot \left(\frac{3k_BT}{E_0(Au_2CO^-) + 3k_BT}\right)^5 \tag{5.25}$$

$$k_d(Au_3^-) = \nu(Au_3CO^-) \cdot \left(\frac{6k_BT}{E_0(Au_3CO^-) + 6k_BT}\right)^8 \tag{5.26}$$

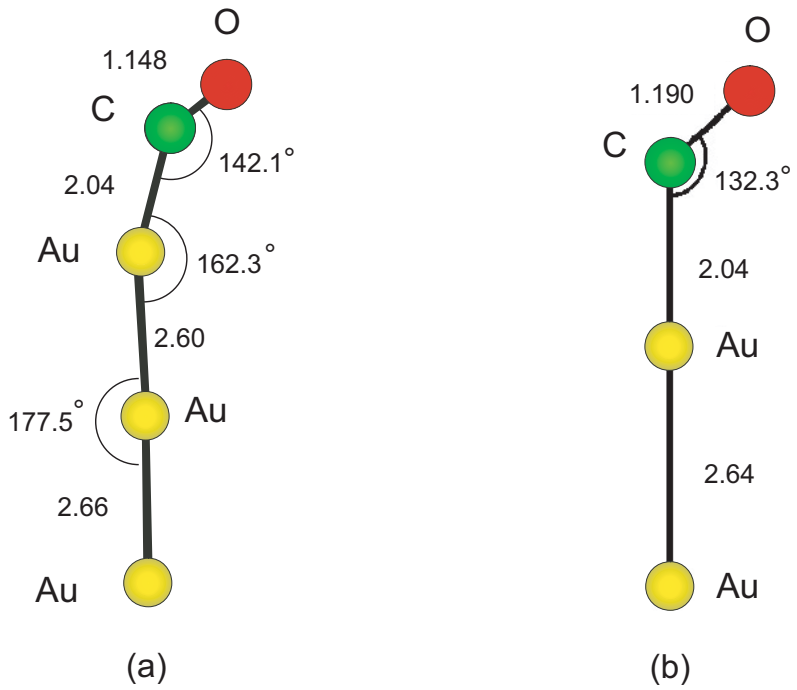

Figure 5.16: The calculated structure of Au_3CO^- (a) and Au_2CO^- (b). The bond lengths are given in $\mathring{A}$: (a) taken from Mitrić and Bonačić-Koutecký;[148] (b) taken from Häkkinen and Landman.[150]

Assuming that the CO binding energies E_0 and the frequencies ν are identical for Au_2^- and Au_3^- clusters,[128,148] the ratio of the experimental termolecular rate coefficients can be calculated as:

$$\frac{k_1^{(3)}(Au_3^-)}{k_1^{(3)}(Au_2^-)} \approx \frac{k_d(Au_3^-)}{k_d(Au_2^-)} = \frac{(E_0 + 6k_BT)^8(3k_BT)^5}{(6k_BT)^8(E_0 + 3k_BT)^5} \tag{5.27}$$

$$\frac{k_1^{(3)}(Au_3^-)}{k_1^{(3)}(Au_2^-)} \approx \frac{(E_0 + 6k_BT)^8}{2^8(3k_BT)^3(E_0 + 3k_BT)^5} \tag{5.28}$$

Considering a reaction temperature of $T = 100\ K$ and the measured termolecular rate constant ratio of $k_1^{(3)}(Au_3^-)/k_1^{(3)}(Au_2^-) \cong 47$, a binding energy of the CO molecule on small anionic gold clusters of $E_0 \cong 0.5\ eV$ is obtained. It is important to note that this value represents a mean value between the assumed similar binding energies of the CO molecule on Au_2^- and Au_3^- clusters.

Comparing the results obtained from RRK and RRKM analysis, it can be observed that the binding energy values for the carbon monoxide molecule on anionic gold clusters are slightly different. Probably the assumption of identical binding energy for Au_2CO^- and Au_3CO^- complexes is not fully appropriate and could explain the discrepancies between the results from RRK and RRKM calculations.

From time-resolved photodetachment experiments on Au_2CO^- clusters, Lüttgens *et al.* estimated the binding energy of the CO molecule on negative gold dimer by using the RRK formalism and a value of about $E_{BE}(Au_2CO^-) = 0.91\ eV$ was obtained. The authors performed density functional calculations as well, where a binding energy of $E_{BE}(Au_2CO^-) = 0.77\ eV$ was found.[151]

In order to determine the structure of the gold-carbonyl complexes and the binding energy of the CO molecule on negatively charged gold clusters, theoretical simulations in the framework of density functional theory have been performed by H. Häkkinen and U. Landman. They found a bent structure for the Au_2CO^- complex and a binding energy of $E_{BE}(Au_2CO^-) = 0.97\ eV$.[150] The result of their calculations is presented in Fig. 5.16 (b).

The DFT calculations carried out in the group of Prof. V. Bonačić-Koutecký predicted a value of $E_{BE}(Au_2CO^-) = 0.5\ eV$ for the binding energy of the first CO molecule on Au_2^- clusters,[143] whereas for the binding of the CO molecule on Au_3^- clusters a value of $E_{BE}(Au_3CO^-) = 0.47\ eV$ has been found.[148] The structure of the Au_3CO^- complex is presented in Fig. 5.16 (a). In these calculations, the modification of the employed basis sets for the theoretical treatment of the binding energy of the CO molecule on Au_2^- clusters leads to a variation of the binding energy values in the range of $E_{BE}(Au_2CO^-) = 0.33\ eV - 0.77\ eV$.[143] The theoretical calculations are in good agreement with the estimated values for the binding energy of the carbon monoxide molecule on negatively charged gold clusters obtained from the experimental measurements presented in this section.

5.4 Reactions of Gold Anions with O_2 and CO

After the investigation of the reactivity of small, negatively charged gold clusters with oxygen and carbon monoxide, respectively, their reactivity in the presence of both reactive gases (O_2 and CO) in the ion trap was studied.[152] These investigations

are of particular interest, since a full catalytic cycle has been theoretically predicted for the gas-phase CO oxidation reaction on free Au_2^- clusters.[150]

The reactive mass spectra for the anionic gold monomer, dimer and trimer, recorded in the presence of oxygen and carbon monoxide are presented in Fig. 5.17. The measurements were performed for different pressures of the reactive gases as well as different reaction temperatures. For the first time, coadsorption products like $Au_2(CO)O_2^-$, $Au_3(CO)O_2^-$ and $Au_3(CO)(O_2)_2^-$ are experimentally observed. From Fig. 5.17, it can be clearly seen that the coadsorption complexes are formed at cryogenic temperatures while no new reaction product could be identified at room temperatures for any investigated reaction parameters.

In the case of the anionic gold monomer, a small peak is observed at a reaction temperature of 100 K, which corresponds to the mass of the Au_1O^- complex. In Fig. 5.17 (a), the mass spectrum for the reaction of Au_1^- with O_2 and CO is shown and for clarity, the cluster signal magnified by a factor of 10 is depicted as well. The small peak which corresponds to the mass of the Au_1O^- complex appears only under special experimental conditions, *i.e.* high reactive gas concentrations in the ion trap as well as long reaction times, which is an indication of an extremely low reactivity. Since the intensity of this product represents almost the lower limit of the detection range available in this experiment, no kinetic measurements could be performed on this reaction product. However, it is important to note that no reactivity of Au_1^- towards O_2 or CO only was observed, as shown in section 5.2 and 5.3. Therefore, the appearance of this peak in the mass spectrum does not indicate a simple dissociative adsorption of an oxygen molecule. It must involve a cooperative process which occurs only in the presence of both reactive gases. Moreover, the presence of the Au_1O^- product in the mass spectra could be an indication of a catalytic CO oxidation reaction on free Au_1^-.

Theoretical calculations have already predicted the catalytic CO oxidation on the Au_1O^- complex. *Ab initio* molecular dynamics simulations (MD) show that once the Au_1O^- product is formed, it will react extremely fast with CO, yielding the products Au_1^- and CO_2 already after 300 fs. Furthermore, the oxidation reaction is highly exothermic, releasing an energy of 3.604 eV.[143,153]

The oxidation reaction of CO on the Au_1O^- complex was experimentally observed by Kimble *et al.*[154] In this experiment, the Au_1O^-, $Au_1O_2^-$ and $Au_1O_3^-$ complexes

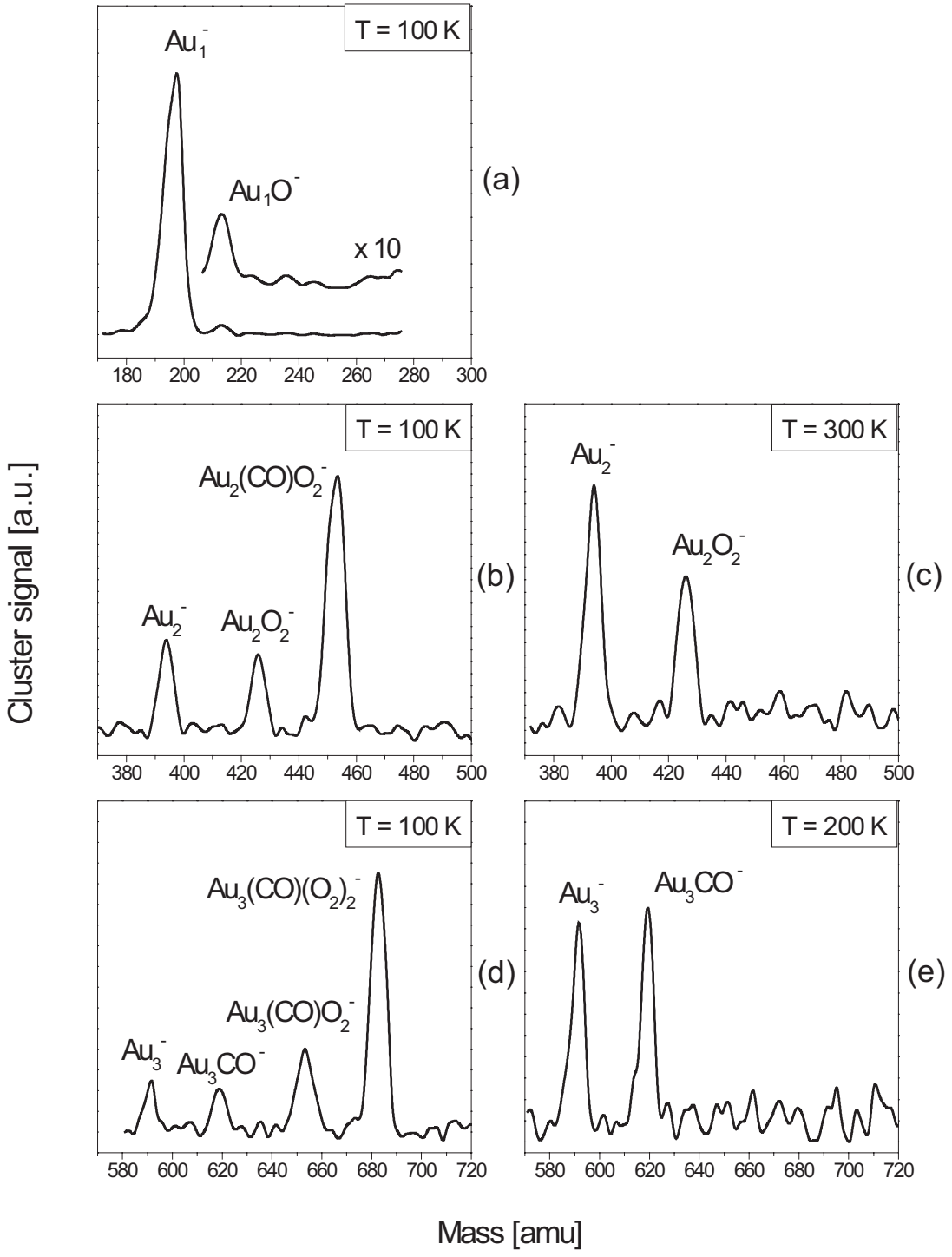

Figure 5.17: Mass spectra for the reaction of Au_1^-, Au_2^- and Au_3^- clusters with O_2 and CO at different temperatures. The reaction parameters are: (a) $p_{He} = 0.75\ Pa$, $p_{O_2} = 0.34\ Pa$, $p_{CO} = 0.34\ Pa$, $t_{reaction} = 2000\ ms$, $T_{octopole} = 100\ K$; (b) $p_{He} = 1.00\ Pa$, $p_{O_2} = 0.05\ Pa$, $p_{CO} = 0.07\ Pa$, $t_{reaction} = 200\ ms$, $T_{octopole} = 100\ K$; (c) $p_{He} = 1.07\ Pa$, $p_{O_2} = 0.11\ Pa$, $p_{CO} = 0.19\ Pa$, $t_{reaction} = 1500\ ms$, $T_{octopole} = 300\ K$; (d) $p_{He} = 0.89\ Pa$, $p_{O_2} = 0.22\ Pa$, $p_{CO} = 0.23\ Pa$, $t_{reaction} = 3000\ ms$, $T_{octopole} = 100\ K$; (e) $p_{He} = 1.08\ Pa$, $p_{O_2} = 0.21\ Pa$, $p_{CO} = 0.19\ Pa$, $t_{reaction} = 2000\ ms$, $T_{octopole} = 200\ K$.

were produced *"in a laser vaporization source by passing a continuous flow of oxygen seeded in helium over the metal plasma formed by ablating a rotating and translating gold rod"*. This implies the formation of the gold oxide products under rather poorly defined thermodynamical reaction conditions which allow dissociated oxygen to react with the negatively charged gold monomer. After the production, the gold oxide complexes react with CO in a flow tube reactor at room temperature. From the analysis of the mass spectra, it was observed that upon addition of CO, the peak corresponding to Au_1O^- decreases slightly, while the bare cluster peak Au_1^- increases. Since no additional reaction product is observed, the authors correlate the decreasing Au_1O^- signal with the CO oxidation reaction.

According to the experiment performed by Kimble *et al.*, the production of gold oxide complexes requires special conditions, which are fulfilled only by adding oxygen to the metal plasma during the cluster formation process.[154] Correlating this finding with the results presented in Fig. 5.17 (a), it can be understood that the experimental conditions employed for the measurements presented in this work do not allow similar observations, since the chemical reactions are carried out under thermodynamically well defined conditions.

In the case of Au_2^- clusters, only the $Au_2O_2^-$ product is observed at room temperature (Fig. 5.17 (c)). At a reaction temperature of 100 K, a new peak appears aside the dioxide complex, which corresponds to the $Au_2(CO)O_2^-$ product (Fig. 5.17 (b)). Interestingly, no Au_2CO^- or $Au_2(CO)_2^-$ carbonyl complexes are observed for any investigated reaction temperature, although these are stable complexes when only CO is present in the ion trap as a reactive gas, as shown in section 5.3. The absence of the carbonyl complexes can be rationalized by comparing the respective termolecular rate constants for the adsorption of an O_2 and a CO molecule, which are presented in table 5.1 and 5.5. From these tables, it can be seen that the reaction rate constant corresponding to the adsorption of an oxygen molecule on Au_2^- clusters is at least one order of magnitude higher than the corresponding reaction rate constant for the adsorption of a CO molecule. Therefore, the adsorption of O_2 is the faster reactive channel, leading to the absence of the carbonyl complexes in the mass spectra.

The formation of $Au_2(CO)O_2^-$ as a final reaction product clearly shows that Au_2^- favors the coadsorption of both, oxygen and carbon monoxide, over the adsorption of just one type of reactive molecule. Many isomeric structures can be assigned for

the coadsorption complex with the mass corresponding to $Au_2(CO)O_2^-$, and the two extreme cases are:

- the $Au_2(CO)O_2^-$ structure, which is formed when the CO and O_2 molecules are adsorbed independently, for example on different sides of Au_2^-;
- the $Au_2(CO_3)^-$ structure, which is formed when a reaction of the two adsorbate molecules (O_2 and CO) takes place, resulting in a carbonate (CO_3) entity. It is important to note that the $Au_2CO_3^-$ product has been proposed theoretically to be a key intermediate in a catalytic CO oxidation cycle on Au_2^- clusters.[150] Therefore, once the $Au_2CO_3^-$ complex is formed, it is very likely to release the CO_2 molecule in a final reaction step, as theoretically predicted.

However, from the mass spectra depicted in Fig. 5.17 (b) and (c), no structural information can be deduced. Hence, it can not be determined whether the $Au_2(CO)O_2^-$ or $Au_2(CO_3)^-$ reaction product is observed, since both complexes have the same mass. A systematical investigation of the reaction of Au_2^- clusters with oxygen and carbon monoxide will be presented in detail in the following subsection.

The previously unknown tendency of small, negatively charged gold clusters to form coadsorption complexes is confirmed by the reactivity of Au_3^- towards O_2 and CO. From the mass spectra depicted in Fig. 5.17 (d) and (e), it can be observed that at 100 K the coadsorption species $Au_3(CO)O_2^-$ and $Au_3(CO)(O_2)_2^-$ are formed, whereas at 200 K only the Au_3CO^- reaction product appears. The formation of the coadsorption complexes is surprising, since bare Au_3^- clusters do not react with oxygen at any investigated temperature, as shown in section 5.2. Therefore, it seems that the CO adsorption on Au_3^- clusters changes the electronic structure of the cluster complex in such a way that favorizes the subsequent reaction with oxygen. These results indicate the existence of a *cooperative adsorption process*: the adsorption of a CO molecule on anionic gold trimer is a necessary prerequisite in order to enable further adsorption of O_2 molecules. Furthermore, no coadsorption complexes are detected at a reaction temperature above 200 K, which is similar to the case of the Au_3^- reaction with CO only (see section 5.3). This finding is an additional indication that a CO molecule has to be adsorbed first on the Au_3^- clusters before subsequent O_2 adsorption becomes possible. The measurements presented in this section represent the first experimental evidence for the existence of a cooperative adsorption process.

In the experiments performed in the group of Prof. L. Wöste, it was observed that anionic silver clusters show as well a cooperative adsorption process. Negatively charged silver clusters present a poor reactivity towards carbon monoxide, but, when they are exposed to a mixture of carbon monoxide and oxygen, coadsorption complexes like $Ag_4(CO)O_2^-$, $Ag_6(CO)O_2^-$ appear in the mass spectra.[79,131] The observation of these reaction products, indicates that the first adsorbed molecule (O_2) changes the electronic structure of the anionic silver cluster in such a way that the adsorption of the second type of molecule (CO) becomes possible.

The observation of the coadsorption complexes $Au_2(CO)O_2^-$, $Au_3(CO)O_2^-$ and $Au_3(CO)(O_2)_2^-$ was the primary motivation for the investigation of the potential catalytic properties of anionic gold clusters towards the CO oxidation reaction.

5.5 Catalytic Oxidation of CO by Au_2^- Clusters

Since a full catalytic cycle for the CO oxidation reaction on Au_2^- clusters that contains $Au_2(CO)O_2^-$ as an intermediate product has already been theoretically predicted,[150] the experimental investigations will focus on the catalytic properties of Au_2^- and a systematic study of the coadsorption complex $Au_2(CO)O_2^-$ will be presented in this section.[57]

After the identification of the $Au_2(CO)O_2^-$ product in the mass spectra at low reaction temperatures, when both reactive gases (oxygen and carbon monoxide) are present inside the ion trap (Fig. 5.17 (b)), kinetic measurements for the reaction of Au_2^- clusters with O_2 and CO were performed. In Fig. 5.18, the kinetic traces for different reaction temperatures and different reactive gas pressures are shown. The open symbols represent the measured ion signals, while the solid lines are the fitted signals. The fitted signal is obtained by using the *Detmech* program.[133] From this figure, one can observe that the ion concentrations vary strongly at short reaction times and reach an equilibrium after a given reaction time (1 s for 100 K and 2 s at 225 K reaction temperature, in the presence of similar amounts of reactive gases). Moreover, the maximum value of the $Au_2(CO)O_2^-$ signal decreases with increasing temperature. The variation of the carbon monoxide partial pressure (from $p_{CO} = p_{O_2}$ in Fig. 5.18 (b) to $p_{CO} = 1.5\ p_{O_2}$ in Fig. 5.18 (c)) leads to a decrease of the equilibrium $Au_2(CO)O_2^-$ signal intensity, which indicates a direct dependence of the

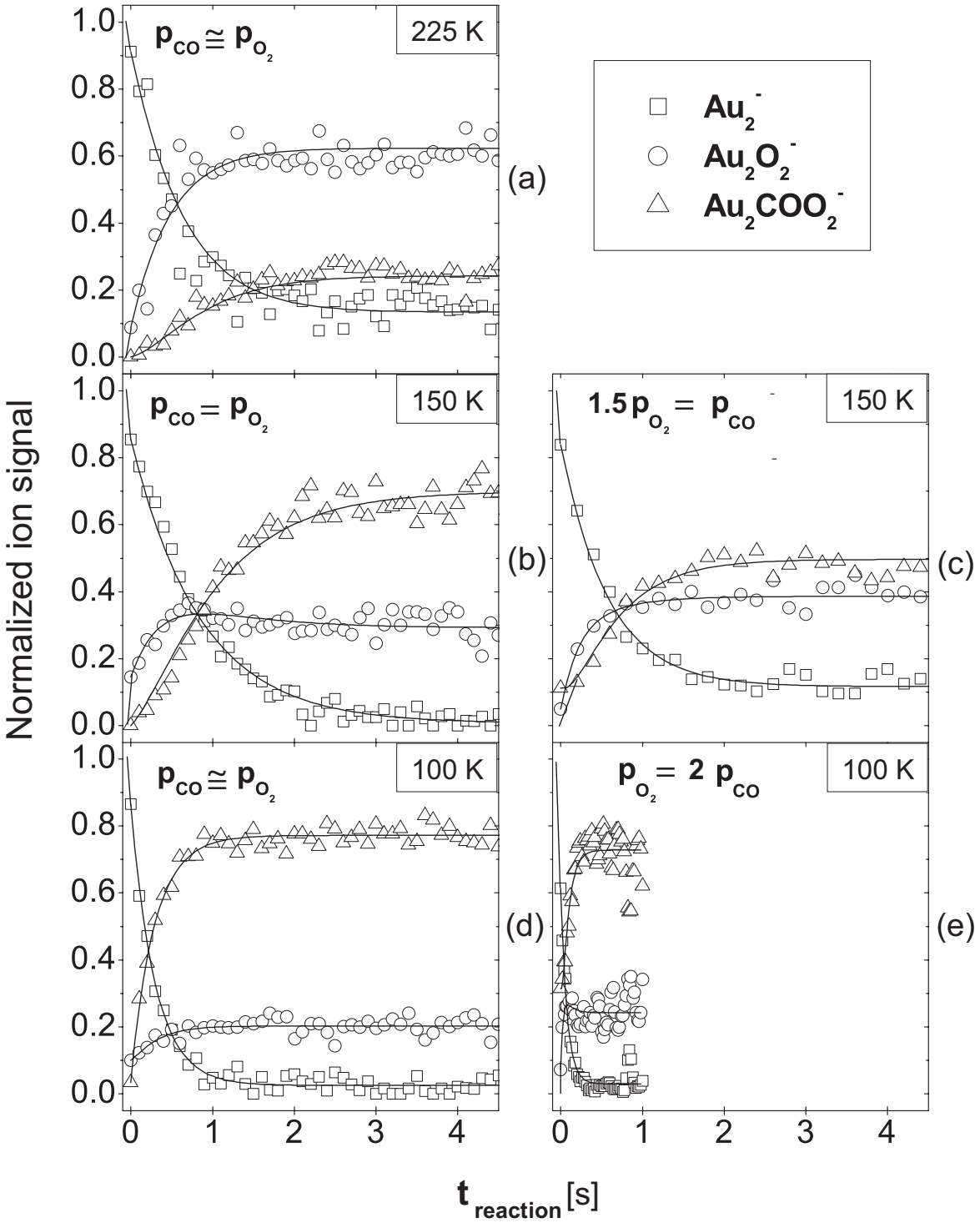

Figure 5.18: Kinetic traces of the reaction of Au_2^- clusters with O_2 and CO at different temperatures. The normalized ion signals (open symbols) and the simulated signals (solid lines) are shown as a function of the reaction time. The reaction parameters are: (a) $p_{He} = 1.07\ Pa$, $p_{O_2} = 0.09\ Pa$, $p_{CO} = 0.10\ Pa$, $T_{octopole} = 225\ K$; (b) $p_{He} = 1.00\ Pa$, $p_{O_2} = 0.04\ Pa$, $p_{CO} = 0.04\ Pa$, $T_{octopole} = 150\ K$; (c) $p_{He} = 1.00\ Pa$, $p_{O_2} = 0.04\ Pa$, $p_{CO} = 0.06\ Pa$, $T_{octopole} = 150\ K$; (d) $p_{He} = 1.01\ Pa$, $p_{O_2} = 0.02\ Pa$, $p_{CO} = 0.03\ Pa$, $T_{octopole} = 100\ K$; (e) $p_{He} = 1.03\ Pa$, $p_{O_2} = 0.08\ Pa$, $p_{CO} = 0.04\ Pa$, $T_{octopole} = 100\ K$.

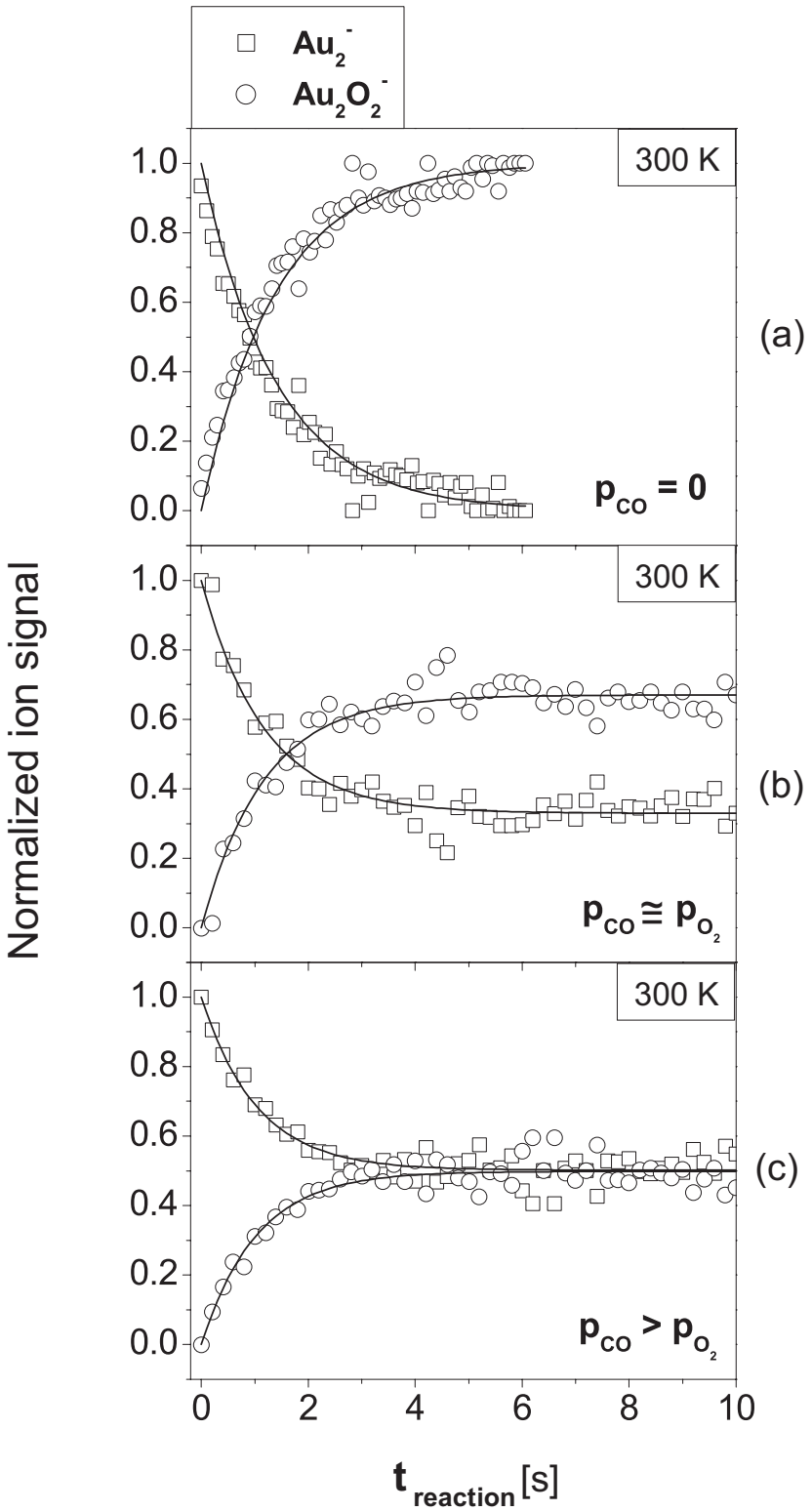

Figure 5.19: Kinetic traces for the reaction of Au_2^- clusters with: (a) O_2 only; (b), (c) with O_2 and CO at 300 K. The reaction parameters are: (a) $p_{He} = 1.00\ Pa$, $p_{O_2} = 0.30\ Pa$, $p_{CO} = 0\ Pa$, $T_{octopole} = 300\ K$; (b) $p_{He} = 0.99\ Pa$, $p_{O_2} = 0.13\ Pa$, $p_{CO} = 0.16\ Pa$, $T_{octopole} = 300\ K$; (c) $p_{He} = 1.01\ Pa$, $p_{O_2} = 0.11\ Pa$, $p_{CO} = 0.25\ Pa$, $T_{octopole} = 300\ K$.

coadsorption product intensity on the CO pressure. This dependence is not observed when the oxygen pressure is modified. Comparing Fig. 5.18 (d) with Fig. 5.18 (e), where p_{O_2} is increased from $p_{O_2} \cong p_{CO}$ to $p_{O_2} = 2\ p_{CO}$, it can be noticed that the equilibrium intensity of the $Au_2(CO)O_2^-$ signal does not change.

Increasing the reaction temperature up to 300 K, the $Au_2(CO)O_2^-$ complex disappears and an offset in the Au_2^- signal is observed after a few seconds reaction time, *i.e.* the equilibrium signal of the Au_2^- clusters does not reach the zero value for long reaction times. This can be seen from Fig. 5.19, where the kinetic traces for the reaction of anionic gold dimers with oxygen only (Fig. 5.19 (a)) and, with oxygen and carbon monoxide (Fig. 5.19 (b), (c)) at a reaction temperature of 300 K are presented. As in the previous graph, the open symbols represent the measured signal, whereas the solid lines illustrate the fitted signal obtained by using the *Detmech* program.[133] It is important to note that the offset of the Au_2^- signal appears in the presence of both reactive gases O_2 and CO and not when only O_2 is introduced inside the ion trap. Moreover, comparing Fig. 5.19 (b) and Fig. 5.19 (c), it can clearly be seen that this offset depends on the CO concentration, becoming larger with increasing CO pressure. This is a key indication that a reaction cycle takes place, where the Au_2^- clusters are reformed at the end of the cycle.

In order to gain more insights into the reaction mechanism, the concentration of all observed ions (Au_2^-, $Au_2O_2^-$, $Au_2(CO)O_2^-$) was monitored as a function of the reaction time under a multitude of different reaction conditions. The dependence of the kinetics on the variation of different reaction parameters (reaction temperature, O_2 partial pressure, CO partial pressure) was investigated. The aim of these investigations is to find a reaction mechanism which fits all the experimental data measured under different reaction conditions. The most simple reaction mechanism that fulfills all these prerequisites is given by the following equations:

$$Au_2^- + O_2 \rightarrow Au_2O_2^- \qquad k_1 \tag{5.29}$$

$$Au_2O_2^- + CO \rightleftarrows Au_2(CO)O_2^- \qquad k_2,\ k_{-2} \tag{5.30}$$

$$Au_2(CO)O_2^- + CO \rightarrow Au_2^- + 2CO_2 \qquad k_3 \tag{5.31}$$

where k_1, k_2, k_{-2} and k_3 represent the reaction rate constants for each elementary step. This reaction mechanism implies that Au_2^- clusters are able to carry out a catalytic cycle for the CO oxidation reaction with $Au_2(CO)O_2^-$ as intermediate complex.

Interestingly, it was found that gold atoms condensed in a CO/O_2 matrix show evidence of catalytic activity at cryogenic temperatures.[155] The authors employed infrared spectroscopy methods and observed that a peak corresponding to the CO_2 molecule appears in the infrared spectra at 40 K. These experiments show that intermediate complexes like $(OC)Au(CO_3)$ and $(OC)Au(O_2CO)$ are involved in the catalytic process.[155]

In Fig. 5.18 and 5.19, the simulated signals (solid lines) are obtained by fitting the experimental data with the reaction mechanism given by the expressions 5.29 - 5.31. The fitting procedure employs the *Detmech* software,[133] which requires the input of a reaction mechanism and calculates the corresponding product ion intensities. It can clearly be seen that an excellent agreement with all measured kinetic data has been achieved (see Fig. 5.18 and 5.19). The fitting procedure is very sensitive to the postulated reaction steps and is able to discriminate against alternative mechanisms. For example, the replacement of the equilibrium step in expression 5.30 by a simple forward reaction step leads to a mechanism that yields an inadequate fit to the experimental data. This is illustrated in Fig. 5.20, where the kinetic traces (open symbols) for the reaction of anionic gold dimer with O_2 and CO at a reaction temperature of 100 K, as well as the simulated signals (solid lines) obtained by fitting a reaction mechanism which does not contain the backward reaction step in equation 5.30 are shown. From this figure, the disagreement between the experimental data and the fitted signals can be observed: the $Au_2O_2^-$ signal disappears at long reaction times, while the experimental curve reaches an equilibrium. Moreover, the respective increase and decrease in the $Au_2(CO)O_2^-$ and Au_2^- signals do not match the experimental data.

The unimolecular reaction rate coefficients are obtained from the fitting procedure and they are presented in tables 5.11 and 5.12. The fitting procedure employs the numerical fit program *Detmech*[133] and these results are cross-checked by taking them as input parameters for the IBM kinetics simulator (*CKS 1.0*)[134] program which generates kinetic traces for given rate constants and reaction mechanisms. The errors in the values of k_1 and k_2 rate constants are primarily due to the uncertainty in the gas pressure measurement ($\pm$ 0.01 Pa). For k_{-2} and k_3, the possible variation of the rate constants resulting in the same fit quality is larger than the uncertainty in the partial pressure and thus determines the error bars of these rate coefficients. The

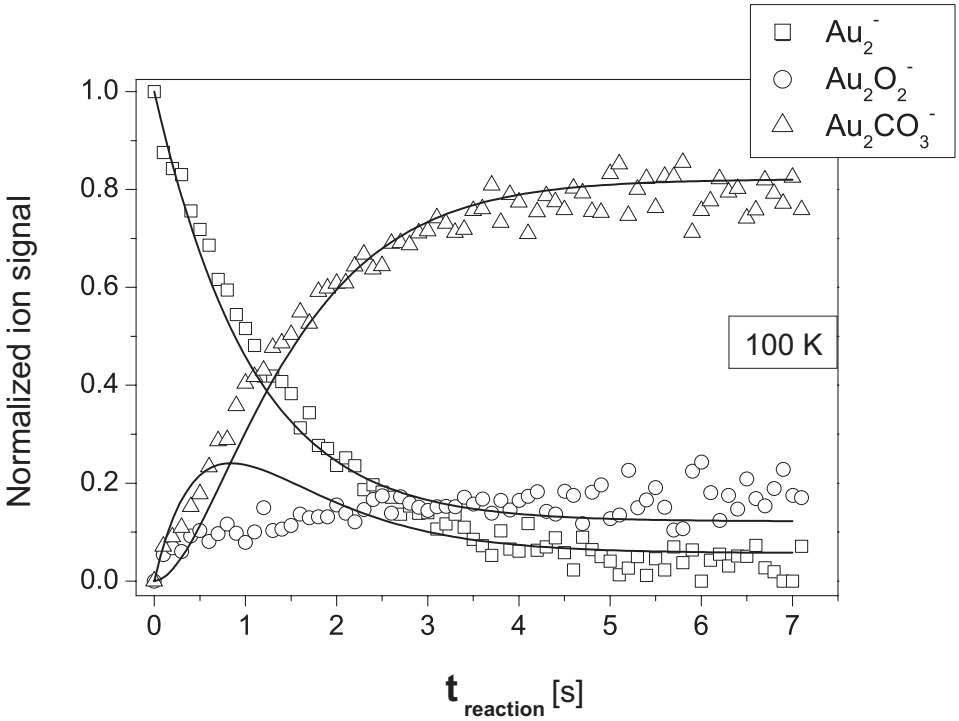

Figure 5.20: Test of the fit quality for the reaction of Au_2^- clusters with O_2 and CO. The kinetic traces (open symbols) and the simulated signals (solid lines) are depicted as a function of the reaction time. The measured data are fitted without introducing the equilibrium step in the reaction mechanism given by the expressions 5.29 - 5.31. The reaction parameters are: $p_{He} = 1.00\ Pa$, $p_{O_2} = 0.02\ Pa$, $p_{CO} = 0.03\ Pa$, $T_{octopole} = 100\ K$.

graphical representation of the reaction rate coefficients as a function of the reactive gas pressures is shown in Fig. 5.21 for 100 K and 150 K reaction temperature.

From tables 5.11 and 5.12 as well as from Fig. 5.21, the pressure dependence of the unimolecular rate constants can be outlined:

- The variation of the O_2 partial pressure leads to a variation of the $k_1^{(1)}$ rate coefficient, while all the other rate constants remain unaffected within the experimental resolution. From table 5.11 as well as Fig. 5.21 (a) and (b), it can be seen that $k_1^{(1)}$ increases linearly with O_2 pressure, as expected for an unimolecular rate coefficient.

- $k_2^{(1)}$ varies linearly with the carbon monoxide pressure (table 5.11). The linear

T [K]	p_{He} [Pa]	p_{O_2} [Pa]	p_{CO} [Pa]	$k_1^{(1)}$ [s^{-1}]	$k_2^{(1)}$ [s^{-1}]
100	1.01	0.02	0.03	3.32 ± 1.66	38.15 ± 12.72
	1.03	0.04	0.04	6.12 ± 1.53	45.53 ± 11.38
	1.02	0.04	0.08	8.20 ± 2.05	76.94 ± 9.62
	1.03	0.08	0.04	12.47 ± 1.56	26.48 ± 6.62
150	1.00	0.04	0.04	1.16 ± 0.29	1.92 ± 0.48
	1.00	0.04	0.06	1.48 ± 0.37	2.97 ± 0.50
	1.00	0.04	0.16	2.20 ± 0.55	14.38 ± 0.90
	1.03	0.06	0.07	3.67 ± 0.61	7.02 ± 1.00
	1.05	0.06	0.11	3.92 ± 0.65	13.46 ± 1.22
	1.04	0.12	0.05	4.27 ± 0.36	3.00 ± 0.60
190	1.05	0.07	0.07	1.78 ± 0.25	2.44 ± 0.35
	1.04	0.08	0.16	2.19 ± 0.27	3.96 ± 0.25
	1.04	0.15	0.08	3.11 ± 0.21	3.17 ± 0.40
225	1.07	0.09	0.10	1.45 ± 0.16	0.84 ± 0.08
300*	1.05	0.13	0.13	0.94 ± 0.07	0.34 ± 0.03
	1.05	0.13	0.26	0.94 ± 0.07	0.67 ± 0.03
	1.05	0.26	0.13	1.61 ± 0.06	0.45 ± 0.03

Table 5.11: The unimolecular rate coefficients $k_1^{(1)}$ and $k_2^{(1)}$ for the reaction of Au_2^- clusters with O_2 and CO for different reaction temperatures and different partial pressures of the reactant gases.
* It is important to note that the intermediate product $Au_2(CO)O_2^-$ is not observed at a reaction temperature of 300 K. Therefore, for fitting the reaction mechanism given by the expressions 5.29 - 5.31, an ion concentration for the $Au_2(CO)O_2^-$ product below the detection limit of the experiment (<1% from the maximal normalized signal) is assumed.

T [K]	$\mathbf{p_{He}}$ **[Pa]**	$\mathbf{p_{O_2}}$ **[Pa]**	$\mathbf{p_{CO}}$ **[Pa]**	$\mathbf{k_{-2}^{(1)}}$ **[s^{-1}]**	$\mathbf{k_{3}^{(1)}}$ **[s^{-1}]**
100	1.01	0.02	0.03	9.92 ± 1.98	0.11 ± 0.06
	1.03	0.04	0.04	10.60 ± 2.12	0.30 ± 0.16
	1.02	0.04	0.08	30.03 ± 6.00	0.62 ± 0.31
	1.03	0.08	0.04	8.31 ± 1.67	0.51 ± 0.26
150	1.00	0.04	0.04	0.79 ± 0.16	0.01 ± 0.005
	1.00	0.04	0.06	1.96 ± 0.39	0.35 ± 0.18
	1.00	0.04	0.16	23.41 ± 4.68	0.69 ± 0.35
	1.03	0.06	0.07	2.49 ± 0.50	0.45 ± 0.23
	1.05	0.06	0.11	10.00 ± 2.00	0.55 ± 0.28
	1.04	0.12	0.05	1.78 ± 0.36	0.67 ± 0.34
190	1.05	0.07	0.07	0.52 ± 0.10	0.29 ± 0.15
	1.04	0.08	0.16	2.38 ± 0.48	0.44 ± 0.22
	1.04	0.15	0.08	1.74 ± 0.35	0.32 ± 0.16
225	1.07	0.09	0.10	1.36 ± 0.27	0.80 ± 0.40
300*	1.05	0.13	0.13	$< 0.01^*$	$> 10^*$
	1.05	0.13	0.26	$< 0.01^*$	$> 10^*$
	1.05	0.26	0.13	$< 0.01^*$	$> 10^*$

Table 5.12: The unimolecular rate coefficients $k_{-2}^{(1)}$ and $k_3^{(1)}$ for the reaction of Au_2^- clusters with O_2 and CO for different reaction temperatures and different partial pressures of the reactant gases.

* It is important to note that the intermediate product $Au_2(CO)O_2^-$ is not observed at a reaction temperature of 300 K. Therefore, for fitting the reaction mechanism given by the expressions 5.29 - 5.31, an ion concentration for the $Au_2(CO)O_2^-$ product below the detection limit of the experiment (<1% from the maximal normalized signal) is assumed. Thus, the values for the rate constants k_{-2} and k_3 shown in the above table represent the upper and the lower limit of the rate coefficients, respectively.

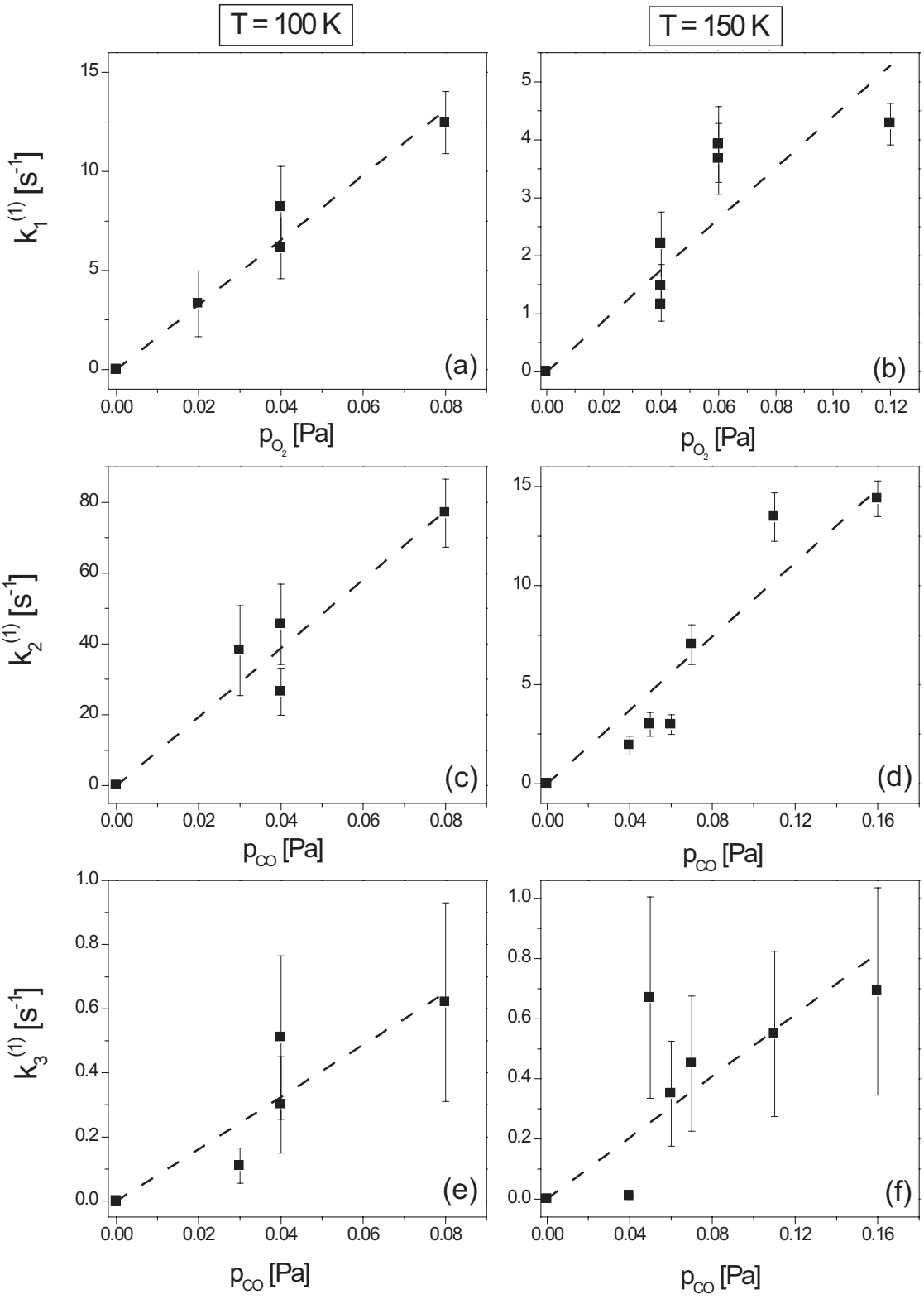

Figure 5.21: The dependence of the unimolecular reaction rate constants $k_1^{(1)}$, $k_2^{(1)}$ and $k_3^{(1)}$ on the reactive gases partial pressure at different reaction temperatures. (a) - (b) show the O_2 pressure dependence of $k_1^{(1)}$; (c) - (d) and (e) - (f) show the CO pressure dependence of $k_2^{(1)}$ and $k_3^{(1)}$, respectively. The dashed lines represent the linear fits to the data.

dependence of the $k_2^{(1)}$ coefficient on the CO partial pressure is depicted in Fig. 5.21 (c) and (d).

- $k_3^{(1)}$ also increases with increasing CO pressure, as can be seen from Fig. 5.21 (e) and (f) as well as table 5.12. This direct dependence is confirmed as well by the kinetic measurements at low and room temperature. Fig. 5.18 (b) - (c) and Fig. 5.19 (b) - (c) show an increase in the Au_2^- offset, which is correlated to $k_3^{(1)}$, when the CO pressure is increased.

- The variation of the CO pressure inside the ion trap affects the $k_{-2}^{(1)}$ rate constant as well. The dependence of $k_{-2}^{(1)}$ on the CO partial pressure is more complicated. The reaction mechanism described by the expressions 5.29 - 5.31 implies that the O_2 adsorption on Au_2^- clusters occurs before the adsorption of a CO molecule, when similar amounts of O_2 and CO are present in the octopole ion trap. This is supported by the fact that no Au_2CO^- reaction product can be observed at any investigated reaction temperature. When Au_2^- clusters are exposed to O_2 or CO only, the adsorption of an oxygen molecule occurs on a much faster time scale than the adsorption of a carbon monoxide molecule, as shown in section 5.2 and 5.3. Moreover, in the case of O_2 adsorption, the value of the termolecular reaction rate coefficient is at least one order of magnitude higher than in the case of CO adsorption. However, the probability of the adsorption of a CO molecule on Au_2^- clusters becomes comparable at high CO partial pressures to the probability of the adsorption of an O_2 molecule and thus, a competing reaction mechanism to the catalytic cycle can take place. This competing mechanism is assumed to involve the adsorption of a carbon monoxide molecule before the oxygen molecule. From this side reaction, a new $Au_2(CO)O_2^-$ product would appear, which should have a different structure than the structure of the intermediate complex from the catalytic cycle presented by the equations 5.29 - 5.31. In this case, the observed increase of the $k_{-2}^{(1)}$ rate constant with the increase of the CO partial pressure could be assigned to the decomposition of this structurally different $Au_2(CO)O_2^-$ product resulting from a CO adsorption that precedes the adsorption of O_2.

As described previously in section 5.2 and 5.3, the experiments were performed in the kinetic low-pressure regime of the Lindemann mechanism, which implies that

an energetically activated reaction complex is formed and stabilizing or activating collisions with the buffer gas molecules have to be considered in the elementary steps of the reaction mechanism. Therefore, the elementary step given by the expression 5.29 as well as the forward step in the expression 5.30, represent ion-molecule reactions and can be described by using the termolecular rate coefficients which are calculated as:

$$k_1^{(2)} = \frac{k_1^{(1)}}{[O_2]} \quad ; \quad k_2^{(2)} = \frac{k_2^{(1)}}{[CO]} \tag{5.32}$$

$$k_1^{(3)} = \frac{k_1^{(1)}}{[O_2] \cdot [He]} = \frac{k_1^{(2)}}{[He]} \quad ; \quad k_2^{(3)} = \frac{k_2^{(1)}}{[CO] \cdot [He]} = \frac{k_2^{(2)}}{[He]} \tag{5.33}$$

where $k_1^{(2)}$ and $k_2^{(2)}$ represent the bimolecular rate coefficients, while $k_1^{(3)}$ and $k_2^{(3)}$ denote the termolecular reaction rates. The backward reaction step from expression 5.30 is described by an overall bimolecular rate constant $k_{-2}^{(2)}$, which is given by the following equation:

$$k_{-2}^{(2)} = \frac{k_{-2}^{(1)}}{[He]} \tag{5.34}$$

The last reaction step (expression 5.31) represents a bimolecular reaction with more than one product and a collision with the buffer gas molecule must not be involved in this elementary step.[20,21] Therefore, this reaction can be described by a bimolecular rate constant $k_3^{(2)}$:

$$k_3^{(2)} = \frac{k_3^{(1)}}{[CO]} \tag{5.35}$$

The values for the bimolecular reaction rate coefficients $k_1^{(2)}$, $k_2^{(2)}$, $k_{-2}^{(2)}$ and $k_3^{(2)}$ for different reactive gas pressures and different reaction temperatures are presented in tables 5.13 and 5.14, while the values for the termolecular rate constants $k_1^{(3)}$ and $k_2^{(3)}$ are shown in table 5.15.

From tables 5.13 and 5.15, it can be noticed that $k_1^{(2)}$ and $k_2^{(2)}$ as well as $k_1^{(3)}$ and $k_2^{(3)}$ show a negative temperature dependence, *i.e.* the reaction rates decrease with increasing temperature. Fig. 5.22 (a) - (b) show the temperature dependence of the termolecular rate coefficients $k_1^{(3)}$ and $k_2^{(3)}$. The observed negative temperature

T[K]	$\mathbf{p_{He}}$**[Pa]**	$\mathbf{p_{O_2}}$**[Pa]**	$\mathbf{p_{CO}}$**[Pa]**	$\mathbf{k_1^{(2)}}$**[cm^{3}s^{-1}]**	$\mathbf{k_2^{(2)}}$**[cm^{3}s^{-1}]**
100	1.01	0.02	0.03	$(40.78 \pm 20.39)\cdot10^{-14}$	$(31.24 \pm 10.41)\cdot10^{-13}$
	1.03	0.04	0.04	$(37.58 \pm 9.40)\cdot10^{-14}$	$(27.96 \pm 6.99)\cdot10^{-13}$
	1.02	0.04	0.08	$(50.36 \pm 12.59)\cdot10^{-14}$	$(23.62 \pm 2.96)\cdot10^{-13}$
	1.03	0.08	0.04	$(38.29 \pm 4.79)\cdot10^{-14}$	$(16.26 \pm 4.07)\cdot10^{-13}$
150	1.00	0.04	0.04	$(8.76 \pm 2.19)\cdot10^{-14}$	$(14.51 \pm 3.63)\cdot10^{-14}$
	1.00	0.04	0.06	$(11.18 \pm 2.80)\cdot10^{-14}$	$(14.96 \pm 2.49)\cdot10^{-14}$
	1.00	0.04	0.16	$(16.62 \pm 4.16)\cdot10^{-14}$	$(27.16 \pm 1.70)\cdot10^{-14}$
	1.03	0.06	0.07	$(18.49 \pm 3.08)\cdot10^{-14}$	$(30.31 \pm 4.33)\cdot10^{-14}$
	1.05	0.06	0.11	$(19.75 \pm 3.29)\cdot10^{-14}$	$(36.98 \pm 3.36)\cdot10^{-14}$
	1.04	0.12	0.05	$(10.75 \pm 0.90)\cdot10^{-14}$	$(18.13 \pm 3.63)\cdot10^{-14}$
190	1.05	0.07	0.07	$(8.60 \pm 1.23)\cdot10^{-14}$	$(11.79 \pm 1.68)\cdot10^{-14}$
	1.04	0.08	0.16	$(9.26 \pm 1.16)\cdot10^{-14}$	$(8.37 \pm 0.52)\cdot10^{-14}$
	1.04	0.15	0.08	$(7.01 \pm 0.47)\cdot10^{-14}$	$(13.40 \pm 1.68)\cdot10^{-14}$
225	1.07	0.09	0.10	$(5.95 \pm 0.66)\cdot10^{-14}$	$(3.10 \pm 0.31)\cdot10^{-14}$
300	1.05	0.13	0.13	$(3.08 \pm 0.24)\cdot10^{-14}$	$(1.12 \pm 0.09)\cdot10^{-14}$
	1.05	0.13	0.26	$(3.08 \pm 0.24)\cdot10^{-14}$	$(1.10 \pm 0.04)\cdot10^{-14}$
	1.05	0.26	0.13	$(2.64 \pm 0.10)\cdot10^{-14}$	$(1.48 \pm 0.11)\cdot10^{-14}$

Table 5.13: The bimolecular rate coefficients $k_1^{(2)}$ and $k_2^{(2)}$ for the reaction of Au_2^- clusters with O_2 and CO for different reaction temperatures and different partial pressures of the reactant gases.

dependence is an indication of a barrierless reaction, which is characteristic for an ion-molecule reaction, as discussed in section 2.2. Deviations from the linear trend in the temperature dependence of the $k_1^{(2)}$ and $k_1^{(3)}$ rate constants are measured for high CO pressures. These deviations can be rationalized by considering the influence of the side reaction which is in competition with the catalytic cycle at high CO pressures, as discussed above.

In the case of $k_3^{(2)}$, a positive temperature dependence can be identified from the

$\mathbf{T[K]}$	$\mathbf{p_{He}[Pa]}$	$\mathbf{p_{O_2}[Pa]}$	$\mathbf{p_{CO}[Pa]}$	$\mathbf{k_{-2}^{(2)}[cm^3s^{-1}]}$	$\mathbf{k_3^{(2)}[cm^3s^{-1}]}$
100	1.01	0.02	0.03	$(2.41 \pm 0.48)\cdot10^{-14}$	$(9.01 \pm 4.50)\cdot10^{-15}$
	1.03	0.04	0.04	$(2.53 \pm 0.51)\cdot10^{-14}$	$(18.42 \pm 9.21)\cdot10^{-15}$
	1.02	0.04	0.08	$(7.23 \pm 1.45)\cdot10^{-14}$	$(19.04 \pm 9.52)\cdot10^{-15}$
	1.03	0.08	0.04	$(1.98 \pm 0.40)\cdot10^{-14}$	$(31.32 \pm 15.66)\cdot10^{-15}$
150	1.00	0.04	0.04	$(0.24 \pm 0.05)\cdot10^{-14}$	$(0.76 \pm 0.38)\cdot10^{-15}$
	1.00	0.04	0.06	$(0.59 \pm 0.12)\cdot10^{-14}$	$(17.63 \pm 8.81)\cdot10^{-15}$
	1.00	0.04	0.16	$(7.07 \pm 1.41)\cdot10^{-14}$	$(13.03 \pm 6.52)\cdot10^{-15}$
	1.03	0.06	0.07	$(0.73 \pm 0.15)\cdot10^{-14}$	$(19.43 \pm 9.71)\cdot10^{-15}$
	1.05	0.06	0.11	$(2.88 \pm 0.58)\cdot10^{-14}$	$(15.11 \pm 7.56)\cdot10^{-15}$
	1.04	0.12	0.05	$(0.52 \pm 0.10)\cdot10^{-14}$	$(40.50 \pm 20.25)\cdot10^{-15}$
190	1.05	0.07	0.07	$(0.17 \pm 0.03)\cdot10^{-14}$	$(14.01 \pm 7.01)\cdot10^{-15}$
	1.04	0.08	0.16	$(0.77 \pm 0.15)\cdot10^{-14}$	$(9.30 \pm 4.65)\cdot10^{-15}$
	1.04	0.15	0.08	$(0.57 \pm 0.11)\cdot10^{-14}$	$(13.53 \pm 6.76)\cdot10^{-15}$
225	1.07	0.09	0.10	$(0.47 \pm 0.09)\cdot10^{-14}$	$(29.56 \pm 14.78)\cdot10^{-15}$
300	1.05	0.13	0.13	$< 0.04\cdot10^{-15}$	$> 32.80\cdot10^{-14}$
	1.05	0.13	0.26	$< 0.04\cdot10^{-15}$	$> 16.40\cdot10^{-14}$
	1.05	0.26	0.13	$< 0.04\cdot10^{-15}$	$> 32.80\cdot10^{-14}$

Table 5.14: The bimolecular rate coefficients $k_{-2}^{(2)}$ and $k_3^{(2)}$ for the reaction of Au_2^- clusters with O_2 and CO for different reaction temperatures and different partial pressures of the reactant gases.

values presented in table 5.14. The graphical representation of the $k_3^{(2)}$ temperature dependence is depicted in Fig. 5.22 (d). The observed positive temperature dependence indicates that an activation barrier is involved in the last elementary step of the reaction mechanism for the catalytic CO oxidation reaction on Au_2^- clusters. This finding can be correlated with the observed decrease of the $Au_2(CO)O_2^-$ signal, as well as the increase of the Au_2^- offset with increasing temperature, as shown in Fig. 5.18 and Fig. 5.19.

$\mathbf{T[K]}$	$\mathbf{p_{He}[Pa]}$	$\mathbf{p_{O_2}[Pa]}$	$\mathbf{p_{CO}[Pa]}$	$\mathbf{k_1^{(3)}[cm^6s^{-1}]}$	$\mathbf{k_2^{(3)}[cm^6s^{-1}]}$
100	1.01	0.02	0.03	$(9.95 \pm 4.98)\cdot10^{-28}$	$(76.25 \pm 25.42)\cdot10^{-28}$
	1.03	0.04	0.04	$(9.00 \pm 2.25)\cdot10^{-28}$	$(66.92 \pm 16.73)\cdot10^{-28}$
	1.02	0.04	0.08	$(12.17 \pm 3.04)\cdot10^{-28}$	$(57.10 \pm 7.14)\cdot10^{-28}$
	1.03	0.08	0.04	$(9.16 \pm 1.15)\cdot10^{-28}$	$(38.92 \pm 9.73)\cdot10^{-28}$
150	1.00	0.04	0.04	$(2.63 \pm 0.66)\cdot10^{-28}$	$(4.36 \pm 1.09)\cdot10^{-28}$
	1.00	0.04	0.06	$(3.36 \pm 0.84)\cdot10^{-28}$	$(4.50 \pm 0.75)\cdot10^{-28}$
	1.00	0.04	0.16	$(5.00 \pm 1.25)\cdot10^{-28}$	$(8.16 \pm 0.51)\cdot10^{-28}$
	1.03	0.06	0.07	$(5.39 \pm 0.90)\cdot10^{-28}$	$(8.84 \pm 1.26)\cdot10^{-28}$
	1.05	0.06	0.11	$(5.65 \pm 0.94)\cdot10^{-28}$	$(10.59 \pm 0.96)\cdot10^{-28}$
	1.04	0.12	0.05	$(3.11 \pm 0.26)\cdot10^{-28}$	$(5.24 \pm 1.05)\cdot10^{-28}$
190	1.05	0.07	0.07	$(2.79 \pm 0.40)\cdot10^{-28}$	$(3.82 \pm 0.55)\cdot10^{-28}$
	1.04	0.08	0.16	$(3.03 \pm 0.38)\cdot10^{-28}$	$(2.74 \pm 0.17)\cdot10^{-28}$
	1.04	0.15	0.08	$(2.29 \pm 0.15)\cdot10^{-28}$	$(4.38 \pm 0.55)\cdot10^{-28}$
225	1.07	0.09	0.10	$(2.05 \pm 0.23)\cdot10^{-28}$	$(1.07 \pm 0.11)\cdot10^{-28}$
300	1.05	0.13	0.13	$(1.25 \pm 0.10)\cdot10^{-28}$	$(0.45 \pm 0.03)\cdot10^{-28}$
	1.05	0.13	0.26	$(1.25 \pm 0.10)\cdot10^{-28}$	$(0.45 \pm 0.02)\cdot10^{-28}$
	1.05	0.26	0.13	$(1.07 \pm 0.04)\cdot10^{-28}$	$(0.60 \pm 0.05)\cdot10^{-28}$

Table 5.15: The termolecular rate coefficients $k_1^{(3)}$ and $k_2^{(3)}$ for the reaction of Au_2^- clusters with O_2 and CO for different reaction temperatures and different partial pressures of the reactant gases.

From table 5.14 and Fig. 5.22 (c), it can be seen that $k_{-2}^{(2)}$ presents a negative temperature dependence. As the forward step of the reaction 5.30 described by the rate constant $k_2^{(2)}$ is found to be barrierless, one would expect that $k_{-2}^{(2)}$ has a positive temperature dependence and thus, an activation barrier. The observed negative temperature dependence of $k_{-2}^{(2)}$ rate coefficient could be due to the participation of different isomers of the $Au_2(CO)O_2^-$ intermediate product in the reaction mechanism: isomers that dissociate back to the $Au_2O_2^-$ reaction product and isomers that do not

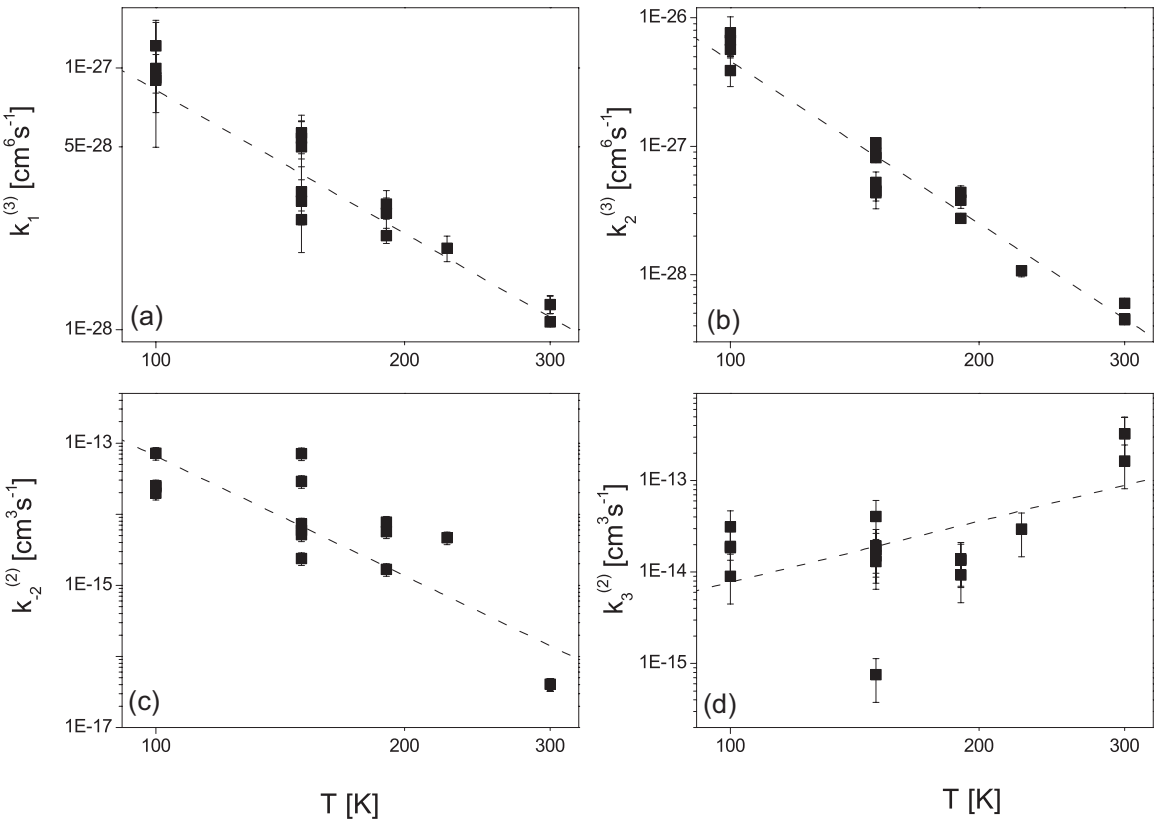

Figure 5.22: Double logarithmic representation of the temperature dependence of $k_1^{(3)}$, $k_2^{(3)}$, $k_{-2}^{(2)}$ and $k_3^{(2)}$ reaction rate constants. The dashed line represents a linear fit of the experimental data.

dissociate but react further with CO, leading to the release of two carbon dioxide molecules. Hence, the relative concentration of stable and dissociating isomers at different reaction temperatures could lead to a negative temperature dependence for $k_{-2}^{(2)}$.

Due to experimental limitations, a direct detection of the produced CO_2 molecules is not possible. However, the CO_2 yield created in the catalytic CO oxidation reaction on Au_2^- clusters can be simulated by using the *CKS 1.0* software.[134] Fig. 5.23 shows the experimental data for the reaction of anionic gold dimers with O_2 and CO at a reaction temperature of 300 K (open symbols) and the fit to the catalytic cycle according to the equations 5.29 - 5.31 (solid lines). From this graph, it can be observed that the CO_2 signal increases non-linearly at short reaction times and after a few

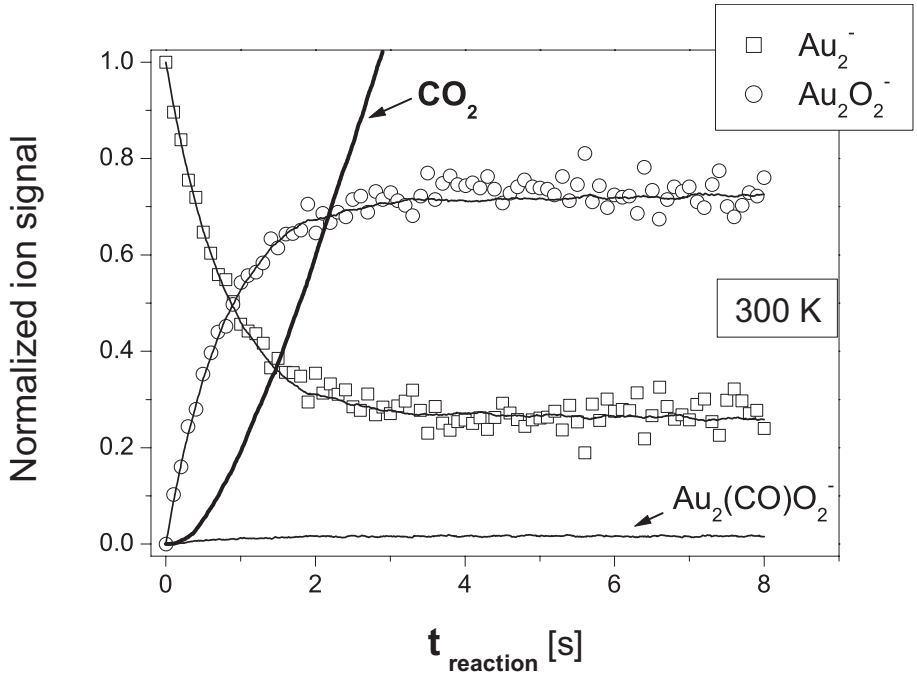

Figure 5.23: Simulation of the catalytic CO oxidation cycle on Au_2^- clusters given by the equations 5.29 - 5.31 at a reaction temperature of 300 K, by using the *CKS 1.0* software. The open symbols represent the experimental data, while the solid lines represent the simulated signals.

seconds, the dependence on the reaction time becomes linear.

From the experimental kinetic traces measured at a reaction temperature of 300 K, the turn-over frequency (TOF) for the CO_2 production can be calculated. Since at this temperature, only $Au_2O_2^-$ appears as an intermediate product in the kinetic traces and the $Au_2(CO)O_2^-$ concentration is below the experimental detection limit, the reaction mechanism can be rewritten schematically as follows:

$$Au_2^- + O_2 \rightarrow Au_2O_2^- \qquad k_I \tag{5.36}$$

$$Au_2O_2^- + 2CO \rightarrow Au_2^- + 2CO_2 \qquad k_{II} \tag{5.37}$$

where k_I and k_{II} represent the reaction rate constants for each elementary step. In the pseudo-first-order approximation the rate law equations can be written as:

$$\frac{d[Au_2^-](t)}{dt} = -k_I[Au_2^-](t) + k_{II}[Au_2O_2^-](t) \tag{5.38}$$

$$\frac{d[Au_2O_2^-](t)}{dt} = k_I[Au_2^-](t) - k_{II}[Au_2O_2^-](t) \tag{5.39}$$

$$\frac{1}{2}\frac{d[CO_2^-](t)}{dt} = k_{II}[Au_2O_2^-](t) \tag{5.40}$$

From Fig. 5.23, one can observe that the reaction product concentrations reach an equilibrium after the reaction time t_{eq}, which can be represented with the following expression:

$$\frac{d[Au_2^-](t_{eq})}{dt} = \frac{d[Au_2O_2^-](t_{eq})}{dt} = 0 \tag{5.41}$$

Furthermore, the concentrations of the reaction educt $Au_2^-(t)$ and product $Au_2O_2^-(t)$ fulfill the normalization condition during the catalytic cycle:

$$[Au_2^-](t) + [Au_2O_2^-](t) = [Au_2^-](0) \tag{5.42}$$

where $[Au_2^-](t)$ and $[Au_2O_2^-](t)$ represent the ion concentrations after a given reaction time t, and $[Au_2^-](0)$ denotes the initial concentration of anionic gold dimers which are present inside the octopole ion trap. Introducing expression 5.41 in the equations 5.38 and 5.39 and using equation 5.42, one can obtain the expression for the anionic gold dimer concentration after the reaction time t_{eq} as a function of the initial gold cluster concentration:

$$[Au_2^-](t_{eq}) = \frac{k_{II}}{k_I + k_{II}}\ [Au_2^-](0) \tag{5.43}$$

The turn-over frequency (TOF) is defined as the number of produced CO_2 molecules per gold cluster in one second. Therefore, by dividing equation 5.40 by the initial concentration of gold clusters and using the expression 5.43, the TOF after the reaction time t_{eq} can be calculated as:

$$TOF = \frac{d}{dt}\ \left(\frac{[CO_2^-](t_{eq})}{[Au_2^-](0)}\right) = \frac{2k_Ik_{II}}{k_I + k_{II}} \tag{5.44}$$

k_I and k_{II} are obtained by fitting the experimental data with the reaction mechanism given by the expressions 5.36 and 5.37, where the fitting program *Detmech* was employed.[133] Using equation 5.44, the turn-over frequency has a value of $TOF = 0.5\, CO_2$ molecules per Au_2^- cluster per second, when similar amounts of O_2 and CO are present

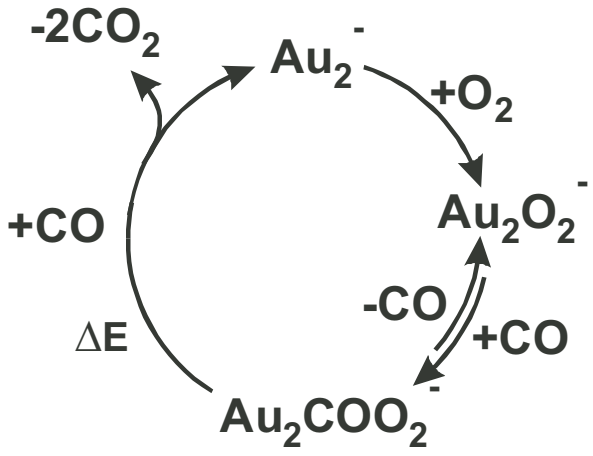

Figure 5.24: The catalytic cycle for the CO oxidation reaction on Au_2^- clusters, derived from the experimental data, according to the equations 5.29 - 5.31.

inside the ion trap. Interestingly, this value is on the same order of magnitude as the catalytic activity of small gold nanoparticles supported on oxide surfaces, where values between 0.25 CO_2 molecules per gold atom per second for particles with 3 nm diameter at 300 K[66] and 4 CO_2 molecules per gold atom per second for particles with 3.5 nm diameter at 350 K[65] have been obtained for the TOF. The experiments presented in this section are the first gas-phase measurements, in which a reliable value for the turn-over frequency could be determined.

Based on the experimental results, the catalytic cycle for the CO oxidation reaction on negatively charged gold dimers can be represented schematically as shown in Fig. 5.24. In summary, the catalytic cycle for the CO oxidation reaction on Au_2^- clusters in the presence of similar amounts of O_2 and CO reactive gases proceeds as follows: in the first step, an oxygen molecule is adsorbed, which leads to the formation of the $Au_2O_2^-$ product. The second step involves the reversible adsorption of a CO molecule and thus, the intermediate complex $Au_2(CO)O_2^-$ is produced. It is important to note that the backward reaction step is a necessary condition in order to obtain a good agreement between the fitted signal and the experimental data. These two processes possess a negative temperature dependence which is an indication of a barrierless reaction. In the third step, a second CO molecule is adsorbed, leading to the release of 2 CO_2 molecules and the reformation of the pure anionic gold dimer.

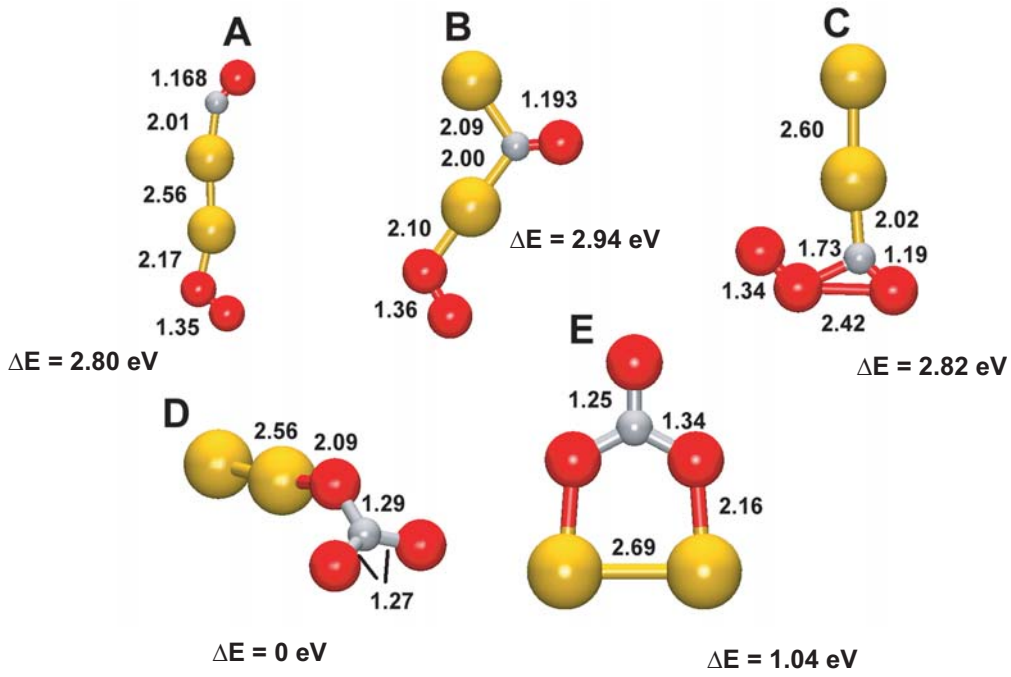

Figure 5.25: Calculated structures for the $Au_2(CO)O_2^-$ reaction product. The bond lengths are given in $\mathring{A}$. The gold atoms are depicted by large yellow spheres, oxygen atoms are represented as red spheres, and carbon atoms are depicted as small grey spheres. The relative structure stability compared to the stability of structure D (for which $\Delta E_{(D)} = 0\ eV$) is also shown.

This last reaction step must involve an activation barrier, since the corresponding reaction rate coefficient shows a positive temperature dependence.

Although the experimental results provide valuable insights into the reaction mechanism, no information about the structure of the $Au_2(CO)O_2^-$ complex can be obtained. However, the measured data point towards the existence of different isomers for the $Au_2(CO)O_2^-$ intermediate product. Moreover, the activation barrier, which appears in the last reaction step has been clearly revealed. In order to elucidate the intrinsic details of the catalytic CO oxidation reaction on Au_2^- clusters, theoretical calculations are needed.

Theoretical investigations in the framework of density functional theory (DFT) are performed by H. Häkkinen and U. Landman.[57,150] The structures of $Au_2O_2^-$ and Au_2CO^- products have already been presented and discussed in detail in section 5.2 and in section 5.3, respectively. In the following, the discussion will focus on the

structure of the $Au_2(CO)O_2^-$ reaction intermediate. The calculations consider that the $Au_2O_2^-$ reaction product is already formed and a CO molecule is coadsorbed on this complex, leading to the formation of the $Au_2(CO)O_2^-$ reaction intermediate. The calculated isomers, denoted as structures A, B, C, D and E for the $Au_2(CO)O_2^-$ complex are presented in Fig. 5.25. The stability of these structures (ΔE) relative to the stability of structure D ($\Delta E_{(D)} = 0$) is also shown in Fig. 5.25. From this figure, it can be seen that structures A and B correspond to a molecular coadsorption of the O_2 and CO molecules on different sides of the anionic gold dimer, whereas the structures C, D and E contain an $O-O-C-O$ group. Furthermore, structures A, B, C and E are planar, while D has a three dimensional structure.

The structure A is obtained through the coadsorption of the O_2 and CO molecules on different terminal sides of the $Au-Au$ axis. Interestingly, the formation of structure A proceeds without an activation barrier. The formation of structure B involves an activation barrier of 0.2 eV, where the carbon monoxide molecule is adsorbed on the bridge site (between the two gold atoms) and the oxygen molecule on the end site of the $Au-Au$ axis. The transformation of structure A into structure B *via* displacement of CO from the terminal site to the bridge site of Au_2^- cluster has a relatively high activation barrier, which has a value of about 0.9 eV. It is important to note that in both structures A and B the $O-O$ bond is activated to a value typical to a superoxo-like species O_2^- (1.35 $\mathring{A}$ and 1.36 $\mathring{A}$ for structure A and structure B, respectively, in comparison to 1.25 $\mathring{A}$ for the free gas-phase O_2 molecule[112]).

The structure C contains a $O-O-C-O$ group that is attached to anionic gold dimer through the carbon atom and the relative stability of this structure is comparable to that of structure A ($\Delta E_{(C)} = 2.82\ eV$, $\Delta E_{(A)} = 2.80\ eV$). The formation of structure C is investigated by considering the Langmuir-Hinshelwood and Eley-Rideal mechanisms, which have been described in section 2.3.1. The Langmuir-Hinshelwood mechanism (LH) involves the migration of the adsorbed CO molecule from the bridging site in structure B to the terminal site in structure C. This migration process has a high activation barrier, which has a value of about 1.1 eV. Therefore, the formation of structure C from structure B is unlikely to occur. The formation of structure C *via* LH mechanism, starting from structure A is also unlikely, since it involves a transformation from structure A to structure B, which has an activation barrier of about 0.9 eV, as discussed above. The Eley-Rideal mechanism (EA) implies

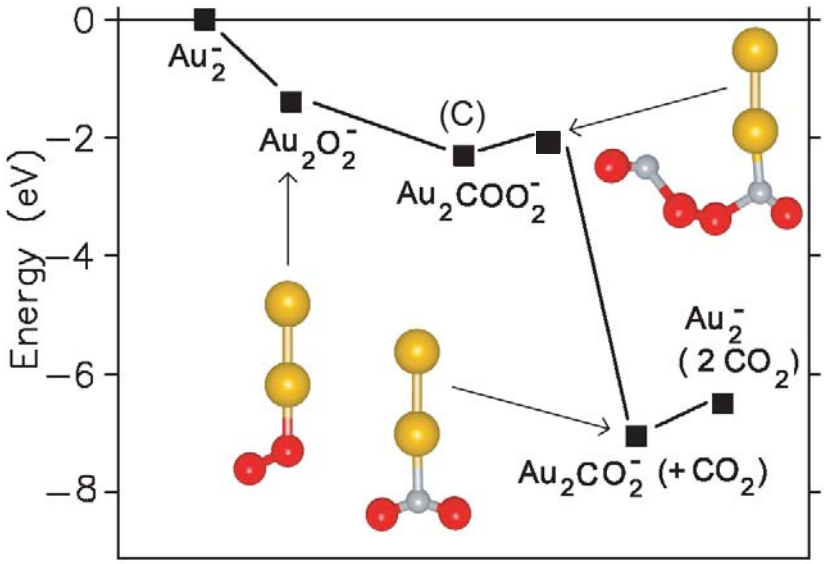

Figure 5.26: Energetics along the reaction path for the catalytic CO oxidation containing structure C, which corresponds to the peroxyformate-like $Au_2(CO)O_2^-$ species as intermediate complex. The initial energy level represents the sum of the total energies of all the reactants ($Au_2^- + O_2 + 2CO$).

that a CO molecule from the gas-phase approaches the preformed $Au_2O_2^-$ complex and adsorbs directly between the gold dimer and oxygen molecule, forming structure C. The theoretical calculations show that this process does not involve an activation barrier and it is therefore, the energetically most favorable pathway for the formation of structure C.

The most stable structure in Fig. 5.25 is the carbonate species D, which is formed by an Eley-Rideal mechanism, where the CO molecule from the gas-phase is inserted into the $O-O$ bond in the $Au_2O_2^-$ complex. This process requires an activation barrier of only 0.3 eV, which can be easily overcome by the thermal excitation under the experimental conditions of the measurements presented here.

The carbonate structure E is formed *via* an ER mechanism from an $Au_2O_2^-$ complex, where the molecular axes of anionic gold dimer and oxygen molecule are parallel to each other. Since this structure of $Au_2O_2^-$ complex is calculated to be about 1 eV less stable than the isomer with the oxygen molecule adsorbed on a terminal site of the gold dimer, it is unlikely to be formed. Hence, structure E is not expected to play a relevant role in the catalytic cycle.

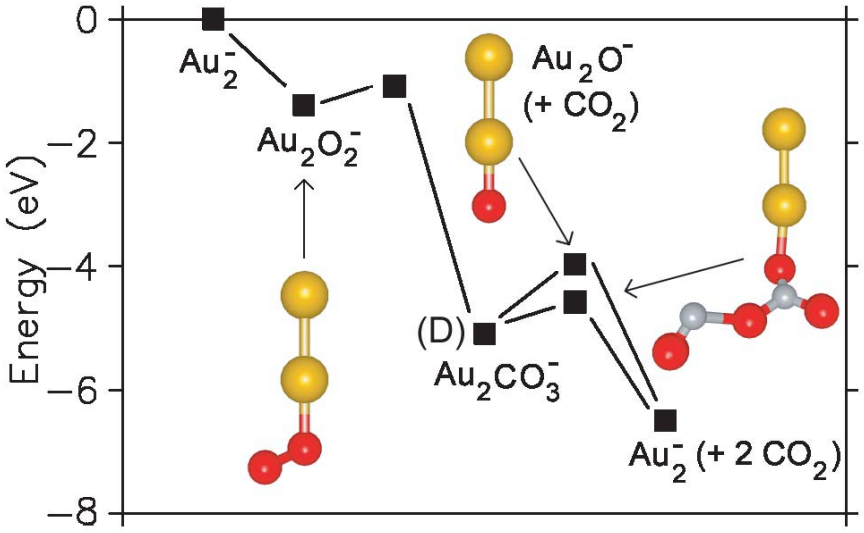

Figure 5.27: Energetics along the reaction path for the catalytic CO oxidation containing structure D, which corresponds to the carbonate species $Au_2CO_3^-$ as intermediate complex. The initial energy level represents the sum of the total energies of all the reactants ($Au_2^- + O_2 + 2CO$).

In the following, the discussion will focus on the last reaction step given by the equation 5.31, in which the second CO molecule is adsorbed, leading to the release of two CO_2 molecules. According to the theoretical calculations, this reaction step can only be carried out by the structures C and D of the intermediate complex corresponding to the mass of $Au_2(CO)O_2^-$. The high energy barriers for the migration of the CO molecule along the $Au - Au$ axis as well as the absence of the $Au_2C_2O_4^-$ reaction product in the experimental mass spectra suggest an Eley-Rideal mechanism for the last reaction step of the catalytic cycle.

The reaction path involving structure C as intermediate reaction product is presented in Fig. 5.26. From this figure, it can be seen that the formation of the $Au_2(CO_2)_2^-$ product starting from structure C involves a small energy barrier of about 0.3 eV. The release of the first CO_2 molecule is barrierless and thus, the $Au_2CO_2^-$ product is formed. The CO_2 group in the $Au_2CO_2^-$ complex is bound to Au_2^- cluster through the carbon atom and the binding energy has a value of about 0.52 eV. However, the heat of reaction released during the formation of the first CO_2 molecule has a value of about 4.75 eV, which is large enough to overcome the

binding energy of the remaining CO_2 molecule to the anionic gold dimer, leading to the desorption of the second CO_2 and the reformation of the bare gold clusters.

The second possible reaction path involves the carbonate species $Au_2CO_3^-$, corresponding to the structure D in Fig. 5.25. This reaction path is shown in Fig. 5.27. It can be noticed that this scenario presents two branches. One reaction path involves a thermal dissociation of the $Au_2CO_3^-$ product and the release of a CO_2 molecule. This process is endothermic by 1.12 eV and leads to the formation of a highly reactive complex Au_2O^-, which further reacts without an activation barrier with a CO molecule to produce CO_2. It is important to note that the Au_2O^- complex was not experimentally observed. The second reaction path assumes an Eley-Rideal (EA) mechanism for the formation of the $Au_2(CO_2)_2^-$ complex. This process involves an activation barrier of 0.5 eV. Once formed, the $Au_2(CO_2)_2^-$ complex will release two CO_2 molecules, since the remaining $Au_2CO_2^-$ product is not stable. Taking into account the experimental conditions, the second path is the most favorable one for the catalytic CO oxidation reaction on an anionic gold dimer.

In Fig. 5.28, the full catalytic cycle for the CO oxidation reaction on negatively

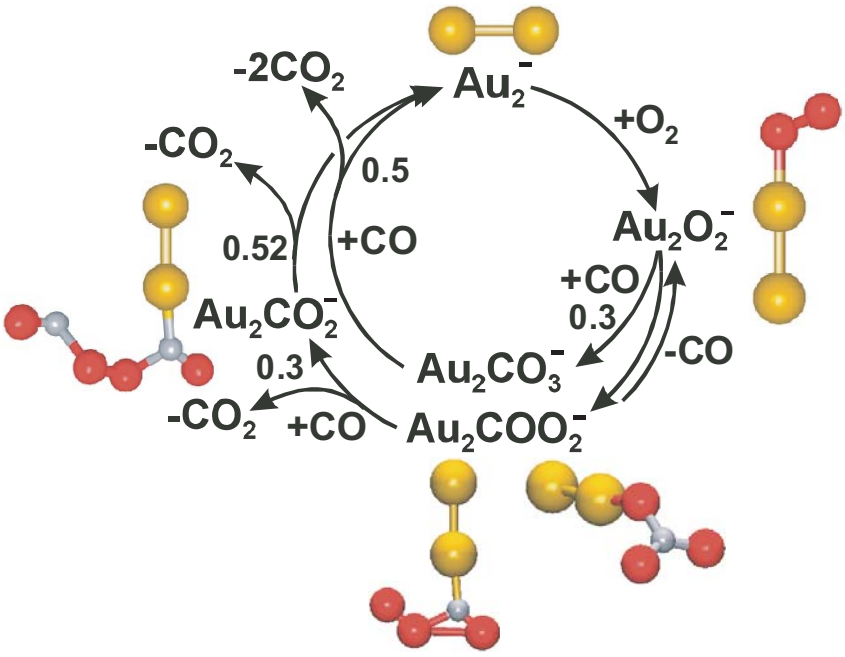

Figure 5.28: The full catalytic cycle for the CO oxidation reaction on negatively charged gold dimers based on the experimental and theoretical results.

charged gold dimers, based on the experimental and theoretical results is presented. The key reaction intermediate corresponding to the mass of $Au_2(CO)O_2^-$, which was observed experimentally is assigned to have two structures (digold carbonate and gold peroxyformate-like), that can lead to the formation of CO_2 molecules and the reforming of the bare gold Au_2^- clusters. In conclusion, the fruitful combination between experimental measurements and theoretical calculations allows for a full understanding of the low temperature catalytic activity of Au_2^- clusters towards the CO oxidation reaction.

5.6 Influence of the Chemical Composition on the Cluster Reactivity

In this section, the influence of the chemical composition on the cluster reactivity will be investigated. For this purpose, a comparison between the reactivity of anionic silver clusters, mixed silver-gold clusters and gold clusters towards oxygen and carbon monoxide will be performed. Mixed silver-gold clusters are of particular interest, since a hetero-polar bonding between gold and silver atom occurs which is the result of an internal charge transfer from silver to gold.[156] The combination between quasi-ionic and metallic properties in mixed silver-gold clusters as well as the possibility to have a negatively charged Au atom embedded in a Ag-surrounding make these type of clusters well suited species for the investigation of their reactivity and catalytic properties.[157] Therefore, it is highly interesting to investigate the chemical behavior of binary noble metal clusters, when going gradually from pure gold to pure silver clusters by successively replacing just one atom of the clusters.

A detailed study of the reactivity of silver and mixed silver-gold clusters with O_2 and CO is presented in the PhD. thesis of Jan Hagen and only a short description will be given here.[79] For the investigation of the reactivity of anionic silver and silver-gold clusters, the same experimental apparatus and measurement procedure, as described in chapter 4 was employed. Fig. 5.29 shows the mass spectra for the reactivity of the anionic dimers Au_2^-, $AuAg^-$ and Ag_2^- towards oxygen and carbon monoxide at a reaction temperature of 100 K and 300 K, respectively.

It can be observed that each anionic dimer adsorbs one O_2 molecule (Fig. 5.29 (a),

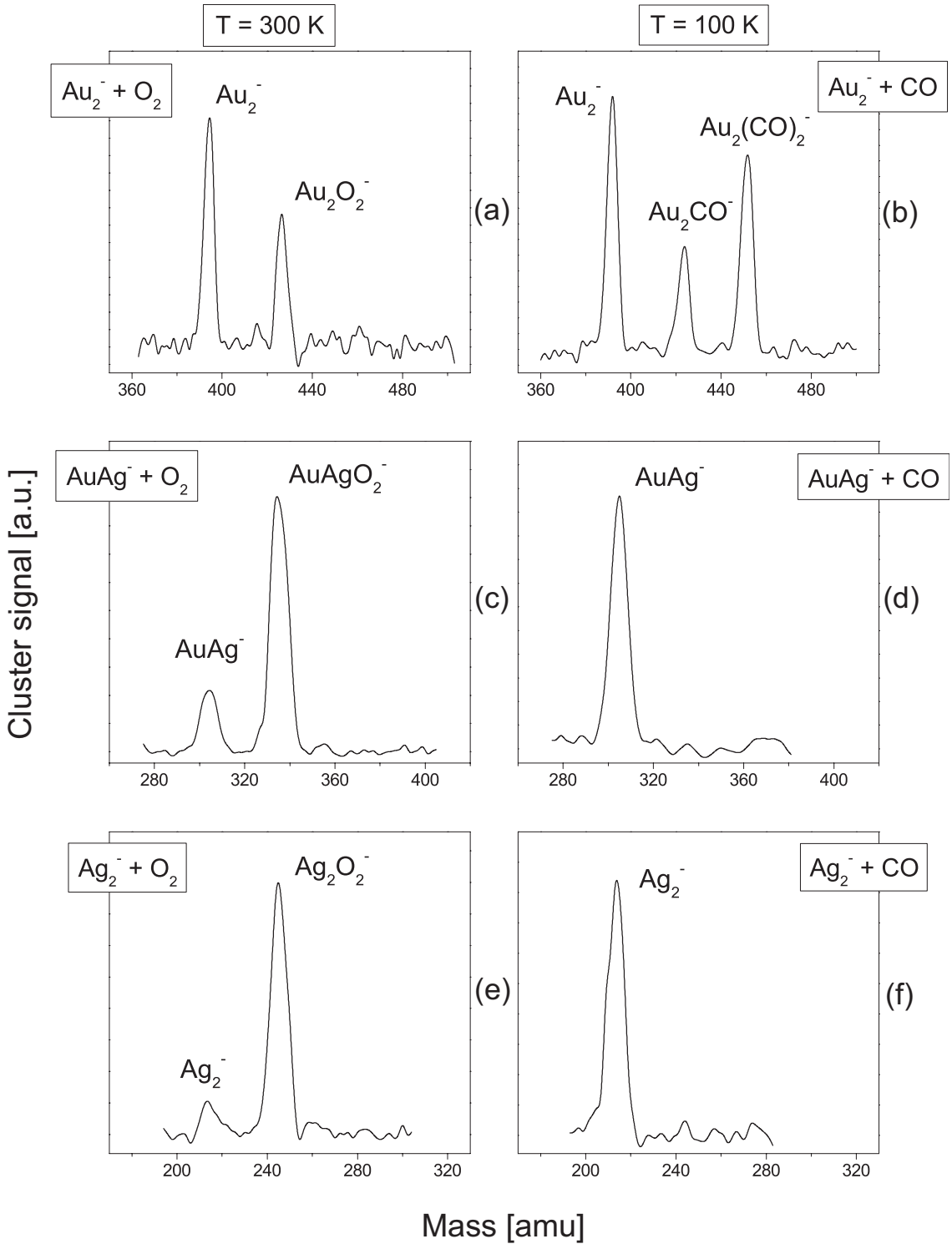

Figure 5.29: Mass spectra for the reaction of Au_2^-, $AuAg^-$ and Ag_2^- clusters with O_2 and CO at a reaction temperature of 300 K ((a), (c), (e)) and 100 K ((b), (d), (f)), respectively. The reaction parameters are: (a) $p_{He} = 1.00\ Pa$, $p_{O_2} = 0.30\ Pa$, $t_{reaction} = 500\ ms$; (b) $p_{He} = 0.96\ Pa$, $p_{CO} = 0.24\ Pa$, $t_{reaction} = 1000\ ms$; (c) $p_{He} = 1.05\ Pa$, $p_{O_2} = 0.12\ Pa$, $t_{reaction} = 500\ ms$; (d) $p_{He} = 1.00\ Pa$, $p_{CO} = 0.26\ Pa$, $t_{reaction} = 5000\ ms$; (e) $p_{He} = 1.06\ Pa$, $p_{O_2} = 0.12\ Pa$, $t_{reaction} = 500\ ms$; (f) $p_{He} = 1.04\ Pa$, $p_{CO} = 0.20\ Pa$, $t_{reaction} = 5000\ ms$.

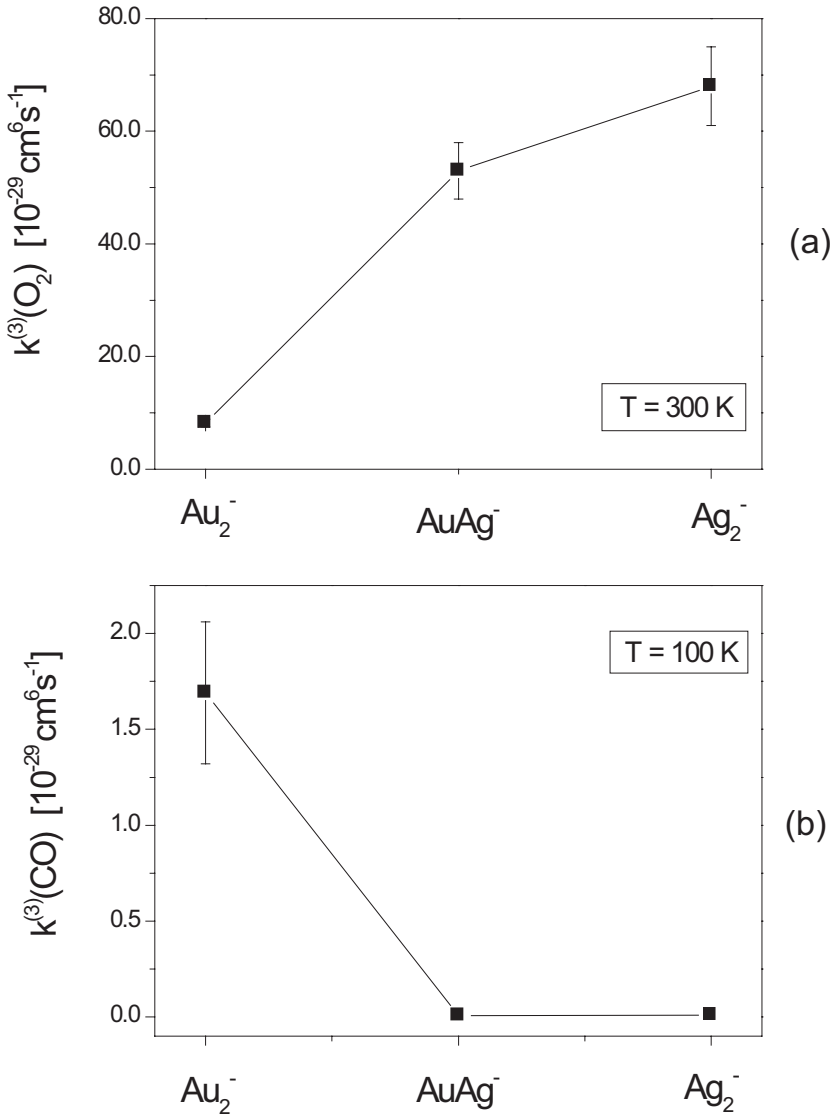

Figure 5.30: (a) Termolecular rate constants for the reaction of Au_2^-, $AuAg^-$ and Ag_2^- clusters with oxygen at 300 K reaction temperature, derived from kinetic measurements. (b) Termolecular rate constants for the reaction of Au_2^-, $AuAg^-$ and Ag_2^- clusters with carbon monoxide at 100 K reaction temperature, derived from kinetic measurements.

(c), (e)) and only Au_2^- clusters react with carbon monoxide (Fig. 5.29 (b)). Surprisingly, $AuAg^-$ and Ag_2^- clusters show no reactivity towards CO within a storage time of up to 10 seconds inside the octopole ion trap ($t_{reaction} = 10\ s$) for all investigated

reaction temperatures and CO gas pressures (Fig. 5.29 (d), (f)).

By recording the variation of the reaction product and educt concentrations as a function of time, the kinetic traces for a specific reaction can be measured. Fitting the kinetic data, by using the *Detmech* program,[133] the values for the reaction rate constants can be extracted.

A comparison of the reactivity of Au_2^-, $AuAg^-$ and Ag_2^- clusters towards O_2 and CO is shown in Fig. 5.30. The termolecular rate coefficients for the reaction of Au_2^-, $AuAg^-$ and Ag_2^- clusters with O_2 are depicted in Fig. 5.30 (a). From this graph, it can be clearly seen that the termolecular rate coefficient for the reaction of anionic silver dimers with oxygen has a higher value than the termolecular rate constant for $AuAg^-$ and Au_2^-: $k_{O_2}^{(3)}(Ag_2^-) > k_{O_2}^{(3)}(AuAg^-) > k_{O_2}^{(3)}(Au_2^-)$. Thus, the reactivity towards molecular oxygen increases gradually from Ag_2^- to $AuAg^-$ and Au_2^- clusters. From the reaction rate constants, the binding energies of the oxygen molecule onto negatively charged noble metal dimers can be calculated by employing the RRK/RRKM theory. The binding energies have the values: $E_{BE}(Ag_2O_2^-) = 0.94 \pm 0.09\ eV$[79] $> E_{BE}(AuAgO_2^-) = 0.89 \pm 0.09\ eV$[79] $> E_{BE}(Au_2O_2^-) = 0.64 \pm 0.10\ eV$. One can observe that the values of the binding energy of the oxygen molecule on negatively charged metal dimers increases as well from anionic gold dimer to silver dimer.

As discussed in section 5.2, the binding mechanism of an O_2 molecule involves an electron transfer from the highest occupied molecular orbital (HOMO) of the cluster into one of the half occupied π^* antibonding orbitals of the oxygen molecule ($2p_x\pi^{*1}$ or $2p_y\pi^{*1}$).[85,129] As previously shown in section 5.2, the reactivity towards oxygen can be rationalized in terms of cluster electron affinity (EA). The values of the electron affinity are correlated to the values of the vertical detachment energy (VDE)[d]. The electron affinity and the vertical detachment energy of pure and binary noble metal dimers have been determined by using photoelectron spectroscopic methods. In the case of gold, silver and mixed silver-gold dimers, the following values have been found: $E_{VDE}(Au_2^-) = 2.01\ eV$,[138,158] $E_{VDE}(AuAg^-) = 1.43\ eV$,[159] $E_{VDE}(Ag_2^-) = 1.06\ eV$.[138,160] These values show that the vertical detachment en-

[d]The vertical detachment energy (VDE) is defined as the energy necessary for the transition from the electronic ground state of an anionic system (vibrational ground state $\nu(X^-) = 0$) into the electronic ground state of the neutral system with a vibrational state $\nu(X) = k$ that corresponds to a vertical electronic transition according to the Franck-Condon principle.

ergy and implicitly, the electron affinity increases gradually from the pure silver to the silver-gold dimer and has the highest value in the case of the gold dimer. This increase in the values of the electron affinity corresponds to the experimentally observed increase in the reactivity of noble metal dimers from Au_2^- to Ag_2^-: the silver dimer has a low EA and therefore can donate more easily an electron to the oxygen molecule ligand than the silver-gold and gold dimers, which have a higher EA and consequently show a lower reactivity towards O_2.

In the case of the reactivity towards CO, Fig. 5.29 (b), (d), (f) and Fig. 5.30 (b) show that only Au_2^- clusters are able to adsorb two CO molecules, whereas Ag_2^- and $AuAg^-$ do not react with carbon monoxide. As presented in section 5.1, the binding mechanism of the CO molecule implies a double charge transfer: CO donates two σ electrons ($2s\sigma^{*2}$) into the lowest unoccupied molecular orbital of the metal cluster (LUMO), while occupied π and δ orbitals from the metal cluster back-donate into the unoccupied antibonding π^* orbital of the CO molecule ($2p_x\pi^*$ or $2p_y\pi^*$).[127] The bond strength of the carbon monoxide ligand depends on the interplay between the σ charge donation (from CO to cluster) and the π back-donation (from cluster to CO).

As discussed in section 5.1, gold shows different chemical and physical properties in comparison to silver due to the presence of strong relativistic effects. This particular behavior of gold is also referred to as the *gold anomaly*.[161] The unusually high ionization potentials, the strong spin-orbit coupling, the yellow color of gold compared to the grey metallic color of silver are only a few of the manifestations of the relativistic effects.[120,121] The contraction of the s-orbitals and the delocalization of the d-orbitals leads to a small $s-d$ band gap in gold clusters, in comparison to silver clusters. Calculations based on density functional theory, performed by Lee *et al.*, have shown that the $s-d$ band gap increases from Au_2 to $AuAg$ and has the highest value for Ag_2 clusters.[162] Since the position of the cluster d-orbitals relative to the position of the molecular orbitals of CO is significant for the π back-donation in the CO bonding mechanism, the non-reactivity of $AuAg^-$ and Ag_2^- clusters towards CO can be correlated with the energetic position of the d-orbitals. In gold clusters, the delocalization of the d-orbitals due to the presence of relativistic effects, energetically favorizes the binding of the CO molecules. In anionic silver and mixed silver-gold dimers, it appears that the relative position of the molecular orbitals does not allow the charge transfer between cluster and CO ligand and thus, no reactivity towards

CO can be observed.

In section 5.5, it was shown that Au_2^- clusters are able to catalyze the carbon monoxide oxidation reaction. In the case of $AuAg^-$ clusters, a catalytic cycle for the CO oxidation reaction was theoretically predicted.[156] Under the experimental conditions of the measurements presented in this work, no reaction product where both CO and O_2 molecules are coadsorbed on the cluster was identified for $AuAg^-$ and Ag_2^-. Furthermore, from the analysis of the kinetic data in the case of $AuAg^-$ and Ag_2^- clusters, no catalytic activity for the CO oxidation reaction could be detected.

The reactivity of anionic pure silver and gold trimers as well as mixed silver-gold trimers towards O_2 and CO is presented in Fig. 5.31. The mass spectra for the reactivity of Au_3^-, Au_2Ag^-, $AuAg_2^-$ and Ag_3^- with O_2 at a reaction temperature of 300 K are depicted in Fig. 5.31 (a), (c), (e), (g), while the mass spectra for the reactivity of negatively charged mixed clusters with CO at reaction temperature of 100 K are shown in Fig. 5.31 (b), (d), (f), and (h). One can notice that the transition in the reactivity towards oxygen and carbon monoxide from pure gold clusters Au_3^- to bare silver clusters Ag_3^- does not occur gradually, but it appears as an "on-off switch" of the chemical reactivity.

From these mass spectra, it can be observed that only Ag_3^- clusters adsorb two O_2 molecules, whereas pure gold and mixed silver-gold trimers do not show any reactivity towards oxygen under the experimental conditions of the measurements presented here. It is important to note that no reactivity of Au_3^-, Au_2Ag^- and $AuAg_2^-$ clusters with O_2 was observed upon any variation of the experimental parameters (reaction temperature, reactive gas pressure, buffer gas pressure). A comparison of the reactivity of Au_3^-, Au_2Ag^-, $AuAg_2^-$ and Ag_3^- clusters towards O_2 at a reaction temperature of 300 K is shown in Fig. 5.32 (a), where the value of the termolecular rate coefficient for the reaction of Ag_3^- with O_2 is derived from kinetic measurements.

As in the case of anionic noble metal dimers, the reactivity of the trimers towards oxygen can be correlated with the values of the electron affinity (vertical detachment energy). The values obtained from photoelectron spectroscopy measurements are: $E_{VDE}(Au_3^-) = 3.9\ eV$,[158,163] $E_{VDE}(Au_2Ag^-) = 3.86\ eV$,[159] $E_{VDE}(AuAg_2^-) = 2.97\ eV$[159] and $E_{VDE}(Ag_3^-) = 2.43\ eV$.[160] Thus, the electron affinity increases from Ag_3^- to Au_3^-. Interestingly, replacing one Ag atom by a Au atom in Ag_3^- clusters leads to a significant increase of the electron affinity of about 0.5 eV. Apparently,

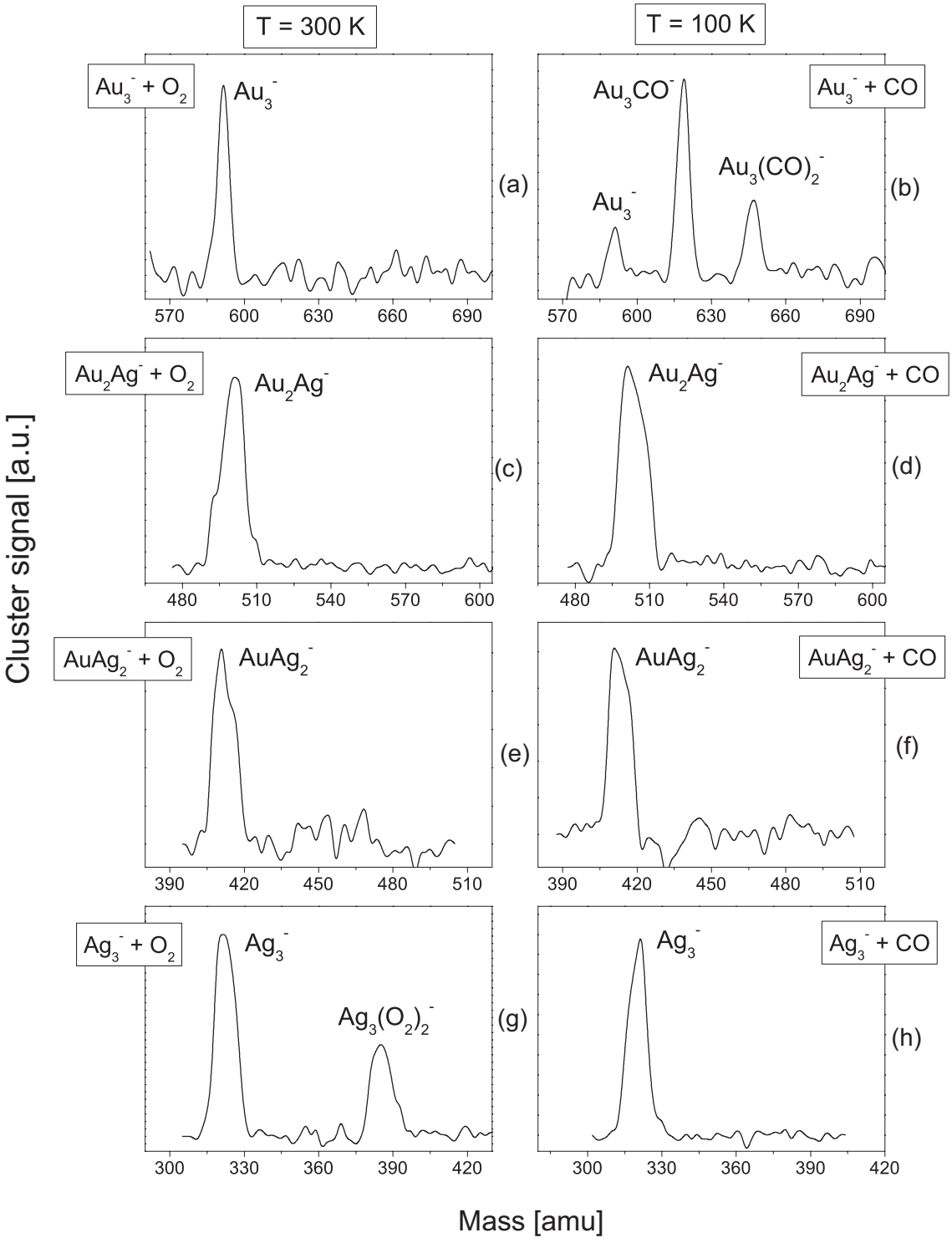

Figure 5.31: Mass spectra for the reaction of Au_3^-, Au_2Ag^-, $AuAg_2^-$ and Ag_3^- clusters with O_2 and CO at 300 K ((a), (c), (e), (g)) and 100 K ((b), (d), (f), (h)) reaction temperature, respectively. The reaction parameters are: (a) $p_{He} = 1.00\ Pa$, $p_{O_2} = 0.30\ Pa$, $t_{reaction} = 1000\ ms$; (b) $p_{He} = 1.03\ Pa$, $p_{CO} = 0.02\ Pa$, $t_{reaction} = 500\ ms$; (c) $p_{He} = 1.05\ Pa$, $p_{O_2} = 0.24\ Pa$, $t_{reaction} = 5000\ ms$; (d) $p_{He} = 1.00\ Pa$, $p_{CO} = 0.15\ Pa$, $t_{reaction} = 5000\ ms$; (e) $p_{He} = 1.05\ Pa$, $p_{O_2} = 0.24\ Pa$, $t_{reaction} = 5000\ ms$; (f) $p_{He} = 1.00\ Pa$, $p_{CO} = 0.15\ Pa$, $t_{reaction} = 5000\ ms$; (g) $p_{He} = 1.04\ Pa$, $p_{O_2} = 0.23\ Pa$, $t_{reaction} = 5000\ ms$; (h)$p_{He} = 1.02\ Pa$, $p_{CO} = 0.24\ Pa$, $t_{reaction} = 5000\ ms$.

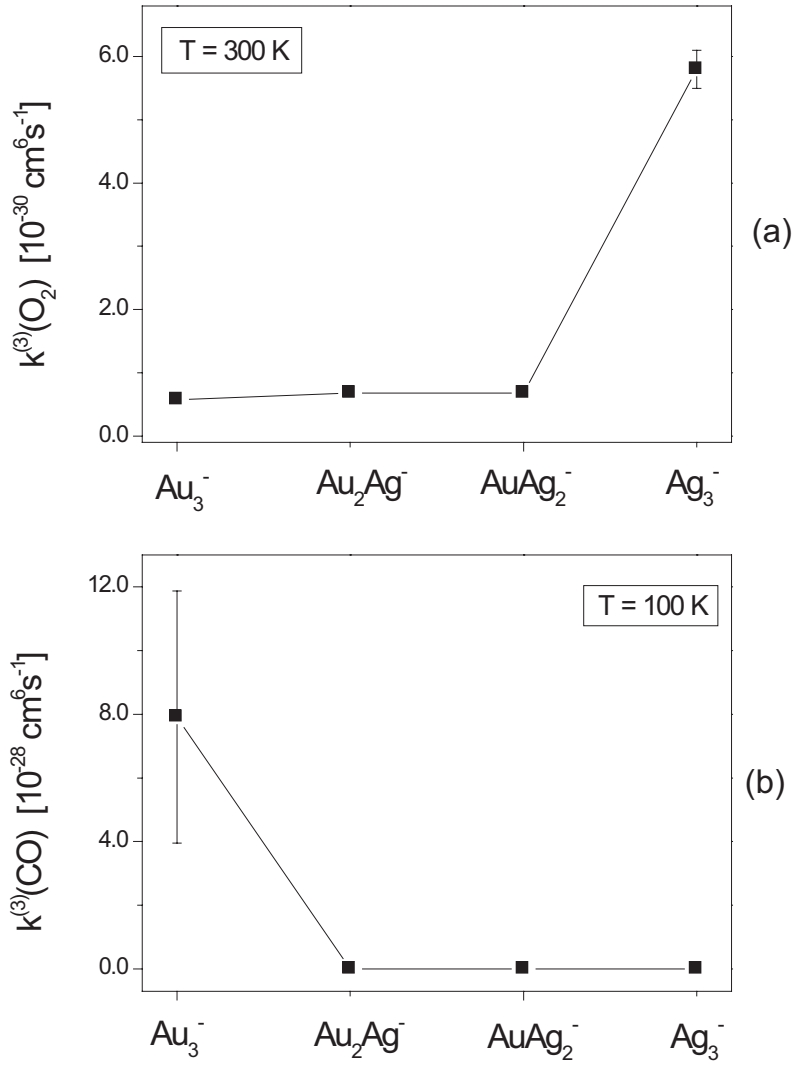

Figure 5.32: (a) Termolecular rate constants for the reaction of Au_3^-, Au_2Ag^-, $AuAg_2^-$ and Ag_3^- clusters with oxygen at 300 K reaction temperature, derived from kinetic measurements. (b) Termolecular rate constants for the reaction of Au_3^-, Au_2Ag^-, $AuAg_2^-$ and Ag_3^- clusters with carbon monoxide at 100 K reaction temperature, derived from kinetic measurements.

this is sufficient to inhibit the charge transfer from the $AuAg_2^-$ cluster to O_2, leading to the observed non-reactivity of $AuAg_2^-$ clusters towards oxygen. The transition from $AuAg_2^-$ to Au_2Ag^- induces a further increase of the cluster electron affinity by almost 1 eV and both these clusters show no reactivity towards oxygen. This par-

ticular reactive behavior of binary silver-gold clusters is another consequence of the strong relativistic effects, which are present in gold atoms.

From the mass spectra depicted in Fig. 5.31 (b), (d), (f), (h) and the values of the termolecular reaction rates shown Fig. 5.32 (b), it can be observed that in the case of the mixed noble metal trimers reactivity towards carbon monoxide only Au_3^- clusters are able to adsorb up to two CO molecules, while Au_2Ag^-, $AuAg_2^-$ and Ag_3^- do not show any reactivity towards CO. As discussed above, the bonding mechanism of a carbon monoxide molecule implies a double charge transfer, which is influenced by the relative energetic position of the cluster and CO molecular orbitals. Similar to the case of mixed silver-gold dimers, the replacement of one gold atom by a silver atom in Au_3^- clusters leads to the disappearance of the reactivity towards carbon monoxide.

In conclusion, the variation of the chemical composition of pure and mixed silver-gold clusters leads to a significant change in the cluster reactivity. In extreme cases, replacing only one silver atom by a gold atom or *vice versa* can lead to a "on-off switch" of the cluster chemical reactivity.